Design, Synthesis and Evaluation of Novel Agents to Treat Alzheimer's Disease

THESIS

Submitted in partial fulfillment
of the requirements for the degree of

DOCTOR OF PHILOSOPHY

by

PRITI JAIN

Under the Supervision of

PROF. HEMANT R JADHAV

BITS Pilani
Pilani | Dubai | Goa | Hyderabad

BIRLA INSTITUTE OF TECHNOLOGY AND SCIENCE, PILANI

2015

BIRLA INSTITUTE OF TECHNOLOGY AND SCIENCE, PILANI

CERTIFICATE

This is to certify that the thesis entitled '**Design, Synthesis and Evaluation of Novel Agents to Treat Alzheimer's disease'** and submitted by **Ms. Priti Jain,** ID No **2009PHXF037P** for award of Ph.D. degree of the Institute embodies original work done by her under my supervision.

Signature of the Supervisor

Name in capital letters: **Prof. HEMANT R JADHAV**

Designation: **Associate Professor, Dept of Pharmacy**

Associate Dean, Academic Research Division

Birla Institute of Technology and Science Pilani, Pilani Campus

Date:

Dedicated to My Family

ACKNOWLEDGEMENTS

Namo Arihantanam (I bow in reverence to Arihants), Namo Siddhanam (I bow in reverence to Siddhas), Namo Ayariyanam (I bow in reverence to Acharyas), Namo Uvajjhayanam (I bow in reverence to Upadhyayas), Namo Loye Savva Sahunam (I bow in reverence to all Sadhus)

Working on the Ph.D. has been a wonderful and often overwhelming experience. It is hard to say whether it has been grappling with the topic itself which has been the real learning experience, or grappling with how to write papers and proposals, give talks, work in a group, stay up until the birds start singing, and stay focused. Though words are seldom sufficient to express gratitude and feelings, it gives me an opportunity to acknowledge those who helped me during the tenure of this study.

I am indebted to many people for making the time working on my Ph.D. an unforgettable experience. It is impossible to come up with the list of individuals who have inspired, encouraged and helped in this achievement however; I will try to list few of those who have served as guideposts along my path.

I would first like to express gratitude from the depth of my heart to the Almighty for His blessings and the strength showered upon me to carry on the daunting task. The next name that comes to my mind while writing these lines is of my revered guide Prof. Hemant R Jadhav, Associate Professor, Dept of Pharmacy; Associate Dean, Academic Research Division, BITS Pilani, Pilani Campus. He went over each section of this text with a fine-toothed comb and made many valuable suggestions to enhance its didactic value. I would like to take this opportunity to thank him profusely for his great help, personal interest, guidance and inspiration bestowed upon me during my Ph. D work, which I shall cherish forever.

I am also highly indebted to Doctoral Advisory Committee (DAC) members Dr S Murugesan and Dr Atish Paul for their suggestions and critical evaluation of this work.

I am immensely thankful to the Vice-Chancellor, Prof. B. N. Jain, Director Prof. A. K. Sarkar, and Dean, Administration, Prof. S. C. Sivasubramanian of Birla Institute of Technology & Science Pilani, Pilani campus for providing me the opportunity to pursue my doctoral studies and providing necessary facilities.

My gratitude to Prof Sanjay Kumar Verma, Dean, ARD and Doctoral Research Committee members of Department of Pharmacy for their support and encouragement. I overwhelmingly acknowledge the teaching and nonteaching staff of ARD and Department of Pharmacy, for their help in one form or other.

I sincerely thank Mr. Satish Dighe and Mr. Pankaj Wadhwa for their continuous help and support. They have been helpful for their constructive suggestions and also moral support. I acknowledge SAIF, Panjab University, Chandigarh for their technical support to access NMR spectroscopy. I also thank University Grants Commission (UGC), Govt. of India for the financial support in the form of minor project during the whole tenure.

Further, my sincere thanks to Dr. Shvetank Bhatt, Dr. Gautam Singhvi, Mr. Mahaveer Singh, Ms. Archana K Kakkar for making the journey a memorable one. They all have been a constant support personally as well as professionally. I also would like to thank all research scholars of Department of Pharmacy, especially Almesh, Ankur, Arghya, Deepali, Emil, Garima, Prashant, Pallavi, Sourabh, Vadiraj, Vibhu and Yeshwant. My sincere thanks to Mr. Rajesh Bhatt and Mr. Amar Singh for all support and help levied by them. I also thank Prof. Saha, Dr. Charde, Mr. Pandey, Dr. Taliyan, Dr. Gaikwad for their support and guidance all the way long. I would also like to thank Dr. S. K. Dubey, Dr. Anil Jindal, Dr. Deepak Chitkara and Dr. Anupama Mittal.

I sincerely express gratitude to my beloved parents, parents-in-law who blessed me with patience and vigour to complete this work; they were always with me whenever and wherever I needed them. They have always been a source of inspiration to me. Thank you with all my heart!

Whole heartedly I thank my husband, Dr. Munendra Jain for all his support and care he has showered all this long. The work could never be accomplished without his help. Finally, the liitle one, my daughter Adwita Jain. I offer my sincere thanks and apologies for all the time she had to spent without my care. But she has always been a great support through her smile and made me a stronger person. I am deeply sorry for the time we spent apart.

I am also thankful to all those who have been of immense help to me, either directly or indirectly and whose names I have unknowingly missed out.

"The trouble with research is that it tells you what people were thinking about yesterday, not tomorrow. It's like driving a car using a rear view mirror – Bernard Loomis".

Priti Jain

LIST OF TABLES

Table No.	Caption	Page
Table 1	Current treatments for Alzheimer's Disease	14
Table 2	Status of interventions based on mechanism based approach	15
Table 4.1	*In silico* docking results of Acridin-9-yl hydrazide derivatives	34
Table 4.2	Physicochemical properties of Acridin-9-yl hydrazide derivatives	36
Table 4.3	*In silico* docking results of *N*-Phenyl-2-[(phenylsulfonyl)amino]acetamide derivatives	40
Table 4.4	Physicochemical properties of *N*-Phenyl-2-[(phenylsulfonyl)amino]acetamide derivatives	43
Table 4.5	*In silico* docking results of 2-amino pyrimidine derivatives	47
Table 4.6	*In silico* docking results of 2-thio pyrimidine derivatives	49
Table 4.7	*In silico* docking results of 2-hydroxy pyrimidine derivatives	50
Table 4.8	Physicochemical properties of substituted pyrimidine derivatives	53
Table 4.9	*In silico* docking results of substituted allylidene hydrazinecarboximidamide derivatives	57
Table 4.10	Physicochemical properties of substituted allylidene hydrazinecarboximidamide derivatives	61
Table 6.1	*In vitro* assay data for Acridin-9-yl hydrazide derivatives	91
Table 6.2	*In vitro* assay data for *N*-Phenyl-2-[(phenylsulfonyl)amino]acetamide derivatives	94
Table 6.3	*In vitro* assay data for substituted pyrimidine derivatives	98
Table 6.4	*In vitro* assay data for substituted allylidene hydrazinecarboximidamide derivatives	101

LIST OF FIGURES

Figure No.	Caption	Page
Figure 1.1	Generation of neurofibrillary tangles from Tau protein	5
Figure 1.2	Downstream events of amyloid cascade hypothesis and Aβ-targeted therapeutic strategies	7
Figure 1.3	APP processing by α-, β- and γ-secretases	8
Figure 2.1	Chemical structure of BACE-1 inhibitor OM99-2	18
Figure 2.2	Structure of 8,8-diphenyl-2,3,4,8-tetrahydroimidazo[1,5-*a*]pyrimidin-6-amine showing various interactions	19
Figure 2.3	Representative BACE-1 inhibitors based on substrate and structure based design	22
Figure 2.4	Representative BACE-1 inhibitors based on fragment based approach	25
Figure 4.1	Docking validation of 2OHP	32
Figure 4.2	Docked pose of Acridin-9-yl hydrazide derivative AA-11 in BACE-1 active site	33
Figure 4.3	Docking poses of few Acridin-9-yl hydrazide derivatives	35
Figure 4.4	Design of *N*-Phenyl-2-[(phenylsulfonyl)amino]acetamide derivatives	37
Figure 4.5	Predicted binding mode of compound 2.1 in active site of BACE-1	38
Figure 4.6	Docking poses of few *N*-Phenyl-2-[(phenylsulfonyl)amino]acetamide derivatives	42
Figure 4.7	Rationale for designing 2-amino pyrimidines	45
Figure 4.8	Binding mode of compound 2.1G to 2OHP	46
Figure 4.9	Docking poses of representative substituted pyrimidine derivatives	52
Figure 4.10	Docking pose and 2D interaction plot of compound C1A	56
Figure 4.11	Docking poses of representative substituted allylidene hydrazinecarboximidamide derivatives	60

LIST OF ABBREVIATIONS

°C	degree centigrade
µl	micro liters
AChE	Acetylcholinestrase
AD	Alzheimer's disease
ADAM	A Disintegrin and Metalloprotease domain protein
AICD	APP Intracellular Domain
Ala	Alanine
Aph-I	Anterior Pharynx-I
ApoE	Apolipoprotein E
APP	Amyloid Precursor Protein
Arg	Arginine
Asn	Aspargine
Asp	Aspartic acid
Aβ	Amyloid-β peptide
BACE-1	Beta site APP Cleaving Enzyme- 1
CNS	Central Nervous System
CSF	Cerebrospinal Fluid
Cys	Cysteine
Da	Dalton
DAPT	*N*-[*N*-(3,5-difluorophenacetyl)-L-alanyl]-S-phenylglycine t-butyl ester
DCM	Dichloromethane
DRAP	Down's Region Aspartic Protease
EDC-HCl	*N*-(3-Dimethylaminopropyl)-*N'*-ethylcarbodiimide hydrochloride
EtOH	Ethanol
Ex/Em	Excitation/Emission
FAD	Familial Alzheimer's disease
FBDD	Fragment-based Drug Discovery
FRET	Fluorescence Resonance Energy Transfer
g	Gram
Glu	Glutamine
Gly	Glycine
GSI	γ-secretase Inhibitors

GSK	Glaxosmithkline
HBA	Hydrogen Bond Acceptor
HBD	Hydrogen Bond Donor
HE	Hydroxyethylene
HOBt	Hydroxybenzotriazole
hr	hour
HTS	High-Throughput Screening
i.v.	Intravenous
IC_{50}	Inhibitory Concentration 50
IR	Infra Red
kcal	kilocalorie
LE	Ligand Efficiency
Leu	Leucine
LogP	Log partition coefficient
Lys	Lysine
MCI	Mild Cognitive Impairment
Met	Methionine
mg	Milligram
ml	Milli Litres
mM	Milli Moles
MM2	Molecular Mechanics 2
mol	Mole
MP	Melting Point
MR	Molar Refractivity
MW	Molecular Weight
Na_2CO_3	Sodium Carbonate
$NaHCO_3$	Sodium Bicarbonate
$NaNO_2$	Sodium Nitrite
NaOH	Sodium Hydroxide
Nct	Nicastrin
NFTs	Neurofibrillary Tangles
NMDA	*N*-methyl-D-aspartate
NMR	Nuclear Magnetic Resonance
NSAID	Non-Steroidal Anti-Inflammatory Drugs

OPLS	Optimized Potentials for Liquid Simulations
PDAPP	PDGF Promoter Expressing Amyloid Precursor Protein
PDB	Protein Data Bank
Pen-2	Presenilin Enhancer-2
Phe	Phenylalanine
PKC	Protein Kinase C
ppm	Part Per Million
PS	Presenilin
PSA	Polar Surface Area
RMSD	Root Mean Square Deviation
SAR	Structure Activity Relationship
$SnCl_2$	Stannous chloride
Sol	Solubility
TACE	Tumour Necrosis Factor-Alpha Converting Enzyme
TEA	Triethylamine
Tg	Transgenic
TGN	Trans-Golgi network
THF	Tetrahydrofuran
Thr	Threonine
TLC	Thin Layer Chromatography
TM	Transmembrane
TMS	Trimethylsilane
Tyr	Tyrosine
Val	Valine
WHO	World Health Organization
XP	Extra Precision

TABLE OF CONTENTS

Chapter 1 Introduction

1.1 Alzheimer's Disease 1

1.2 AD symptoms and progression 2

1.3 Pathological Features of AD 3

1.4 Therapeutic approaches for the treatment of AD 6

Chapter 2 β-site APP cleaving enzyme (BACE-1)

2.1 Biology, functions and structural features 17

2.2 Rationale for BACE-1 as target 20

2.3 BACE-1 Inhibition 20

Chapter 3 Aims and objectives 27

Chapter 4 Design of BACE-1 inhibitors

4.1 Methodology 28

4.2 Selection and validation of 3D crystal structure of BACE-1 31

4.3 Acridin-9-yl hydrazide derivatives as BACE-1 inhibitors 32

4.4 *N*-Phenyl-2-[(phenylsulfonyl)amino]acetamide derivatives as BACE-1 inhibitors 37

4.5 Substituted pyrimidine derivatives as BACE-1 inhibitors 44

4.6 Substituted allylidene hydrazinecarboximidamide derivatives as BACE-1 inhibitors 55

Chapter 5 Synthesis and characterization

5.1 Synthesis of Acridin-9-yl hydrazide derivatives 63

5.2 Synthesis of *N*-Phenyl-2-[(phenylsulfonyl)amino]acetamide derivatives 67

5.3 Synthesis of substituted pyrimidine derivatives 73

5.4 Synthesis of substituted allylidene hydrazinecarboximidamide derivatives 81

Chapter 6 *In vitro* screening and *in silico* - *in vitro* correlation

6.1 *In vitro* BACE-1 inhibition assay 89

6.2 Results and discussion 90

Chapter 7 Summary and Conclusion 103

Future Perspectives 106

Chapter 8 References 107

Appendix

List of publications 118

Biography of Priti Jain 121

Biography of Prof. Hemant R Jadhav 121

CHAPTER 1

INTRODUCTION

1.1 Alzheimer's Disease

Memory is known to influence the everyday life of an individual. Almost every activity of our daily life ranging from thinking, decision making, personal relationships, self care etc. involves the use of memory functions. Memory deficits and lapses becomes a major problem for elderly, putting them in embarrassing situations at times. It becomes frustrating and devastating for an individual when he/she is not able to recall his/her own past as well as daily activities are disturbed. This happens in Alzheimer's disease, a type of dementia.

Alzheimer's disease (AD) is a remarkably, and to date inexplicably, most common neurodegenerative disorder. It usually affects the population of 65 years and older. The population suffering from AD is projected to expand with increase in life expectancy [1]. As per National Institute on Aging, USA, 5.3 million Americans have been reported to suffer from AD in 2015 with 5.1 million being from the age group of 65 and older. It bears an annual cost of approximately $226 billion– a cost that does not address the impact of the disease on families, individuals, and society. It is therefore ranked as costliest chronic disease to the society [2, 3]. Every 70 seconds, someone in America develops Alzheimer's which will reduce to 33 seconds by mid-century [www.alz.org]. The racial discriminations are known to cause significant effect. African-Americans (twice) and Hispanics (1.5 times) are at higher risk for developing Alzheimer's than whites for whom the impact of health conditions like high blood pressure and diabetes are considered responsible [4-6]. It is estimated that one in every six women above age of 65 [7] will suffer from AD. AD stands out among the neurodegenerative diseases as one of the major leading cause of death in the developed countries and the most common cause of acquired dementia in the elderly population. Thus, AD is unfolding as one of the most important global health concerns.

Parallel to the increase in afflicted population, the speed of drug research has accelerated noticeably in the last decade. However, the numbers of therapeutic options on the market remain severely narrow. Currently available drugs for AD are unable to alter or prevent disease progression. They are, instead approved for the symptomatic treatment only. Several years after the discovery of AD, the scientific consensus is that although the pathogenesis of AD is not yet fully understood, it is a multi-factorial disease caused by genetic, environmental, and endogenous factors, as with other neurodegenerative disorders. These factors include excessive protein misfolding and aggregation, often related to oxidative stress and free radical formation; impaired bioenergetics, mitochondrial abnormalities, and neuroinflammatory processes [8]. Knowledge of these factors, together

with ongoing discoveries about AD pathogenesis, have provided the rationale for research on possible treatments directly targeting AD molecular causes. However, there are following challenges:

1. Multiple therapeutic targets: Alzheimer's disease is a complex disorder and there exist several hypotheses. A number of genetic risk factors and environmental risk factors have been implicated. Comorbidities such as high cholesterol, homocysteine, diabetes, and hypertension may also play a role. Potential targets include the β-amyloid and tau pathology, inflammation, and oxidative stress. These targets are currently the subject of research, as well as drug-discovery and drug-development efforts [8-9].

2. Lack of adequate animal models: The available animal models of AD do not provide the full spectrum of neuropathological and clinical aspects of the disease. So far, transgenic mouse models of β-amyloid production and deposition have been developed. Models of tau pathology are also under development. However, access to the available models for drug screening is the bottleneck. Being transgenic, the models are also very costly to adopt [8-9].

3. Lack of funding and interest: These programs also suffer from the lack of investment. Developing new drugs for AD is considered high risk by business managers. For small companies, attracting capital, especially for early-stage, high-risk projects, is difficult [9].

1.2 AD symptoms and progression

AD is a neurodegenerative disorder which leads to decline in cognitive abilities, deterioration of behavioral functions, communication problems, personality changes, erratic behaviour, dependence and loss of control over bodily functions. Early symptoms include confusion, disturbances in short-term memory, problems with attention and spatial orientation, changes in personality, language difficulties and unexplained mood swings. Although these symptoms will likely vary in severity and chronology, overlap and fluctuate, the overall progress of the disease has fairly been identified. The disease begins with the effect on short-term memory, progresses with neuronal degeneration and neuronal death in cortical regions of the brain which changes the personality and behavior of an individual dramatically [10].

The progression of symptoms varies from patient to patient but can be roughly divided into three stages: mild, moderate and severe [9]. The progression of symptoms can be ascribed to the sequential and progressive loss of neuronal functions and synaptic connections, and neuronal cell death in different regions of the brain.

a. In the mild stage, AD manifests with loss of memory as neurons in the region for memory formation, the hippocampus, are affected. Patients may forget words and names with

increasing frequency and get lost even in familiar places. Some believe that these incipient cases of AD are equivalent to a clinical condition known as mild cognitive impairment (MCI). Not all MCI patients will convert to AD. A 36 month study shows that the conversion rate from amnestic MCI to AD is about 16% per year [10, 11].

b. In the moderate stage, cortical regions responsible for reasoning become affected and AD patients may begin to lose their logical thinking and experience confusion. They may need help putting on proper clothing appropriate for the season. They may have difficulty recognizing and identifying family members. Changes in personality may also occur, for example, making accusations of theft and fidelity, cursing, and inappropriate kicking and screaming [11, 12].

c. In the severe stage, additional brain regions are damaged resulting in loss of control over many normal physiological functions and responses to the external environment. AD patients are unable to take care of their daily chores and lose their ability to speak coherently. They may need help with feeding, toilet use and walking [11, 12].

Once diagnosed, the median survival time is 4 to 6 years [10], although some individuals can live up to 20 years. Death results from deterioration of the brain's control of vital physiological functions resulting in complications including pneumonia, urinary tract infections or a physical fall.

1.3 Pathological Features of AD

What distinguishes AD from other neurodegenerative diseases is the presence of its pathologies in the brains of these patients: amyloid plaques and neurofibrillary tangles (NFT's). Since Alois Alzheimer's seminal report of November 1906, several scientists have considered the defining and key pathological hallmarks of the disease to be diffuse and neuritic extracellular amyloid plaques often surrounded by dystrophic neurites and intracellular neurofibrillary tangles. The disease is further characterized by neuroinflammation, and neuronal dysfunction, ultimately leading to neuronal death [5]. Another hallmark commonly observed in AD patients is focal demyelination in the plaque core areas. Plaques and tangles therefore are considered as signature notions of AD. These pathological changes are frequently accompanied by reactive microgliosis and loss of neurons, white matter and synapses [13]. The etiological mechanisms underlying these neuropathological changes remain unclear, but are probably caused by both environmental and genetic factors. The various pathologies that have been considered to be involved in AD are discussed below.

1.3.1 Cholinergic deficit

According to cholinergic hypothesis of Alzheimer's dementia, the destruction of cholinergic neurons in the basal forebrain and the resulting deficit in the central cholinergic transmission contributes substantially to the characteristic cognitive (memory loss, problem with language, disorientation, poor or reduced judgement, problem with learning) and non-cognitive symptoms (changes in mood or behaviour, changes in personality, loss of initiative) observed in the patients [14].

1.3.2 Glutamate mediated neurotoxicity

Glutamate excitotoxicity mediated through excessive excitation of NMDA receptors is believed to play a role in neuronal death observed in AD. Excessive activation of NMDA receptor is believed to cause increase in intracellular Ca^{+2} on myelin sheath and oligodendrocytes, which impairs synaptic functions, especially long term synaptic plasticity that ultimately leads to neurodegeneration [15].

1.3.3 Amyloid Pathologies/ Amyloid cascade hypothesis

The dominating hypothesis to explain the mechanisms leading to AD is the amyloid cascade hypothesis. It states that Aβ, a fragment produced by proteolytic cleavage of large trans-membrane protein APP, by β- and γ-secretases, is an oligonuleotide of 39-42 amino acid chain and is deposited in parenchyma of the amygdala, hippocampus, and neocortex. The most common isoforms are Aβ-40 and Aβ-42; the shorter form, Aβ-40 is typically produced by cleavage that occurs in the endoplasmic reticulum while the longer form is produced by cleavage in the trans-golgi network [16]. The Aβ-40 form is the more common of the two, but Aβ-42 is the more fibrillogenic and is thus associated with disease state. It is believed that accumulation of Aβ-42 in the brain initiates a cascade of events that ultimately lead to neuronal dysfunction, neurodegeneration and dementia [17, 18].

1.3.4 Tau Pathologies

Tau are microtubule associated proteins found in the axons of healthy neurons that form the cytoskeleton of neuron. They interact with tubulin and promote tubulin assembly into microtubules and further stabilize microtubules. Hyperphosphorylation of the tau protein, results in the self-assembly of paired helical filaments and straight filaments into neurofibrillary tangles (NFT's) (Figure 1.1) [19].

There are at least two schools of thoughts on how tau pathologies may cause neurodegeneration: loss of essential functions and gain of toxic functions [20, 21]. In addition to loss of microtubule stabilizing activity, hyperphosphorylated tau tends to aggregate and sequester normal tau from binding microtubules. The aggregated tau

continues to form paired helical filaments and straight filaments approximately 10 and 15nm in diameter, respectively. The former constitutes about 95% and the latter about 5% of the tau filaments found in AD brains [22]. This leads to microtubules disassembly (loss of essential functions). The disintegration of microtubules then leads to disruption of axonal transport, atrophy of distal neuritis and eventually neuronal cell death. The gain of toxic functions school proposes that these abnormally aggregated tau species (not limited to NFTs) may be toxic to neurons. The exact mechanisms by which tau overexpression induces degeneration and dysfunctions of neurons remains to be elucidated. Reduction of tau pathologies and/or tau toxicities is certainly an important area [23].

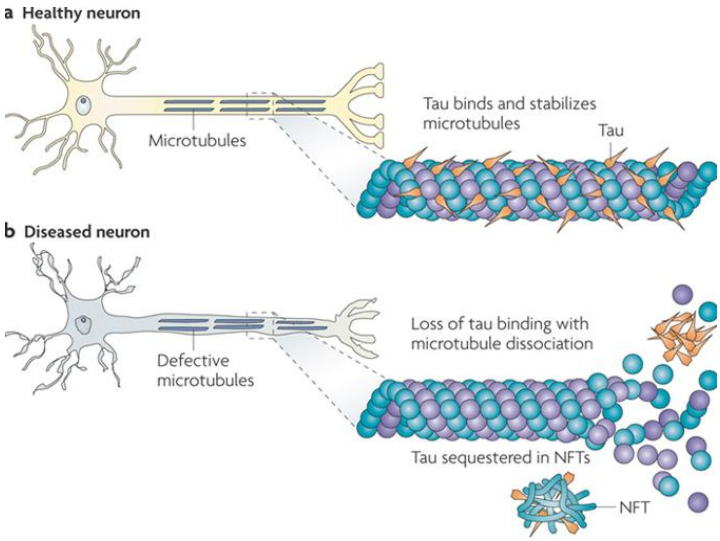

Figure 1.1: Generation of neurofibrillary tangles from Tau protein [22]

1.3.5 Microgliosis

Surrounding the amyloid plaques in AD brains are clusters of reactive microglia, a phenomenon known as microgliosis. Microglia are immune cells of the brain derived from bone marrow, equivalent to macrophages in blood. On one hand, activated microglia can release a variety of toxic substances detrimental to neurons, e.g. proinflammatory cytokines, reactive oxygen species, proteases and complements [24–28]. On the other hand, activated microglia may be one of the defense mechanisms to clean up amyloid plaque deposits. It is the bone marrow-derived microglia and not resident microglia that are critical in eliminating brain amyloid deposits [29-32]. Attraction of blood microglia cells to the brain depends on the microglial surface chemokine (C–C) motif receptor, CCR2, in response to its ligand, chemokine (C–C) motif ligand 2 (CCL2). Mice deficient in CCR2 crossed with APP transgenic mice display a dramatic reduction in the number of microglial cells in the brain, a concomitant elevation of amyloid plaques and increased mortality [33]. Interestingly,

overexpression of the ligand CCL2 in APP transgenic mice appears to lead to inactivation or desensitization of microglia and exacerbates plaque deposition [34]. Finally, recent success in using Aβ immunotherapy to reduce amyloid plaque deposition in mice has been shown to depend at least in part on the activation of microglial cells [35].

1.4 Therapeutic approaches for the treatment of AD

1.4.1 Current therapeutic approaches

Currently, treatment of Alzheimer's disease includes acetylcholinesterase (AChE) inhibitors for mild to moderate cases, and NMDA (*N*-methyl-D-aspatarte)-receptor antagonists for the treatment of moderate to severe Alzheimer dementia.

Reduced cholinergic neurotransmission is one of the cause and hence AChE inhibitors are employed [5, 9]. Four acetylcholinestrase inhibitors being used are tacrine, donepezil, rivastigmine and galantamine [36] [Table 1]. Tacrine needs to be administered four times a day, co-inhibits both acetyl and butyryl cholinestrase and has side effects like hepatotoxicity, poor bioavailability and poor tolerance by patients. While donezepil is used widely, there is no significant improvement in functional outcome; of quality of life or of behavioural symptoms. Rivastigmine leads to nausea and vomiting with corresponding loss of appetite, fatigue and weight loss. Galantamine is obtained from the bulbs and flowers of *Galanthus woronowii* (Amaryllidaceae) and related genera like *Narcissus* (daffodil), *Leucojum* (Snowflake) and *Lycoris* including *Lycoris radiata* (Red Spider Lily). It does not alter the course of the underlying dementing process and is poorly tolerated [37-39].

Excessive excitation of NMDA receptors is also believed to play a role in neuronal death observed in AD [40]. Memantine is a non-competitive NMDA-receptor antagonist that protects neurons while leaving physiological NMDA-receptor activation unaffected. It does not have disease modifying property and very high cost is also one of the factors considered while prescribing [41, 42].

Although beneficial in improving cognitive, behavioural, and functional impairments, these drugs have side effects and do not address the molecular mechanisms that underlie the pathogenic processes. Current AD drug development programs focuse primarily on mechanism based approaches particularly anti-amyloid disease-modifying agents.

1.4.2 Aβ-based therapeutic approaches: In 1990's, emphasis was given to the development of agents that could restore the neurotransmitter imbalances resulting from neuronal cell death. These gave symptomatic relief but could not stop the progression of disease. Hence, newer approaches were sought for. Amongst which amyloid cascade hypothesis got the utmost attention because of its relationship to formation of neurofibrillary tangles. The main

approach till today is to design molecules that act upon Aβ42, to increase its clearance or to stop/ slow down its generation. Genetic and pathological evidence strongly supports the amyloid cascade hypothesis of AD. Key experimental evidences that support this theory are: i) amyloid deposits provide early pathological evidence of AD and neuritic plaques are a key diagnostic criterion; ii) in peripheral amyloidosis (unrelated to Aβ and AD), amyloid burden drives tissue dysfunction, thereby suggesting that brain amyloid is pathogenic as well; iii) Aβ oligomers show acute synaptic toxicity effects, whereas plaque-derived Aβ fibrils have pro-inflammatory effects and cause neuronal toxicity [18]; iv) the most important genetic risk factor, ApoE4, is associated with increased amyloid burden; v) most importantly, all mutations that cause familial early-onset AD increase Aβ42 production or the ratio of Aβ42 compared to the less aggregation-prone Aβ40 isoform [43].

Based on these evidences, several Aβ-targeted therapeutic strategies are being pursued, as given below:

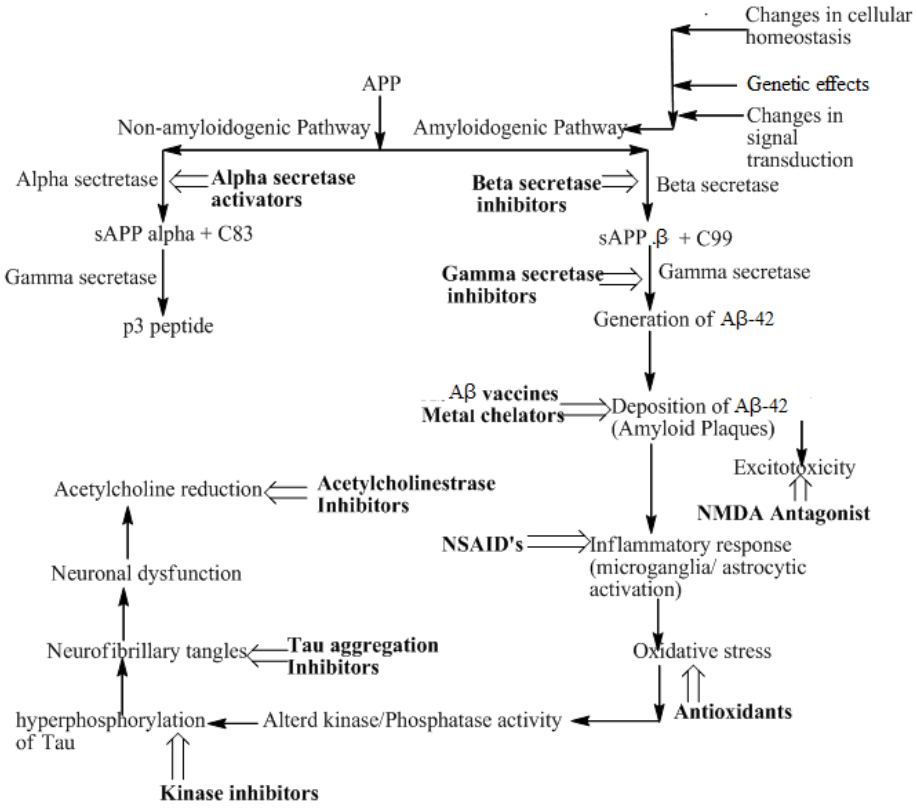

Figure 1.2: Downstream events of amyloid cascade hypothesis and Aβ-targeted therapeutic strategies [8]

1.4.2.1. Interfering with the APP proteolytic processing

i. The secretases

The production of Aβ-42 occurs by the sequential cleavage of APP by α, β and γ secretases as shown in Figure 1.3. The maximum amount of APP is cleaved by α-secretases regulated by protein kinase C (PKC) through phosphorylation [44]. The activity of α-secretases is associated with three members of ADAM (A disintegrin and metalloprotease domain protein) family: ADAM 9, 10 and 17. A minor fraction of APP is cleaved by β-secretase at distal side of the membrane to produce soluble APPß and a longer C-terminal fragment, C99, which is further cleaved by γ-secretase within the transmembrane domain to generate Aβ fraction 39-42 along with AICD (APP Intracellular Domain). Aβ-40, which is normal product, is generated majorly and another minor peptide generated is Aβ-42, which is amyloidogenic in nature [45,46]. Being highly hydrophobic, Aβ-42 aggregates to form oligomers and gets deposited in the brain, aggregates further and starts forming fibers, which eventually precipitate and accumulate in the disease defining amyloid plaques. As the ratio of Aβ-40/ Aβ-42 decreases, the risk of AD increases [45]. Since β- and γ-secretases are involved in amyloidogenic pathway, synthesis of their inhibitors has been an attractive strategy to combat AD.

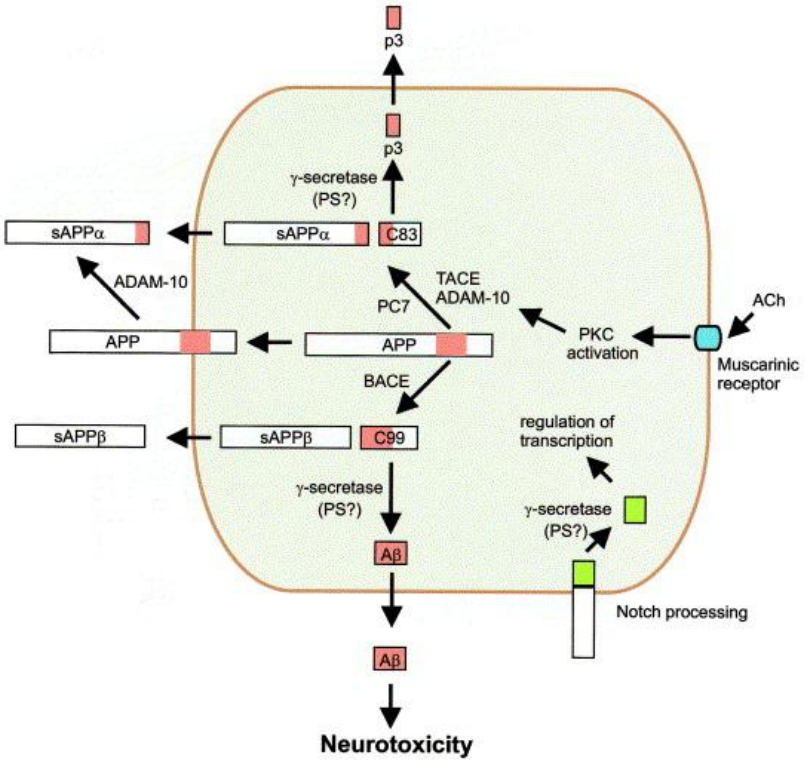

Figure 1.3: APP processing by α-, β- and γ-secretases [46]

i a. β-secretase: β-secretase also known as BACE-I (beta-site APP cleaving enzyme-I) or Memapsin-2 is an aspartyl protease family transmembrane protein of 501 amino acids. It is predominantly located intracellularly in the stacks of the Golgi complex and in endosomes, also detectable somewhat in plasma membrane. It requires low pH for optimal activity, which is easily achieved in golgi and early endosomal compartments [46]. BACE-1 inhibition holds promise as transgenic mice lacking the BACE gene produce little or no Aβ, and do not display any robust negative phenotype. More details about the enzyme and its inhibitors are given in literature review.

1 b. γ-secretase: Once APP is cleaved by α-secretase or β-secreatse, γ-secretase acts on the cleaved peptide. This aspartyl protease is responsible for the final intramembrane cleavage of APP. A set of four proteins, PS-I or PS-II (Presenilin-I or Presenilin-II), Nct (Nicastrin), Aph-I (Anterior Pharynx-I), Pen-2 (Presenilin enhancer-2) are required to built the γ-secretase complex. It may lead to imprecise cleavage of C99 fragment resulting from β-secretase cleavage of APP to generate small fraction of Aβ-42. FAD (familial Alzheimer's disease) is characterized by increased Aβ-42 resulting from mutations in presenilins [47]. Presenilins are polytopic transmembrane (TM) proteins with eight domains, predominantly found in the endoplasmic reticulum and intermediate Golgi complex. PS1 is considered to be the catalytic site of the γ-secretase active complex, having two transmembrane aspartic acid moieties (Asp257, Asp385), one in TM6 and other in TM7 [48]. The finding that transition-state inhibitors limit the γ-secretase activity and are bound directly to PS1, supports this theory of PS-I being catalytic site. However, PS is not the only requirement for γ-secretase activity, it also requires Aph-I, Nct and Pen-2 [49-50]. Besides APP, it also acts upon many other substrates like Notch, Delta, and Tumour necrosis factor-alpha converting enzyme (TACE) [50]. Hence, its inhibition may cause disruption of other important functions of other substrates that may lead to unwanted side effects.

Initially, transition state analogues were designed as γ-secretase inhibitors (GSI) and most were peptidomimetics. They failed because they were orally not bioavailable and had poor blood brain penetration [51]. Then the trend changed and there were attempts to design low molecular weight agents with drug like properties. Number of novel, bioavailable GSI's have been reported to reduce Aβ-42 levels in both transgenic and non-transgenic animal models [52].

N-[N-(3,5-difluorophenacetyl)-L-alanyl]-S-phenylglycine t-butyl ester (DAPT) was the first semi-peptidic inhibitor having *in-vivo* efficacy. Unfortunately, it was reported to severely interfere with Notch signaling in zebra fish embryos, indicating that putative side-effects

(embryogenesis, control of gliogenesis and neural stem cell differentiation) can be expected during long-term treatment in humans [53].

Further, small, potent inhibitors that selectively act upon APP binding site rather than substrate binding site were designed. Petit *et al* reported isocoumarins as GSI, not interfering with notch signaling *in-vitro* and *in-vivo* [54]. Mayer *et al* reported the design and synthesis of a novel thiophene sulfonamide γ-secretase inhibitor - GSI-953 (Begacestat) (Table 2). It demonstrated nanomolar potency in cellular and cell-free assays and selectively inhibits APP. In healthy human volunteers, oral administration of a single dose of GSI-953 produces dose-dependent changes in plasma Aβ levels, confirming pharmacodynamic activity of GSI-953 in humans giving a hope for it to serve as a potential drug candidate [55-57].

Eli-lilly and company designed LY-450139 as γ-secretase inhibitor, now known as Semagacestat. In Phase II trial, it was shown to cause reduction in plasma Aβ-42 significantly but not in CSF [58]. Another Phase II trial was done to evaluate its safety, tolerability and Aβ response in AD patients. It was well tolerated upto a dose of 140 mg taken daily for 14 weeks, based upon which the first phase III trial for this drug commenced in March, 2008 [59]. The trial was known as IDENTITY (Interrupting Alzheimer's Dementia by EvaluatiNg Treatment of AmyloId PaThologY). Recently, the development was halted due to the worsened results on cognition in Phase III studies. The trials were done on approximately 2600 patients with mild to moderate AD and compared with placebo. The results revealed that cognition and activities of daily living worsened significantly in patients treated with semagacestat as compared to placebo treated patients [http://www.medscape.com/viewartical/727021; http://newsroom.lilly.com/releasedetail.cfm?releaseid=499794].

Besides GSI, γ-secretase modulators are another class of compounds that lack notch inhibition. These are believed to act upon APP and not γ-secretase. Ibuprofen is also reported to reduce plaque deposition and brain inflammation in a mouse AD model [60-62]. It is hypothesized that NSAID's might decrease the inflammatory reactions caused due to β-amyloid deposits, leading to diminished neurotoxicity and also attenuate the production of inflammatory cytokines, microganglia and its reactive products such as ApoE, implicated in amyloid deposition [61]. From amongst many, Tarenflurbil (R-flurbiprofen) (Table 2) is reported to improve the cognitive abilities on chronic administration in APP transgenic mouse model. University of Toronto presented its Phase II results and found that the drug is safe and well tolerated with fewer side effects. On the basis of these results Phase III trials

for this drug were conducted and unfortunately it demonstrated lack of efficacy due to low penetration in cerebrospinal fluids [62-64].

ii. Interfering with downstream events of amyloid cascade hypothesis:

Many other strategies based on downstream events of amyloid cascade hypothesis have also been utilized to find newer AD treatment.

ii a. Active immunization: Active immunization with full length Aβ42 or an Aβ42 immunoconjugate, or passive administration of monoclonal anti-Aβ42 antibodies is reported to be an important approach in attenuating the AD pathological symptoms. For this purpose, PDGF (Platelet Derived Growth Factor) promoter expressing amyloid precursor protein (PDAPP) transgenic mice immunized with β-amyloid peptide as an immunogen demonstrated reduction in plaque formation and deposition [65]. Many other studies have been done on animal models to prove the efficacy of the immunization and reported to reduce neuritic dystrophy and synaptic degeneration. Antibodies enter the brain, bind to Aβ42 in the plaques, and dissociate the plaque. These Aβ-antibody complexes are then degraded by microglia via FcR-mediated (Fc receptor) or FcR-independent phagocytosis. Alternatively, antibodies to Aβ bind to peripheral Aβ causing disequilibrium between plasma and brain amyloid leading to reduction in brain amyloid deposition [66].

AN-1792 was the first vaccine to enter the Phase trial. This synthetic form of Aβ 1-42 peptide is known to prevent or reverse the development of the neuropathological hallmarks of AD. It was administered with adjuvant QS-21 and reported to be well tolerated in Phase I trials but unfortunately its Phase II-A trials were halted in 2002 due to T cell mediated aseptic meningoencephalitis in about 6% population [66-67]. Hence approaches that could avoid T-cell response and eliminate putative risk factors as given below are tried [68].

ii b. Immunoconjugation: This is a type of active immunization technique wherein synthetic fragment of Aβ42 is conjugated with carrier protein providing helper T- cell epitope is administered. Elan Pharmaceuticals and Wyeth pharmaceuticals evaluated the immunoconjugate ACC-001 for its safety, tolerability, and immunogenicity, and had reported the suspension of Phase II trial in 2008 after noticing skin lesions and vasculitis in one of the patients (www.thestreet.com/story/10412498/wyeth-elan-halt-alzheimer-drugtrial.html). It was started again in October 2008 and was over in late 2013 (www.clinicaltrials.gov/ct/show/NCT00498602) but results have not yet been revealed. Phase II trial for CAD-106 (Novartis) is also underway. There have been reports for immunoconjugates like AD vaccine consisting of the N-terminus of A*β* (A*β*28) conjugated to mannan [69], dendrimeric Aβ1-15 (16 copies of Aβ1-15 on a lysine antigen tree), 2xAβ1-15 (a

tandem repeat of two lysine-linked Aβ1-15 peptides), and 2xAβ1-15 with the addition of a three amino acid RGD motif (R-2xAβ1-15) [70].

ii c. Passive immunization: As compared to active immunization, passive immunization includes the administration of monoclonal antibodies and shows many advantages both in terms of efficacy and safety. It has demonstrated beneficial effects on synaptic plasticity and neuronal function. Bapineuzumab (AAB-001) (Table 2) is a humanized monoclonal antibody developed by Elan/Wyeth with specificity for Aβ peptides, proposed to bind and clear Aβ, with the potential added benefit of a better safety and tolerability profile. In 2008, Phase II-A results were reported and is currently under Phase III trial in stratified ApoE4 groups [71-72]. Vasogenic edema was the only side effect observed (www.alzforum.org/new/detail.asp ?id=1894).

Since the scientific basis of immunotherapy is well founded [73], further developments in this field can be expected. Compared to other strategies used for AD, immunotherapy provides higher overall efficacy when employed before the aggregation of Aβ and tau, and before amyloid accumulates in cerebral blood vessels.

ii d. Beta amyloid aggregation inhibitors: Clearance or inhibition of the neurotoxic entities such as amyloid plaques and NFT's is considered to be a method of avoiding the generation of oligomers and further cascade of amyloid hypothesis. The search began with the design of short peptide inhibitors, and the first one was Aβ 16-20 by Tjernberg *et al*. It prevented the assembly of Aβ into fibrils. Later on, many researchers developed peptide inhibitors and N-methylated peptides were reported to improve half-life *in-vivo* and also generated soluble monomeric β-sheet peptides [74]. Further, small molecule inhibitors based on the amyloid dyes such as Congo red, chrysamine D, thioflavin S were tested for the activity. Fraser *et al* reported that congo red inhibited fibrillization but it could not cross BBB and was also carcinogenic if given orally. Other dyes could cross the BBB and also were effective in inhibiting fibrillization. Elan Pharmaceuticals designed agents which could clear Aβ42 and developed ELND-005 (formerly known as AZD-103), a possible disease modifying therapeutic for AD [75]. Its Phase I trial was completed by Transition Therapeutics in 2006, which displayed good pharmacokinetic, safety and tolerability results. Elan began with its Phase II trial which is still going on (clinicaltrials.gov/ct2/show/NCT00568776).

ii e. Metal chelators: Metal ions like iron and copper are known to play an important role in protein aggregation. It seems to be a link between the pathological processes of protein aggregation and oxidative damage. Bush *et al*, 2003 have revealed a close association between brain metal dishomeostasis and the onset and/or progression of AD. As the age

increases, oxidative stress also increases and ultimately leads to neurodegeneration, attributed to the interaction of metal ions with proteins causing oxidative damage [76]. Aβ-42 is a metallo-binding protein, possessing binding sites for Zn^{+2}, Cu^{+2} and Fe^{+3}. Hence, metal chelators have been considered to be a therapeutic approach for AD. Clioquinol (PBT-1), a metal chelator, entered Phase II clinical trials but could not make to Phase III studies due to toxic impurities (di-iodo form of clioquinol) [77]. Another drug, PBT-2 entered Phase II clinical studies (Prana Biotechnology Ltd.) [78] in 2008 and has recently been reported to fail in this trial. (http://www.alzforum.org/news/research-news/pbt2-takes-dive-phase-2-alzheimers-trial; accessed 15 May 2015). Besides Zn^{+2} and Cu^{+2}, Fe^{+3} has recently been considered for design of chelators that bind iron(III) more tightly than iron (II). Dimethyl derivative of hydroxypyridine-4-one (Deferiprone) has been proposed for the same effect [79].

ii f. Tau aggregation inhibitors: The strong correlation between tangles and AD, and genetic evidence suggesting role of tau aggregation, due to mutations in the tau gene, indicates that tau aggregation inhibitors could possibly be useful in the treatment. The first compound reported to inhibit tau aggregation is Rember (Methylthionium Chloride) developed by TauRx Therapeutics. The Phase II data of this drug suggested it to be effective (www.msnbc.msn.com/id/25918231/). It acts by inhibiting the assembly of soluble tau into multimeric structures thus preventing the development of toxic species. Recently, Claude *et* al have reported that Phase III trials for Rember are underway [80]. N744 is another dye like compound known to inhibit tau aggregation but at higher doses increases the tau assembly [81]. Pickhardt *et al* have reported a number of anthraquinones (Daunorubicin, adriamycin) as tau inhibitors after completing HTS of about 2,00,000 compounds [82-83].

1.4.3 Targeting Microgliosis

Microglial activation can be inhibited by non-steroidal anti-inflammatory drugs (NSAIDs). Epidemiological studies show that NSAID usage is associated with a lower risk of AD. However, clinical trials of NSAIDs in AD patients have been largely disappointing [84]. The lack of efficacy of NSAIDs can be ascribed to their potential use only for prevention but not treatment, inappropriate doses or a faulty hypothesis. In contrast to NSAIDs, Aβ immunotherapy may depend at least in part on the activation of microglia [85].

Table 1: Current treatments for Alzheimer's Disease.

Name	Application	Side effects
Donepezil	All stages of AD	Nausea, vomiting, loss of appetite and increased frequency of bowel movements, anorexia, dreams, insomnia, muscular cramps.
Rivastigmine	Mild to moderate AD	Nausea, vomiting, loss of appetite and increased frequency of bowel movements, anorexia, dreams, insomnia, muscular cramps.
Galantamine	Mild to moderate AD	Nausea, vomiting, loss of appetite and increased frequency of bowel movements, anorexia, dreams, insomnia, muscular cramps.
Tacrine	Mild to moderate AD	Hepatotoxicity
Memantine	Advanced stages of AD	Fatigue, pain, dizziness, headache, pain in joints etc.

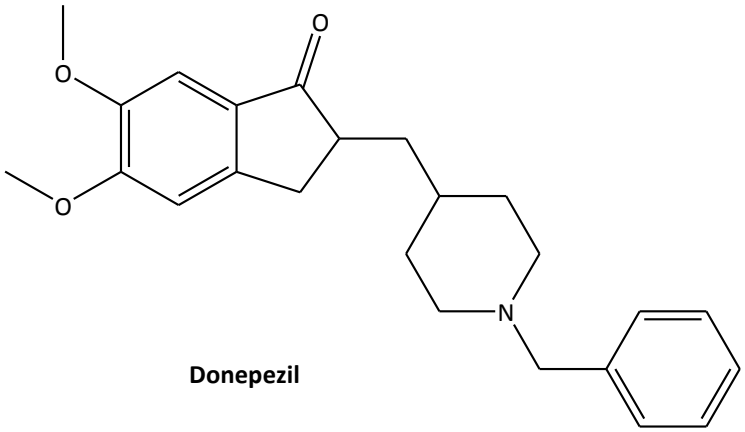

Donepezil

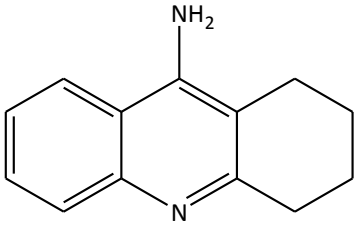

Tacrine

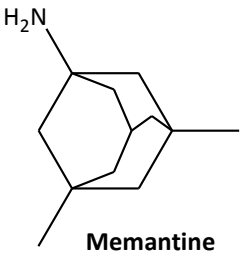

Memantine

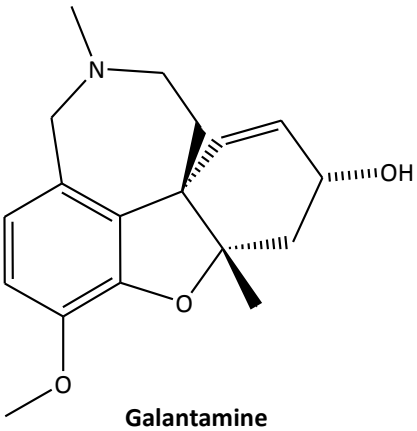

Galantamine

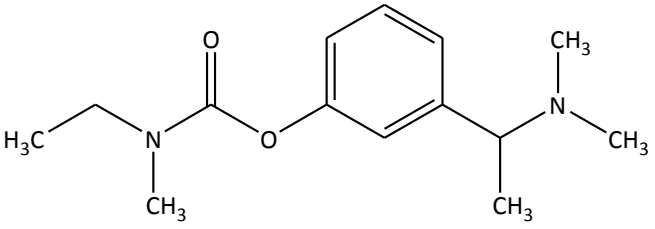

Rivastigmine

Table 2: Status of interventions based on mechanism based approach

Name	Mode of action	Present status
KMI-429	β-secretase inhibitor	Presently in preclinical trial
DAPT	γ-secretase inhibitor	Presently in preclinical trial
Begacestat (GSI-953)	γ-secretase inhibitor	Phase I trial completed
Semagacestat (LY-450139)	γ-secretase inhibitor	Phase III trial recently halted
Tarenflurbil	γ-secretase modulator	Failed in Phase III trial
AN-1792	Vaccine (Active immunization)	Phase II trials halted
ACC-001, CAD-106	Vaccine (Immunoconjugate)	Presently in Phase II trial
Bapineuzumab (AAB-001)	Humanized monoclonal antibody for passive immunization	Undergoing Phase III trial
Solanezumab (LY2062430)	Humanized monoclonal antibody for passive immunization	Undergoing Phase III trial
Scyllo-inositol (ELND005)	β-amyloid aggregation inhibitor	Undergoing Phase II trial
Clioquinol (PBT-1)	Metal chelator of Copper and Zinc	Failed in Phase III trial
PBT-2	Metal chelator	Failed in Phase II trial
Rember	Tau aggregation inhibitor	Currently in Phase III trial
Ladostigil (TV-3326)	Multi target directed ligand (MTDL) based reversible acetyl cholinesterase and butyryl cholinesterase inhibitor and irreversible MAO-B inhibitor	Currently in Phase II trial
Intravenous immunoglobulin G	Human immunoglobulin preparation containing endogenous polyclonal antibodies to Aβ	Currently in Phase III trial

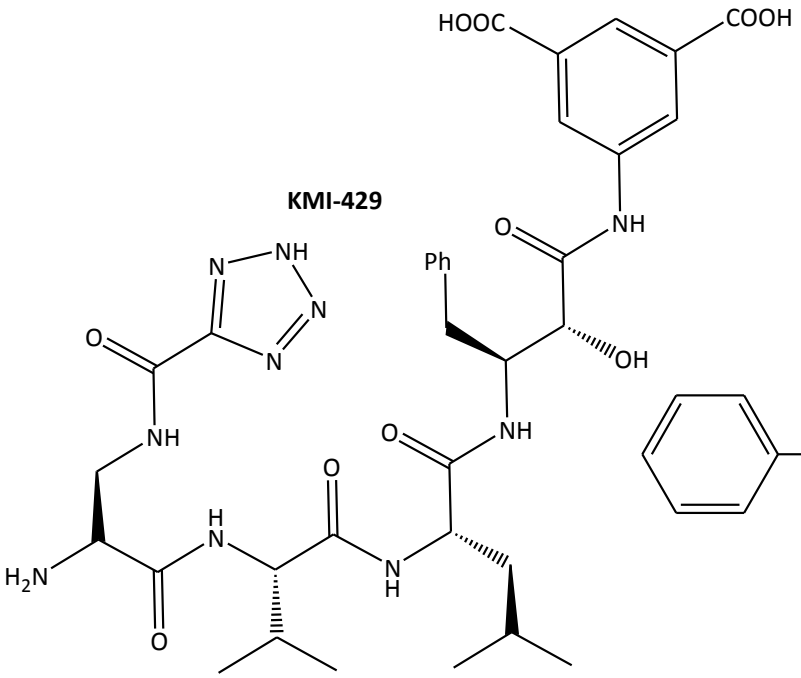

KMI-429

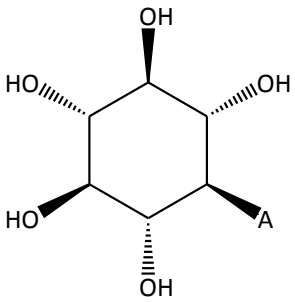

Scyllo-inositol

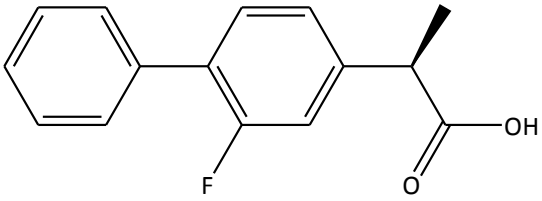

Tarenflurbil

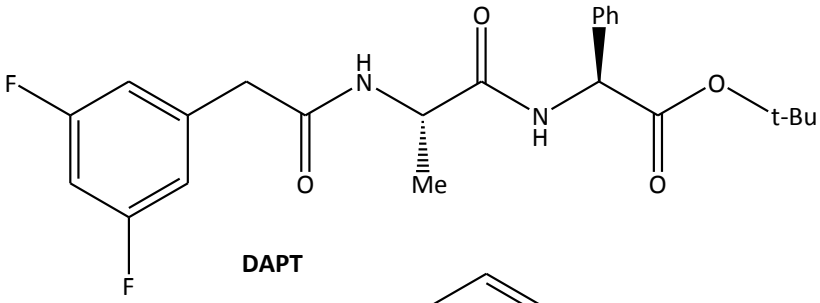

DAPT

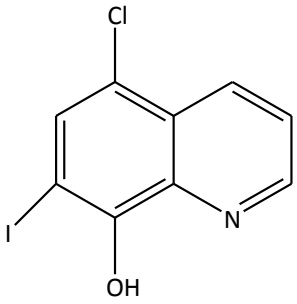

Clioquinol

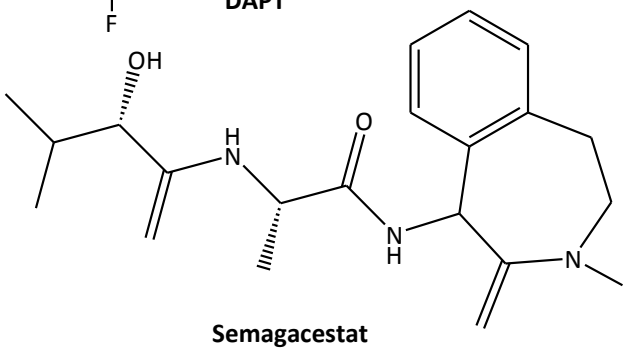

Semagacestat

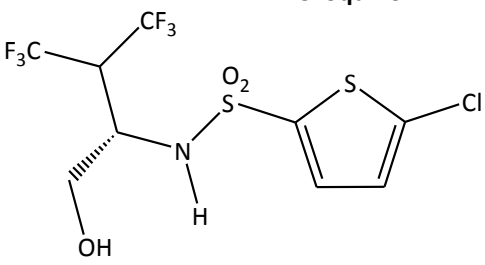

Begacestat

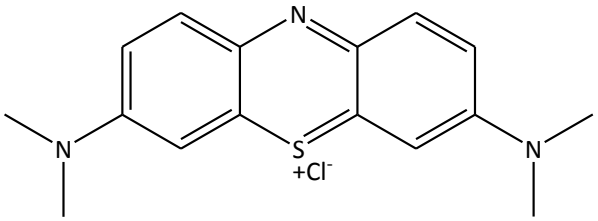

Rember

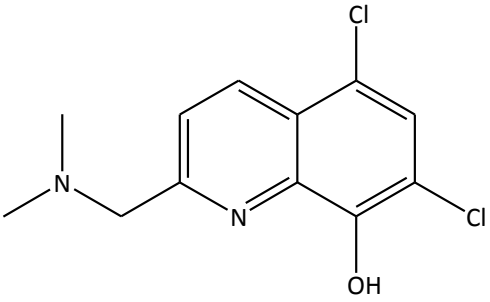

PBT-2

CHAPTER 2

β-SITE APP CLEAVING ENZYME (BACE-1)

2.1 Biology, functions and structural features

The β-secretase APP Cleaving Enzyme is universally recognized as the protease which initiates the cleavage of APP at the β site and, as such, catalyses the rate limiting step in the production of Aβ42. This aspartyl protease was initially named memapsin-2, and Asp-2, though it is now more commonly known as BACE-1 or β-secretase. After the discovery of BACE-1, a homologue was described and identified as BACE-2. BACE-1 and BACE-2 are the members of the A1 aspartic protease family, also called pepsin family. Human aspartic proteases of this family also include pepsin, cathepsin-E, cathepsin-D, renin, pepsinogen-C and napsin. The BACE proteins represent a subgroup of this family, being the first reported aspartic proteases to contain a transmembrane domain and carboxyl terminal extension [86], and also possessing unique disulphide bridge distribution. BACE-1 disulphide bridges maintain correct folding and orientation of BACE, but are not vital to its enzymatic activity [87].

Both BACE-1 and BACE-2 can process APP at the β-site, but BACE-2 has a preference to cleave the APP between amino acids 19 and 20 of the Aβ sequence, thus avoiding Aβ42 formation. BACE-1 cleaves at β and also β´ site (between amino acid 10 and 11) of APP [88-91]**.** BACE-1 mRNA has highest expression level in the mammalian brain. BACE-1 displays optimal activity at pH 4.5, which is consistent with its detection in acidic organelles like endosomes and trans-Golgi network (TGN), the main cellular sites of APP processing and Aβ production [92-95]. BACE-1 plays a crucial and central role in pathogenesis of AD because the prodomain of BACE-1 allows easy access of APP into BACE active site cleft [96]. It cleaves at the N-terminus of Aβ domain at Asp-1 (between Met596 and Asp597 of APP) and Glu-11 (between Tyr606 and Glu607) cleavage sites resulting in heterogeneous cleavage indicating that it is a site-specific protease [96]. Under normal conditions, the Glu11 cleavage site is the major β–cleavage site producing soluble secreted APP (sAPPβ) [97] and the C-terminal membrane-bound fragment (CTF)β product C89. The C89 fragment is then processed by γ-secretase in non-amyloidogenic pathway. However, if it cleaves at Asp-1, it produces sAPPβ596 and CTFβ C99 [98]. C99 fragment is further cleaved by γ-secretase in amyloidogenic pathway to generate Aβ-42.

The main feature of A1 aspartic proteases is bilobar structure, with an essential catalytic aspartic dyad located at the interface of the homologous N- and C-terminal lobes, with maximal enzyme activity occurring in acidic environment [94]. For BACE-1, the catalytic dyad is represented by two aspartic acids, Asp32 and Asp228. The unique transmembrane domain serves to expose the catalytic lobes to lumenal regions of vesicles such as endosomes or

Golgi where the low pH environment sustains their optimal protease activity, while their C-termini are exposed to the cytoplasm, enabling post-translational modification and protein-protein interaction. Although very short, the cytoplasmic domain of BACE-1 plays an important role in orienting BACE-1 cellular trafficking and compartmentalization [94-96].

To date, there are over 100 known structures of BACE-1 in complex with inhibitor and seven without inhibitor (www.pdb.org). The active site of BACE-1 has been elucidated with binding motif of the first reported eight residue transition state analogue inhibitor OM99-2 (Figure 2.1).

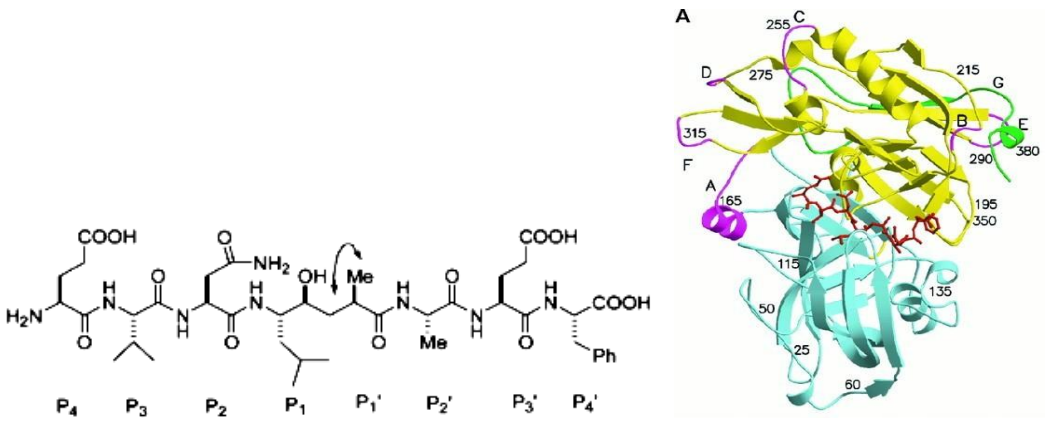

Figure 2.1: Chemical structure of BACE-1 with inhibitor OM99-2. On the left is structure of OM99-2 with constituent aminoacids and their subsite designations (the hydroxyethylene transition-state isostere is between P1 and P1'). On the right, a cartoon model of the crystal structure of BACE-1 complexed to inhibitor OM99-2 (PDB id: 1FKN). The N-lobe and C-lobe are blue and yellow, respectively, except the insertion loops, designated A to G in the C-lobe are magenta and the COOH-terminal extension is green. The inhibitor bound between the lobes is shown in red [106].

OM99-2 is a P4-P4′ peptide (Glu-Val-Asn-Leu*Ala-Ala-Glu-Phe) incorporating a non-cleavable hydroxyethylene isostere between P1 and P1′. It blocks normal proteolytic BACE-1 cleavage between the P1 and P1′ scissile bond (Figure 2.1). Further enzyme subsites were initially identified by comparing crystal structure of enzyme bound to other eight residues and the crystal structure of free BACE-1 [99-101].

Various X-ray crystal structures of β-secretase (PDB ID-2OHP, 3IGB, 1FKN etc.) reveal the groups required for β-secretase inhibitory activity. It proposes the necessity of a group that acts as H-bond donor, so that it can form H-bonding interactions with catalytic Asp-228 and Asp-32 (Figure 2.2). Further, large hydrophobic pockets (S_1, S_3, S_2') are key regions for β-secretase inhibition and demand hydrophobic groups to fill these pockets while the S4, S2, and S3′ are hydrophilic pockets. Outside the catalytic aspartic acid dyad, the S1 specificity

pocket is the most important contributor to both potency and specificity. S1 hydrophobic cleft is formed by the side chains of Tyr71, Phe108, Trp115, Ile118, and Leu30. Tyr71 and Phe108 indicate the presence of aromatic interaction to boost the potency. Like S1, S3 is also largely hydrophobic pocket formed by side chains of Leu30, Trp115, and Ile110, as well as main chain of Gln12, Gly11, Gly230, Thr231, Thr232 and Ser35. It is receptive to simple aliphatic chain as well as aromatic residues. The crystal structure of BACE-1 reveals an important feature called as 10s loop. This 10s loop is located in S3 pocket. It contains Gly11 residue and when a substrate forms hydrogen bond with this residue it allows stabilization of the 10s loop and BACE-1 and substrate interaction. Unlike the S1/S3 cleft, both S2 and S4 are more polar and solvent exposed. Besides residues Thr72, and Glu73, the key feature of the S2 pocket is the side chain of Arg235, which provides polar character. This region has a preference for negatively charged groups, which complement the positive charge of Arg235. The S4 specificity pocket, likewise, is highly polar and is solvent exposed, with Arg235 and Arg307. The S2 pocket is usually left unoccupied in order to minimize molecular weight and increase brain penetration. Among remaining minor pockets, S2′ (Ile126, Trp76, Val69, Arg128) has been extensively explored while S3′ and S4′ (Pro70, Glu125, Arg195, Trp197, and Tyr198) do not show much preference for specific interactions [102-103]. Crystal structures of BACE-1 inhibitor complexes have revealed key features regarding the possible protein-ligand interactions, and information related to the nature of binding sites has been of critical importance in the design and development of inhibitors as potential anti-AD drug candidates.

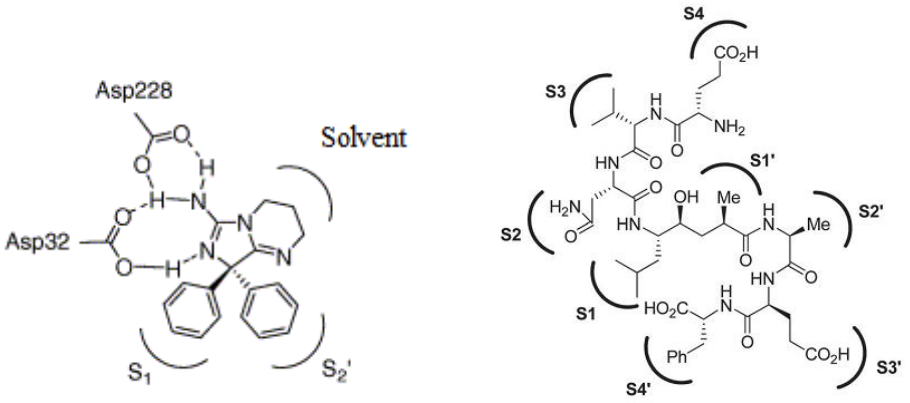

A **B**

Figure 2.2: Structure of 8,8-diphenyl-2,3,4,8-tetrahydroimidazo[1,5-*a*]pyrimidin-6-amine showing various interactions. A: shows hydrogen bonding interactions between the guanidine moiety and Asp32 and Asp228 of BACE1, and the two phenyl groups projecting into S_1 and S_2′ pockets; B: Structure of OM99-2 showing different subsites of BACE-1 [104]

2.2 Rationale for BACE-1 as target

β-secretase has been established as target for AD treatment. Following are evidences supporting it:

1. As per amyloidogenic pathway, in abnormal conditions, BACE-1 cleaves at Asp-1 producing sAPPβ596 and CTFβ C99 fragment, which is further cleaved by γ-secretase in to generate Aβ-42 [98].

2. β-secretase initiated cleavage of APP at the β site is considered the rate limiting step in the production of Aβ42 [105].

3. Transgenic mice lacking the BACE gene produce little or no Aβ [106].

4. Primary neuronal cultures derived from these transgenic mice showed complete loss of all Aβ forms [107-108].

5. Increased levels of BACE is associated with increased processing at the APP β-site and vice versa [108].

6. Several BACE-1 inhibitors, described in later section, showed improvement in condition and reduction of Aβ plaques.

Hence, these evidences support the conclusion that β - secretase catalyzes the rate limiting in Aβ production and is a valid target.

2.3 BACE-1 inhibition

In the last decade several drug discovery strategies have been exploited in the search for BACE-1 inhibitors as potential anti-AD drug candidates. The inhibitors with therapeutic potential would require, besides good potency and pharmacokinetic properties, low molecular weight (<500 daltons) and high lipophilicity in order to penetrate the blood-brain barrier [109-110]. Research aimed at the discovery of BACE-1 inhibitors has been strengthened by the large amount of available information, particularly, on the proteasic domain which is structurally well-defined, opening new opportunities for rational drug design. More than 550 BACE-I patent citations can be found on Scifinder for last 5.5 years which is indicative of the efforts that have been put till date to overcome the challenges in the design of BACE-I inhibitors.

2.3.1 Substrate-based method and structure-based design

Substrate-based methods have been used as the starting point for developing BACE-1 inhibitors. The first substrate-based BACE-1 inhibitor, P10–P4´ StatVal, was developed by Elan Pharmaceuticals. This peptidic inhibitor is a P1 (S)-statine substituted substrate analogue with an *in-vitro* half-maximal inhibitory concentration (IC_{50}) of ~ 30 nM [111-112]. Tang and Ghosh reported the crystal structure of BACE-1 in complex with the octapeptidic,

hydroxyethylene (HE) isostere-based transition-state analogue inhibitor OM99-2. Inspite of its excellent inhibitory potency *in- vitro* (Ki = 1.6 nM), the bulky peptidic structure of OM99-2 precluded its use *in-vivo* [102, 113].

KMI-008 (cellular IC_{50} = 413 nM) was developed by Kiso's group employing a hydroxymethylcarbonyl (HMC) isostere as a transition-state mimic [114]. Further chemical modifications of KMI-008 yielded more potent pentapeptidic BACE-1 inhibitors KMI-420 (*in-vitro* IC_{50} = 8.2 nM) and KMI-429 *(in-vitro* IC_{50} = 3.9 nM) [115-119]. In particular, KMI-429 significantly reduced brain Aβ secretion when directly injected into the hippocampus of both wild-type mice (> 30% decrease in soluble Aβ) and APP transgenic mice Tg2576 (> 60% decrease in soluble Aβ) [112].

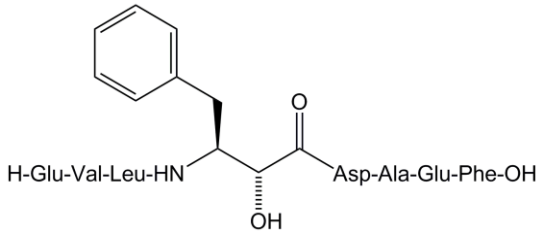

KMI-008

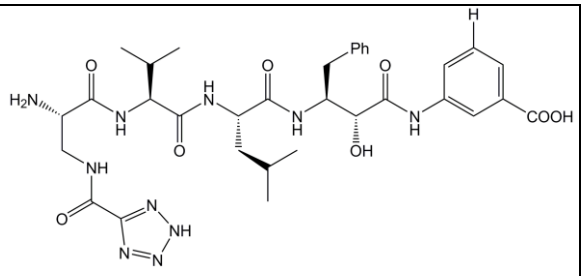

KMI-420

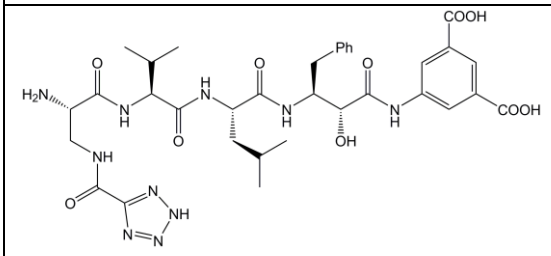

KMI-429

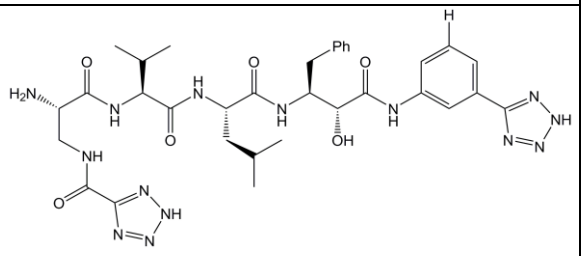

KMI-684

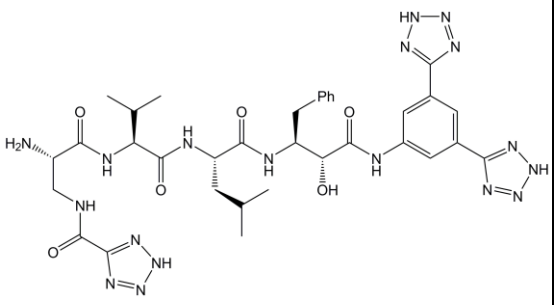

KMI-570

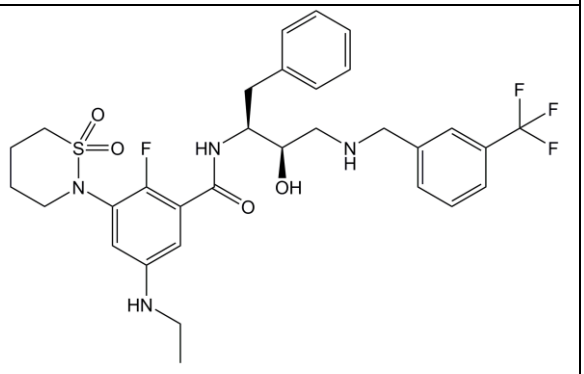

GSK-188909

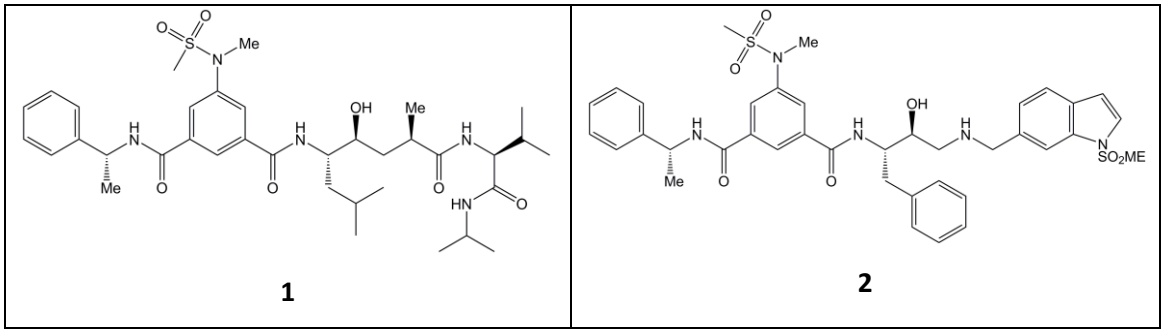

Figure 2.3: Representative BACE-1 inhibitors based on substrate and structure based design

At the same time, more substrate-based peptidomimetic inhibitors were also developed by big pharmaceutical companies and other academic research groups. Unfortunately, despite their nanomolar affinity *in-vitro*, these peptidomimetic BACE-1 inhibitors did not present a valuable pharmacokinetic profile (i.e., large size, poor brain permeability, short half-life *in-vivo*, and low oral availability) making them unsuitable drug candidates. On the other hand, based on the large amount of structural information and guided by a structure-based approach, these first-generation inhibitors have laid the foundation for the rational design of later generations of smaller, non-peptidic BACE-1 inhibitors that have significantly improved drug properties [113].

The BACE-1 inhibitors, 1 and 2, developed via chemical modifications of OM99-2, are typical examples of BACE-1 inhibitors having less-peptidic features. Both of them exhibited stronger potency (cellular IC_{50} equal to 39 nM and 1 nM, respectively) and impressive *in vivo* efficacy (reduction of plasma Aβ level by 30% and 65%, respectively) when intraperitoneally (*i.p.*) injected into Tg2576 mice [116].

In addition to this, further modifications of KMI-420 and KMI-429 produced tetrazole ring-containing compounds KMI-570 (*in-vitro* IC_{50} = 4.8 nM) and KMI-684 (*in-vitro* IC_{50} = 1.2 nM), which display improved brain permeability [118-119]. In 2007, researchers from GSK reported the first orally available BACE-1 inhibitor GSK188909, a small non-peptidic compound originated from substrate-based design. GSK188909 displayed a cellular IC_{50} of 5 nM and showed excellent selectivity over other aspartic proteases [118].

CoMentis developed CTS-21166 as BACE-1 inhibitor. This compound had shown promising results in Phase I trials. The Phase I results published in 2008 and 2012 were satisfactory enough to advance it to the Phase II clinical trial. This transition-state analog inhibitor possesses excellent properties of brain penetration, selectivity, metabolic stability, and oral availability. The data from human Phase I studies suggested that this compound was safe at dose of 225 mg, and when intravenously injected into AD patients, it caused a dose-

dependant reduction of plasma Aβ levels (www.alzforum.org/new/detail.asp?id=1790) [120].

2.3.2 Fragment-based lead generation methods

Though many BACE-1 inhibitors were successfully designed as substrate-based analogues mimicking the transition state, most of non-peptidic BACE-1 inhibitors were developed using fragment-based lead generation method. Many big pharmaceutical companies employed High Throughput Screening (HTS) to identify hit compounds from different chemical libraries. In 2001, Takeda reported the first series of non-peptidic BACE-1 inhibitor with *in-vitro* IC_{50} of 0.35–2.93 μM using this approach [120]. Subsequently, Wyeth reported WY-25105 (*in vitro* IC_{50} = 3.7 μM, cellular IC_{50} = 20 μM) containing an acylguanidine moiety that forms key interactions with the aspartic catalytic dyad [121]. Using the similar approach, Johnson & Johnson developed the BACE-1 inhibitor **3** having a stronger affinity for BACE-1 (Ki = 11nM) and exhibiting excellent brain permeability and oral availability [122].

In contrast to HTS, which uses libraries of relatively high molecular weight compounds, the fragment-based drug discovery (FBDD) approach takes advantage of libraries comprising more diverse and smaller-sized compounds (fragments) to identify hits that can be efficiently developed into potent leads with drug-like properties. After the hit identification, chemical modifications result in lead compounds and further these leads are optimized into suitable drug candidates. AstraZeneca has reported a FBDD based BACE-1 inhibitor **4** with cellular IC_{50} ≈ 0.47 μM [123]. Huang et al. reported non-peptidic BACE-1 inhibitors using fragment screenings by a computer-assisted docking simulation method [113, 124]. They have reported phenyl urea derivative having IC_{50} of 97 μM (inhibitor **5**). A series of (1,3,5-triazin-2-yl) hydrazone BACE inhibitors was discovered by the same group, inhibiting BACE enzyme with IC_{50} of 28± 4 μM (inhibitor **6**) [125]. The Astex group worked on aminoquinoline moiety and moved to aminopyridine derivatives. Irrespective of the low potency (2mM), the group worked on these motifs considering the low molecular weight and high ligand efficiency. The modifications helped increase the potency from 25 μM to 4.2 μM (inhibitor **7**) (126). Stahl *et al* have synthesized tyramine analogues having IC_{50} in the range of 2000 μM to 60 μM (inhibitor **8**) [127]. Gianpaolo *et al* reported the design and synthesis of 2-amino imidazole derivatives as low molecular weight inhibitors, and IC_{50} observed for most potent compound (inhibitor **9**) was 5.59 μM [128]. Malamas *et al* have reported substituted hydantoin derivatives while Cumming *et al* have reported piperazine derivatives as BACE-1 inhibitors [129-130]. Gerritz *et al* (2012) have demonstrated acyl guanidine as BACE-1 inhibitors and found compound **10** to have IC_{50} of 3.9 μM [131]. The series was reported to

possess good plasma exposure but poor brain permeability. Recently, Peng Lui *et al* have reported 4-Oxo-1,4-dihydro-quinoline-3-carboxamides as BACE-1 inhibitors. Amongst this series, compound **11** displayed IC_{50} of 2.20 µM but had molecular weight above 500 daltons [132].

Here, it should be emphasized that each of the previously mentioned strategy of drug discovery has its pros and cons. While substrate-based BACE-1 inhibitors usually show high potency and selectivity, their poor oral availability and permeability across the blood-brain barrier frequently makes them unsuitable drug candidates. By contrast, the HTS method has the advantage of generating hits with high diversity, smaller size, and more drug-like properties (i.e., oral availability and brain penetration). However, the hit rate of HTS tends to be extremely low and the hits generally have lower potency and selectivity than substrate-based inhibitors. Compared to the traditional HTS method, however, fragment-based screening and structure-based approach enjoy much higher hit rates, and like HTS, can identify leads with favorable drug properties. On the other hand, fragment leads are too small to exhibit satisfactory potency and selectivity, thus require considerable subsequent chemical modifications. Overall, a combinatorial approach associated with computational structure-based studies that carefully integrates the strengths of different design strategies may find its successful application in the future design of more applicable BACE-1 inhibitory drugs.

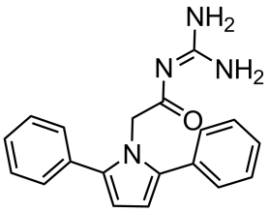

WY-25105

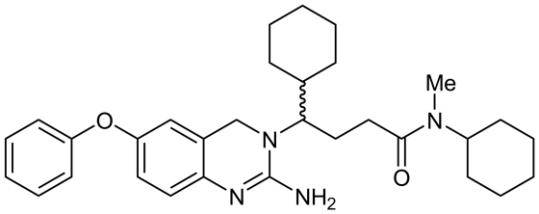

3

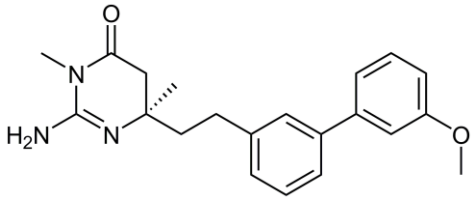

4

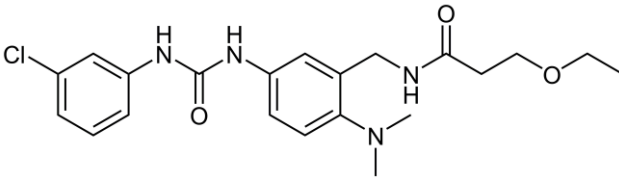

5

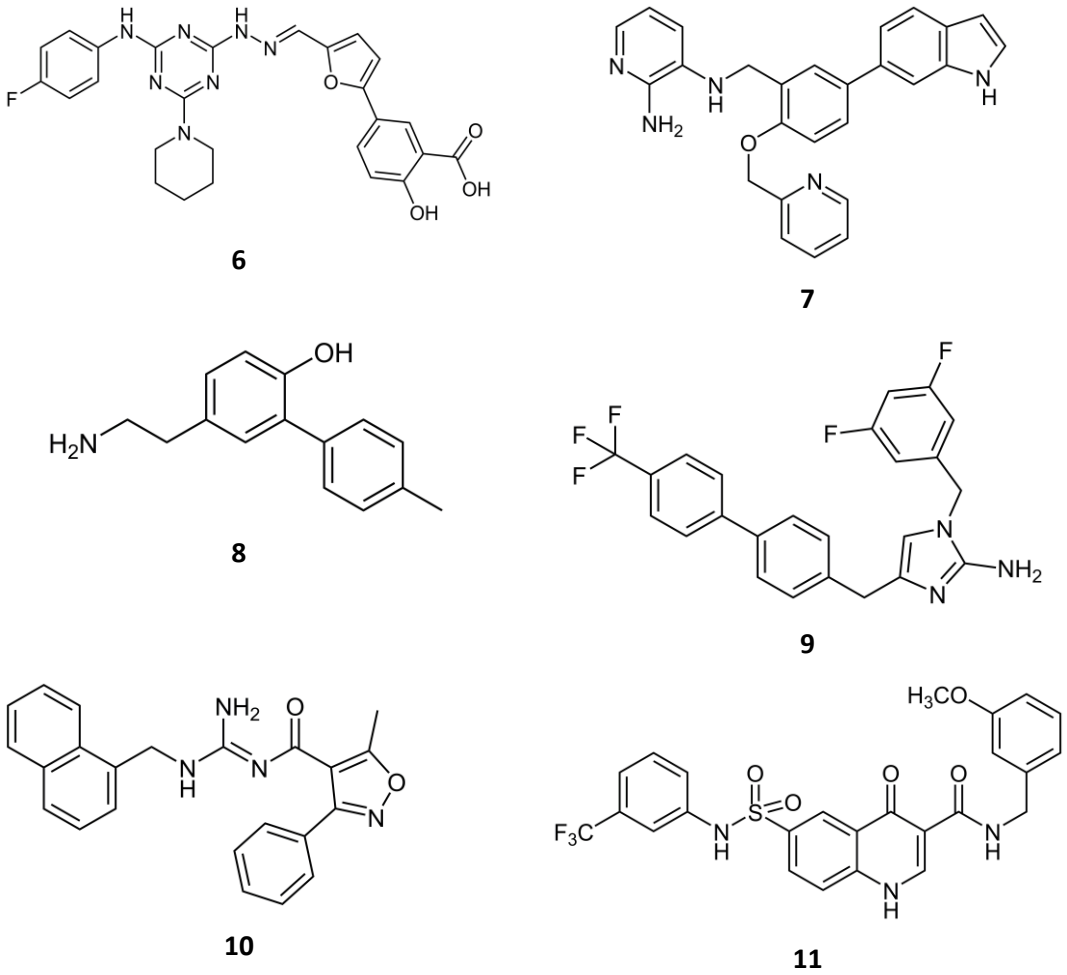

Figure 2.4: Representative BACE-1 inhibitors based on fragment based approach

2.4 Conclusion

Given the assumption that Aβ in neuritic plaques from AD brain is causally linked to disease progression, research focused on β-secretase and γ-secretase. Of the two, β-secretase has many advantages as a target. Perhaps most importantly, BACE is a single molecular entity belonging to a large and well - characterized mechanistic set of proteolytic enzymes; its structure and mechanism are well established. This opens the door to structure - based drug design, an activity that has been underway in the search for inhibitors of related enzymes like rennin. Another argument in favor of the β-secretase target is that the γ-secretase cannot function without prior cleavage at the β-site so that, in fact, a β-secretase inhibitor would also silence γ-secretase. Finally, results from the BACE knockout mice indicate that these mice show absence of Aβ in the circulation, and do not appear to show phenotypic liabilities of any kind. Knockouts of components of the γ-secretase complex are often lethal.

Further, the crystal structures of BACE-1 inhibitors complexes have revealed key features required for protein-ligand interactions, and information related to the nature of binding

sites has been of critical importance in the design and development of inhibitors as potential anti-AD drug candidates. Therefore, BACE-1 has emerged as a promising target for the treatment of AD and its inhibition represents a possible therapeutic strategy to drastically reduce Aβ42 levels.

CHAPTER 3

AIMS AND OBJECTIVES

3.1 Aims and objective

Currently marketed drugs for treatment of AD provide symptomatic relief from the neurotransmission deficits observed in these patients and they fail to halt disease progression. There is a large unmet clinical need for disease modifying therapies. The design of drugs for aspartyl proteases has always been challenging and is exemplified by various HIV protease inhibitors. Akin to the HIV protease inhibitor field, the majority of BACE inhibitors are also based on transition - state mimetic approach. Consequently, it is not totally unexpected that the development of drug - like BACE inhibitors has been plagued by ADME problems. Being located in brain, BACE inhibitors need to cross the blood–brain barrier if they are to demonstrate efficacy. This represents another major challenge for BACE inhibitor development.

Considering these facts, the present thesis work was aimed to design, synthesize and evaluate BACE-1 inhibitors to treat Alzheimer's disease. It was also decided to generate structurally diverse library of compounds to obtain leads of different structural scaffolds. Previously, many groups have worked on focused libraries around the lead compounds and have not succeeded due to several reasons that include structural complexity, poor pharmacokinetics and poor brain-barrier penetration. For these reasons, small molecular inhibitors (having low molecular weight) were the focus of this work. Further, advances in computational techniques have allowed the researchers to speculate on probable success in their efforts. The availability of several pdb crystal structures also gave enough idea about binding interactions in the BACE-1 active site. Therefore, the present work adopted *in silico* guided approach to design the small molecular, structurally diverse libraries.

To achieve the aim, following steps were envisaged:

Step 1: To design *in silico* database of small molecular, structurally diverse compounds using structure-based design approach and to predict their binding in the BACE-1 enzyme active site.

Step 2: To synthesize *in silico* designed compounds showing significant binding affinity by different synthetic approaches followed by purification and characterization.

Step 3: To screen synthesized compounds for their *in vitro* BACE-1 inhibitory potential.

Step 4: To analyze the results and derive structure activity relationship of these compounds.

Chapter 4

DESIGN OF BACE-1 INHIBITORS

4. Design of BACE-1 inhibitors

Structure-based design approaches have led to identification of lead compounds that retain the activity even after modification. In literature, several structurally complex BACE-1 inhibitors have been reported. Since the aim was to look at small molecules, prototypes from literature having moderate BACE-1 inhibition were chosen. These compounds were then modified to preserve the desired interactions and additionally occupy adjacent hydrophobic pockets of the active site. Following the reductionist approach, initially, a structure similar to prototype was docked and the poses were analyzed. Further, a library of compounds having electron donating and electron withdrawing substitutents on the selected structure was designed. Using the docking results of first library, design of further libraries to overcome the problems was envisioned.

4.1 Methodology

4.1.1 Docking protocol

A. Docking with Molegro Virtual Docker (MVD)

Crystal structure of human BACE-1 protein (2OHP) was downloaded from Brookhaven protein data bank and prepared using the preparation wizard of MVD [135]. During protein preparation, the system assigns missing bonds, bond orders, hybridization states, explicit hydrogen, charges and flexible torsion to the protein. It also repairs and modulates the improper amino acids. The ligands to be docked were drawn using Chemdraw Ultra 11 and their 3D structure was energy minimized using MM2 (molecular mechanics 2) force field in Chem 3D Pro, version 11.0 [136]. All the energy minimized ligands were further prepared and corrected for bonds, bond orders, hybridization and charges through ligand preparation wizard. For the docking purpose, grid was generated around the standard molecule. The docking wizard was then utilized to carry docking simulations with grid resolution 0.3Å, 1500 iterations for each run and moldock SE module. The system generates 5 possible energy minimized conformers for each ligand, which were visualized for interactions using ligand energy inspector and best pose was scored.

B. Docking with Glide

Protein (BACE-1, 2OHP) was prepared using protein preparation wizard of Maestro [137]. The prepared protein was used as an input file for generating the receptor grid file, which was used as input file for docking simulation. Grid of active site was created using Maestro. A centroid at 8.0, 6.0, 25.0 on x, y, z axis respectively was used to define the grid box. Grid box length was set to 6Å, 14Å and 10Å along x, y and z directions respectively. Preparation of ligands was performed using “LigPrep” module of Schrodinger Suite 2013. The use of LigPrep

is to create a single, low-energy, 3D structure with correct chirality for each successfully processed input structure. LigPrep can also produce a number of structures from each input structure with numerous ionization states, tautomers, stereochemistries, and ring conformations, and eliminate molecules using various criteria including molecular weight or specified numbers and types of functional groups present. All the compounds were drawn using Chemaxon Marvin Sketch [138] and prepared with ligand preparation wizard of Maestro. The ionization states in a given pH range of 7 ± 2 were produced by adding or removing protons from the ligand using EPIK 2.1 module [139]. OPLS 2005 Force Field was selected for energy minimization. During docking simulation, using different modules of Schrödinger suite, potential of non-polar parts of ligands was softened by scaling Vander Waals radii of ligand atoms by 0.8Å with partial charge cut-off of 0.15. During docking simulation, glide first places the centre of ligand at various grid positions of a 1Å grid and then by rotating ligand in all the Euler angles it generates various possible conformations which pass through a filter series composed of initial rough positioning followed by scoring phase. The docking simulation was performed by allowing flexible torsions in ligands with the use of XP mode. The parameter selected for docking run was default and a model energy function named Glide score (Gscore) [137] is used which combines force field and empirical terms for selecting the best docking pose, generated as output. The molecular docking simulations output file, having all the thermodynamics information in the form of Glide score, were analyzed using Glide XP visualizer, which enables visualization of ligand-receptor interactions in an interactive manner.

4.1.2 Prediction of Oral Bioavailability and BBB penetration

Predicting oral bioavailability is very important both in the early stage of drug discovery to select the promising compounds for further optimizations and at later stage to identify candidates for clinical trials. Various physicochemical properties of ligands that influence oral bioavailability like molecular weight, hydrogen bond donor (HBD) count and hydrogen bond acceptor count (HBA), polar surface area (PSA), and log partition coefficient (logP) were determined using Chemaxon Jchem for Excel [140].

HBD is defined as number of oxygen or nitrogen atoms with at least one hydrogen attached. Whereas HBA is defined as number of oxygen and nitrogen atoms present in the molecule with at least one lone pair of electrons. PSA is defined as the sum of polar atom surfaces in the molecule [141]. LogP is the calculated logarithm of partition coefficient between octanol and water. All these parameters affect solubility and partitioning between biological barriers which can have direct correlation with oral bioavailability. Based on observation of approved

drugs with these properties various rules were developed to predict oral bioavailability. One such rule is Rule of five or Lipinski rule [142], which states that for good oral bioavailability given molecule should not violate more than one of the following rules:

a. Molecular weight should be less than 500 Da.
b. LogP should be less than 5
c. Should have less than 10 hydrogen-bond acceptors (sum of oxygen and nitrogen atoms)
d. Should have less than 5 hydrogen bond donors (sum of hydroxyl and amine groups)

It is reported that BBB permeability is affected by Polar Surface Area (PSA) and compounds having PSA less than 90Å^2 will be able to cross BBB though all the compounds with PSA less than 140Å^2 will be highly absorbed through oral route (>90%) [143]. Therefore, PSA was taken as one of the parameter to predict the BBB permeation. To further supplement the understanding, BBB permeation was predicted using online BBB permeation predictor software available at http://www.cbligand.org/BBB/. As per the software, any compound having SVM_MACCSFP BBB Score of more than 0.02 will be able to cross BBB.

4.1.3 Toxicity Prediction

The prediction of toxicity of chemical structure at an early phase can provide valuable information and contribute to the reduction of animal usage in screening out the potentially toxic compounds. All compounds should hence be tested for biological safety in order to minimize the risk of elimination at the later phase of clinical development. Some of the common toxicity screening tests involve study of mutagenicity, tumorigenicity, skin irritation, reproductive toxicity, cardiotoxicity, etc. In this study, the toxicity risk assessment was carried using OSIRIS property explorer [144-145], a software of Actelion Pharmaceuticals Ltd., Switzerland, hosted on www.organic-chemistry.org website.

Drug likeliness score takes into account physicochemical properties and groups present in marketed drugs. It may be defined as a complex balance of various molecular properties and structure features which determine whether particular molecule is similar to the known drugs. These properties, mainly hydrophobicity, electronic distribution, hydrogen bonding characteristics, molecule size and flexibility and of course the presence of various pharmacophoric features influence the behavior of molecule in a living organism, including bioavailability, transport properties, affinity to proteins, reactivity, toxicity, metabolic stability and many others. Whereas Drug score considers toxicity risk and drug likeliness score. Drug likeliness should be a positive value. Compounds with higher values represent

the significant pharmacokinetic similarity with ideal drug. The Drug score is calculated directly from LogP, logS (solubility), molecular weight while drug likeness takes into account the drug score and risk factors [146]. Risk alerts are calculated based on presence of fragments with known risk factors. However, these risk alerts are nor fully reliable and absence of risk alerts does not indicate that compounds are free of toxicity.

4.2 Selection and validation of 3D crystal structure of BACE-1

Although several 3D crystallographic structures of BACE-1 have been reported in protein data bank, based on experimental details, best structure was selected for design studies. Pdb structure 2OHP was selected as it has resolution of 2.25Å and it was a monomer. The docking process using 2OHP was validated using extracted ligand (6IP-389) and further validated using external data set of 20 molecules reported as BACE-1 inhibitors by different research groups [128, 129, 130, 147, 148]. The validation of docking protocol is essential to govern the reliability and reproducibility of docking parameters used for given study.

The protein 2OHP was docked with the extracted ligand (6IP-389) considering the same as reference. The protocol was established using Molegro Virtual Docker (MVD) software. The chemical structure of ligand was drawn using Chemdraw ultra 11.0 and 3D energy minimized structures were obtained using Chem 3D Pro 11.0 applying MM2 calculations for energy minimization. Further, the protein structure was prepared in MVD and corrected for all errors and protonation states. The grid box had resolution of 0.30Å. Moldock SE algorithm was employed with 1500 iterations per run and population size of 50 generating 5 minimum energy conformers.

The docking study revealed that the docked ligand superimposed well on the reference ligand (co-crystallized ligand) with RMSD value of 0.385Å (figure 4.1) and moldock score of -76.8. The docked ligand also displayed hydrogen bonding interactions with amino acids Asp 32 and 228 (1.79Å, 2.62Å; 2.72Å, 2.96Å respectively). Further, indole ring occupied S1 cavity showing π-π stacking with Tyr71 and other interaction with amino acids of S1 cavity.

Similar validation protocol was followed using Schrodinger (Glide). It was observed that the extracted ligand superimposed well with reference ligand and showed similar binding interactions with glide score of -6.47.

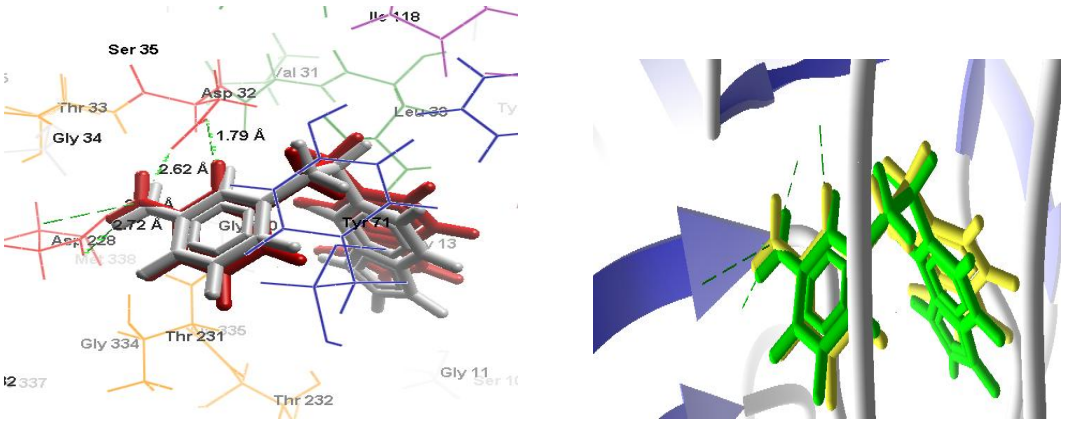

A B

Figure 4.1: Docking validation of 2OHP (A) Redocked pose of 6IP-389 (red) superimposed with the co-crystallized ligand (grey); (B) Secondary view of docked ligand and co-crystallized ligand.

For cross validation, an external data set of 20 molecules reported in literature as BACE-1 inhibitors was used. These compounds were docked over 2OHP using MVD as well as Schrodinger (Glide) to get an idea of the binding interactions. It was observed that the interactions seen match with those reported in the reports. Thus, 2OHP was considered further for design and docking studies.

4.3 Acridin-9-yl hydrazide derivatives as BACE-1 inhibitors

4.3.1 Design

BACE-1 belongs to the family of aspartyl proteases. For designing BACE-1 inhibitors, it was decided to start with known aspartyl protease inhibitors. This strategy has been used for various other targets and there has been reasonable success. Further, it was expected to show activity by similar interactions in the active site. Hydrazinyl acridine derivatives have been reported to inhibit two aspartyl proteases Plasmepsin-II and Cathepsin-D, *in-silico* as well as *in-vitro* [149]. The hydrazinyl acridine derivatives (representative compound Nar103) were reported to occupy S1 and S3 subsites of plasmepsin-II and cathepsin-D. In plasmepsin-II, only one of the aspartate was hydrogen bonded with –NH- of the ligand while in cathepsin-II none could be bonded. The activity of acridine derivatives on BACE-1 has not been reported. Taking this into account, design of acridine derivatives as BACE-1 inhibitors was attempted.

When the report was analyzed, it was observed that the two methyl substituents do not take part in interactions. Therefore, these two methyl groups were not included in design of compounds and compound having similar nucleus with nitro substituent placed on aromatic ring (Compound AA-11) was considered for initial design.

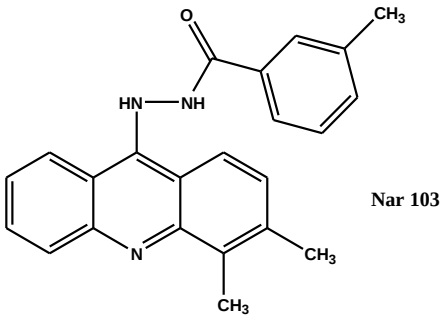

Nar 103

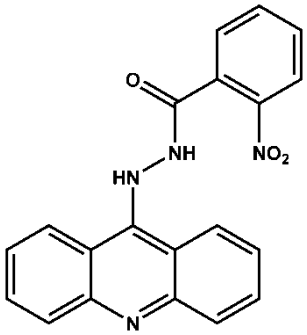

AA-11

When compound AA-11 was docked in protein 2OHP, it was observed that the enzyme-inhibitor complex was primarily stabilized by hydrogen bonds between the hydrazide part of the inhibitor and Asp32. The acridinyl moiety showed π-π stacking with Tyr71, occupied the S2′ region while the phenyl ring was buried in S1 cavity. It showed significant interactions and accommodation of substrate binding clefts and a good moldock score of -84.34 which is better than the standard ligand 6IP-389.

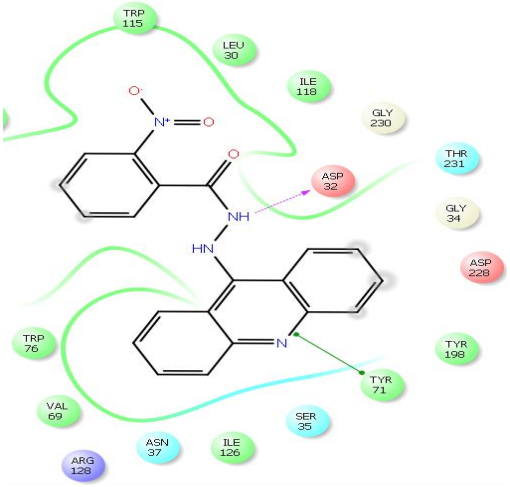

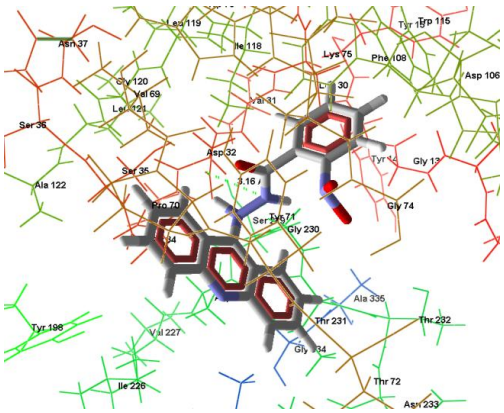

A **B**

Figure 4.2: Docked pose of Acridin-9-yl hydrazide derivative AA-11 in BACE-1 active site (A: 2D Ligplot of compound AA-11, B: Binding mode of AA-11 to 2OHP)

Encouraged by these results, 12 derivatives having electron donating as well as electron withdrawing groups were designed as given in table 4.1. AA-12 with *m*-fluoro group on the phenyl ring displayed interaction of Asp32 with acridine nitrogen through a salt bridge and also formed hydrogen bond with the main chain of Gly230. Acridine ring covered the S2′ cavity and also had π- π stacking with Trp115 while phenyl ring occupied S1 pocket. Placing an *o*-fluoro or *p*-fluoro group (AA-13, AA-14) instead of *m*-fluoro, diminished the aspartate interactions though AA-13 tends to form key interactions with 10s loop (Gly11), Gly230, and

Thr232. AA-16 substituted with *o*-bromo also revealed the desired interactions. Placing *o,p*-dichloro (AA-17) was found to enhance interactions with Asp32, Tyr71 and placed the acridine ring in S1 and S2' cavity while phenyl ring occupied S1 pocket. AA-18 has *p*-acetamido group, which formed contacts with Asp32 and π- π stacking with Tyr71 and Phe108. It showed very high docking score in Glide as well as MVD. Compound AA-19 with *m*-methoxy group showed interaction with Gly11, π-π stacking with Tyr71 by acridine ring and phenyl ring was buried in S1 cavity. However, it did not show any interaction with the aspartate dyad. AA-110 with *m*,*p*-dimethoxy phenyl group had highest moldock score and it also showed hydrogen bonding interaction with Asp32, Phe108 and π- π stacking of both the rings with Tyr71. AA-111, which has *m*-amino and *p*-methyl, gave highest docking score in Glide and had similar interactions. Isonicotinoyl substitution in place of benzoyl (AA-112) was not favoured because it reduced the overall interactions.

Table 4.1: *In silico* docking results of Acridin-9-yl hydrazide derivatives

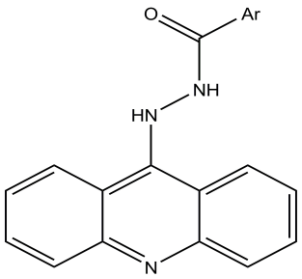

Code	-Ar	Glide Score	Moldock score
AA-11	*o*-NO_2-Ph	-4.48	-84.34
AA-12	*m*-F-Ph	-6.73	-85.30
AA-13	*o*-F-Ph	-5.85	-74.64
AA-14	*p*-F-Ph	-5.64	-78.82
AA-15	*p*-Cl-Ph	-5.92	-78.24
AA-16	*o*-Br-Ph	-6.45	-80.75
AA-17	(*o,p*-di Cl)-Ph	-6.90	-86.95
AA-18	(*p*-$NHCOCH_3$)-Ph	-7.95	-100.70
AA-19	*m*-OCH_3-Ph	-5.68	-84.56
AA-110	(*m,p*-di OCH_3)-Ph	-6.31	-104.57
AA-111	(*m*-NH_2, *p*-CH_3)-Ph	-7.96	-87.48
AA-112	-C_5H_4N (Isonicotinic acid)	-5.68	-77.84

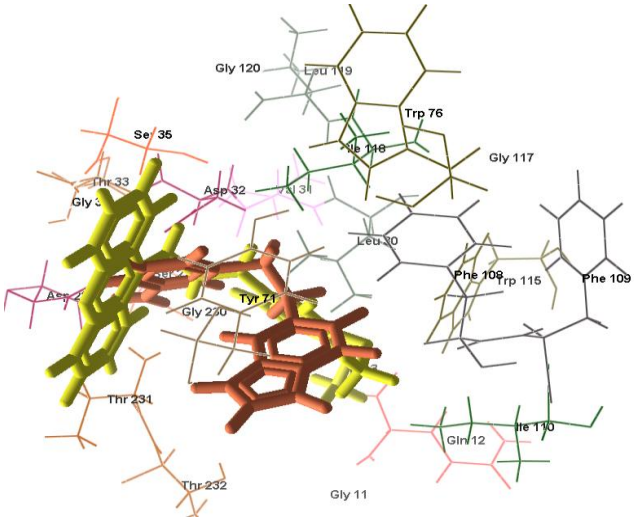

i. Superimposed docked pose of 6IP-389 (orange) and AA-110 (yellow)

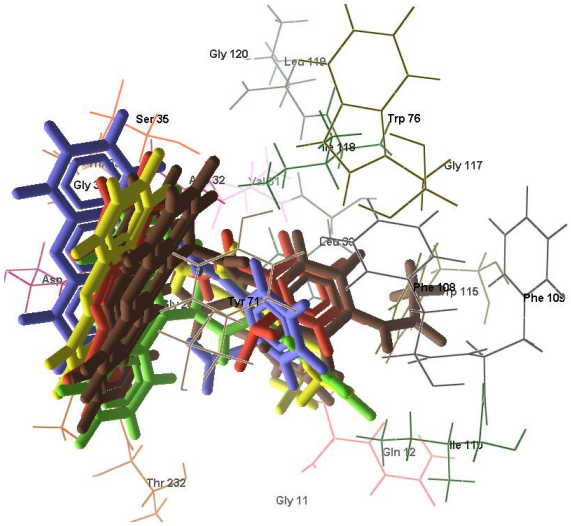

ii. Superimposed docked pose of all acridin-9-yl hydrazide derivatives

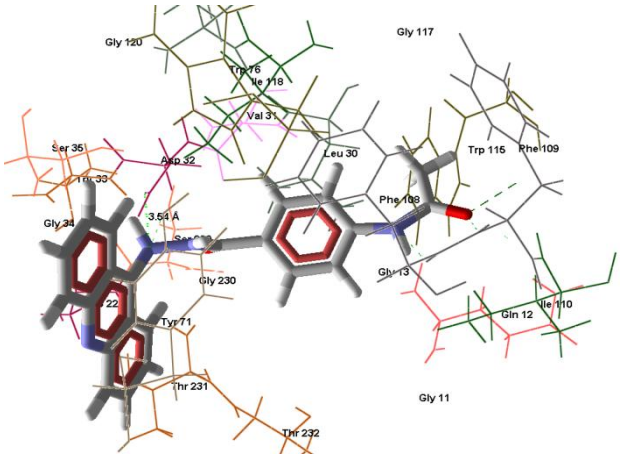

iii. Docking pose of AA-18

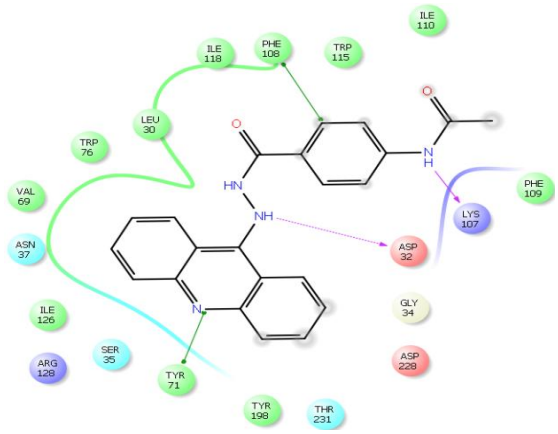

iv. 2D Ligplot of AA-18

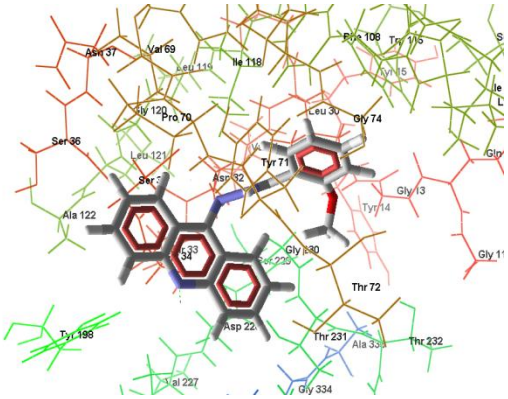

v. Docking pose of AA-19

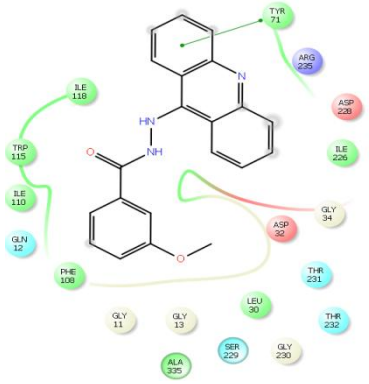

vi. 2D Ligplot of AA-19

Figure 4.3: Docking poses of few Acridin-9-yl hydrazide derivatives

4.3.2 Oral bioavailability and toxicity prediction

All the designed compounds fulfilled the criteria of Lipinski rule. The log P values were within range of 3.24 to 5.66 and hydrogen bond donor count between 2 to 3, hydrogen bond acceptor count from 3 to 5. It is reported that BBB permeability is affected by Polar Surface Area (PSA) and for penetration PSA should be below 90$Å^2$. Except AA-11, all ligands had polar surface area less than or near to 70$Å^2$ and hence BBB permeability for the series was predicted to be good. Further, using online BBB permeation prediction software, BBB permeability was predicted, wherein any compound having SVM_MACCSFP BBB Score of more than 0.02 will be able to cross BBB. It was found that all the compounds had score above 0.02 and hence were predicted to cross BBB. All these parameters indicate that these derivatives will have good oral bioavailability and will cross blood brain barrier.

Acridine derivatives are known to have cytotoxicity [23]. Therefore, all compounds in the series were predicted to have mutagenic, tumorigenic and irritant effects. Due to this, the predicted drug score was low.

Table 4.2: Physicochemical properties of Acridin-9-yl hydrazide derivatives

Code	MW	HBA	HBD	PSA	LogP	M	T	I	RE	Drug likeliness	Drug score	BBB Score
AA-11	358.10	5	2	98.41	4.39	R	R	R	G	-7.60	0.05	0.041
AA-12	331.12	3	2	55.27	4.60	R	R	R	G	-4.09	0.04	0.091
AA-13	331.11	3	2	55.27	4.60	R	R	R	G	-1.62	0.05	0.070
AA-14	331.11	3	2	55.27	4.60	R	R	R	G	-0.44	0.06	0.090
AA-15	347.08	3	2	55.27	5.06	R	R	R	G	1.71	0.07	0.080
AA-16	391.03	3	2	55.27	5.22	R	R	R	G	-3.96	0.03	0.080
AA-17	381.04	3	2	55.27	5.66	R	R	R	G	0.90	0.05	0.062
AA-18	370.14	4	3	84.37	3.69	R	R	R	G	2.28	0.08	0.097
AA-19	343.38	4	2	64.50	4.30	R	R	R	G	-1.67	0.05	0.065
AA-110	373.14	5	2	73.73	4.14	R	R	R	G	2.10	0.08	0.022
AA-111	342.14	4	3	81.29	4.14	R	R	R	G	-2.95	0.04	0.070
AA-112	314.11	4	2	68.16	3.24	R	R	R	R	0.78	0.06	0.094

M=mutagenicity, T= tumorigenic, I= Irritant, RE= reproductive effect. Alphabets in column representing M, T, I and RE imply G= no indication, Y = medium risk and R = high risk.

4.4 *N*-Phenyl-2-[(phenylsulfonyl)amino]acetamide derivatives as BACE-1 inhibitors

4.4.1 Design

From the docking simulation study of acridin-9-yl-hydrazide derivatives, it was observed that, although these compounds were able to occupy S1 and S2' active site, S3 cavity was not fully occupied. Moreover, these could interact with only one of the aspartate instead of aspartate dyad. These results were concurrent to those observed for Plasmepsin-II and Cathepsin-D. Therefore, it was decided to design compounds which could show interactions with aspartate dyad as well as extend in S3 cavity. As acridine derivatives were also predicted to have mutagenicity, modifications in acridines were not considered. Instead, literature reports for compound showing these properties were searched.

Various reports have indicated that sulfonamide derivatives have good CNS penetration [150]. Gerritz et al have reported acyl guanidine derivatives as BACE-1 inhibitors [131]. Replacement of acyl guanidine portion in reported compounds with sulfonyl-amino-acetamide motif was done to check the effect on BACE-1 inhibition. Substituted sulfonamide derivatives possessing two aromatic moieties separated by a sulfonyl-amino-acetamide linker were designed. It was expected that these ligands will have interactions with desired amino acids in S1 as well as S3 substrate binding pockets. 10s loop is located in S3 pocket and it contains Gly11 residue. When a substrate forms hydrogen bond with this residue it allows stabilization of the 10s loop and BACE-1 and substrate interaction. Further, S2' cavity is also an important region which contributes to ligands potency and selectivity [130]. Therefore, through this series, these interactions were targeted.

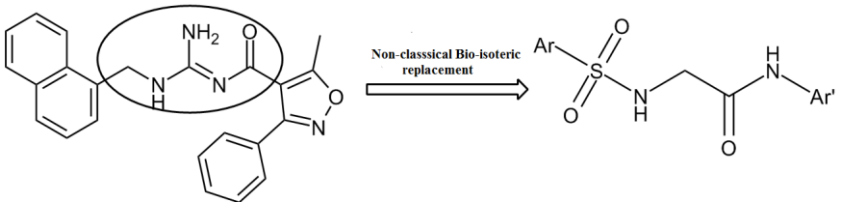

Figure 4.4: Design of *N*-Phenyl-2-[(phenylsulfonyl)amino]acetamide derivatives

Compound 2.1, in which naphthyl ring was reduced to *p*-tolyl and heterocyclic ring replaced by phenyl ring, was taken as prototype. When it was docked over BACE-1 protein (2OHP), it displayed:

i. hydrogen bonding interaction of sulfonamide nitrogen (NH) with side chain of catalytic Asp228 and amide nitrogen with Asp32;

ii. sulfonamide nitrogen (-NH-) forms hydrogen bonding interaction with Thr231 and with carbonyl oxygen of Gly230;

iii. Sulfonyl oxygen also interacts with Thr231;

iv. Amide nitrogen forms hydrogen bond with Gly230;

v. Phenyl ring with *p*-methyl substitution (ring A) is seen to occupy more of S2' cavity than S3 cavity while phenyl ring (ring B) is seen to occupy S1 pocket.

Although, the prototype compound did not occupy S3 cavity completely, these docking results served as an insight to further change the substitution pattern (as shown in Table 4.3) and achieve increased potency. It was expected that the substitution change may affect the conformation in such a way that it would cover S3 cavity and not S2' cavity. Further, it was expected that the amide moiety would be oriented towards Gly11, which is key component of 10s loop.

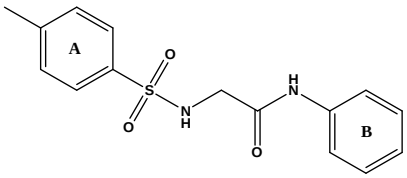

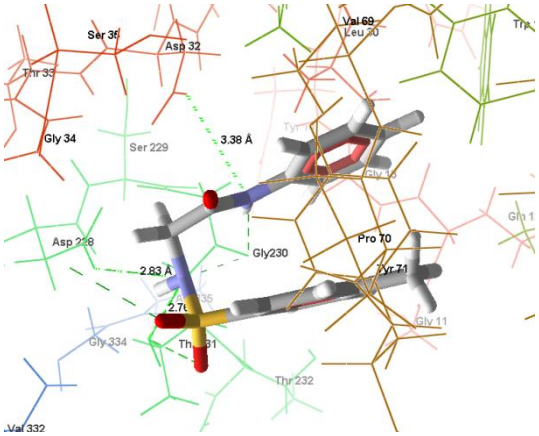

i: Compound 2.1 **ii**

Figure 4.5: Predicted binding mode of compound 2.1 in active site of BACE-1; i: Chemical structure of compound 2.1; ii: Docking pose of 2.1 showing ligand as sticks and protein as shapely residue. The dashed lines represent hydrogen bonding interactions.

Substitution pattern on ring A and B revealed the important groups needed for activity. It was observed that when ring A was not substituted by any group, it failed to show the desired interactions with BACE-1 (compounds 2.2, 2.3, 2.4, 2.5). Substitution of *p*-methyl group on ring A with different substitutions on ring B increased the interactions as compared to compound A. It was observed that among compounds 2.6, 2.7 and 2.8, which had substituents on ring B, 2.8 substituted with *o,p*-dimethyl on ring B showed the best interaction pattern. In this compound (i) nitrogen of sulfonamide formed hydrogen bonding interaction with side chain of Asp228 (3.24Å); (ii) nitrogen of amide formed hydrogen bonding interaction with side chain of Asp32; (iii) Both these nitrogen also formed hydrogen bonding interactions with Gly230 (3.10Å, 4.81Å); (iv) The carbonyl oxygen of amide formed hydrogen bonding interactions with Thr231 (S3 cavity) and also Arg235 (S2 cavity); (v) The phenyl ring bearing *o,p*-dimethyl substitution accommodated S3 cavity; (vi) ring A bearing *p*-methyl substitution was seen to accommodate S2' region with proximity of S1 substrate

binding pocket; (vii) ring A was also seen to establish π-cation interaction with Arg128 (S2' cavity). Compound 2.6 substituted with *p*-chloro on ring B showed hydrogen bonding interactions with aspartate dyad and occupied the S3 pocket well while the rest (2.1 and 2.7) were seen to interact with either of the aspartates instead of both. Substitution of *p*-chloro on ring A (compounds 2.10 to 2.13) influences the binding pattern favorably with better docking score by occupying S2' cavity. Compound 2.13 having *p*-chloro at ring A and *o,p*-dichloro at ring B revealed that its amide nitrogen can form hydrogen bonding with Asp32, ring B was buried into S1 pocket while ring A was present in S2' cavity and formed π-cation interaction with Arg128 (S2' cavity) and its –NH- was seen to form hydrogen bonding interaction with Thr231 (S3 region). Compounds 2.14 to 2.17 having *p*-acetamide group on ring A showed very good interaction pattern with BACE-1 active site. Compound 2.17 with *p*-acetamide substitution on ring A and *o*-*p*-dimethyl group on ring B revealed the ability of the compound to form key interactions with catalytic aspartate dyad. Though the interaction with 10s loop was not observed, it extended its interactions to Tyr71 (π-π interaction and hydrogen bond) and Thr231 occupying the S1 and S3 active sites through hydrophobic contacts. This implies that *p*-acetamide on ring A and *o,p*-dimethyl group on ring B is preferred for the activity.

From amongst compounds having *m*-nitro group on ring A: 2.18, 2.19, 2.20 and 2.21; compounds 2.20 and 2.21 have revealed favourable interactions. Compound 2.20 with *m*-nitro on ring A and *m*-chloro on ring B formed key hydrogen bonding interactions with aspartate dyad; ring A was seen to form π-cation linkage and salt bridge with Arg128 (S2' cavity) because of the presence of nitro group. Ring B occupied S1 cavity while ring A was accommodated in S2' and S3 pockets. Compound 2.19 with *p*-chloro on ring B was seen to interact in the same manner as 2.20 but *p*-chloro substitution orients ring A away from S3 cavity towards S2' cavity. Similarly, 2.21 with *o,p*-dimethyl on ring B showed desired interactions but failed to occupy the S3 cavity though the other two (S1 and S2') were occupied.

It was observed that placing *o*-nitro or *p*-nitro group on ring A in place of *m*-nitro reduced the docking score (compounds 2.22 to 2.29). Only 2.25 (*o*-nitro on ring A and *o,p*-dimethyl on ring B) showed good interactions with catalytic aspartate dyad but failed to occupy the S3 and S2' substrate binding pockets. The reason may be attributed to *o*-nitro group being present in proximity of sulfonamide which tends to move it towards polar group while *p*-nitro group renders the compound linear and thus improper orientation. Placing *p*-methoxy on ring A (compounds 2.30 to 2.33) also does not favour the interactions as needed. Only,

compound 2.30 (*p*-methoxy on ring A and unsubstituted ring B) and 2.33 (*p*-methoxy on ring A and *o,p*-dimethyl on ring B) showed interaction with Asp 228 and compound 2.30 also occupied both S1 and S3 cavity while 2.33 did not.

Table 4.3: *In-silico* docking results of *N*-Phenyl-2-[(phenylsulfonyl)amino]acetamide derivatives

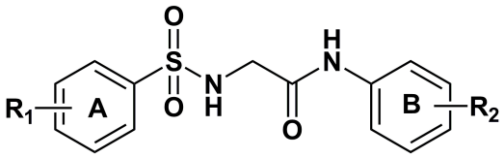

Code no.	R_1	R_2	Moldock score	Glide XP score
2.1	*p*-CH_3	H	-84.57	-6.39
2.2	H	*p*-Cl	-76.82	-4.72
2.3	H	*m*-Cl	-77.39	-5.30
2.4	H	*o,p*-di CH_3	-64.21	-4.24
2.5	H	H	-72.13	-4.28
2.6	*p*-CH_3	*p*-Cl	-84.23	-6.51
2.7	*p*-CH_3	*m*-Cl	-86.75	-5.94
2.8	*p*-CH_3	*o,p*-di CH_3	-83.50	-7.21
2.9	*o*-CH3	H	-79.51	-4.32
2.10	*p*-Cl	H	-74.04	-4.93
2.11	*p*-Cl	*p*-Cl	-90.75	-6.74
2.12	*p*-Cl	*m*-Cl	-96.32	-8.91
2.13	*p*-Cl	*o,p*-di CH_3	-101.02	-8.48
2.14	*p*-$NHCOCH_3$	H	-101.55	-7.17
2.15	*p*-$NHCOCH_3$	*p*-Cl	-97.40	-8.27
2.16	*p*-$NHCOCH_3$	*m*-Cl	-102.09	-9.84
2.17	*p*-$NHCOCH_3$	*o,p*-di CH_3	-111.74	-10.93
2.18	*m*-NO_2	H	-79.19	-4.58
2.19	*m*-NO_2	*p*-Cl	-90.08	-6.79
2.20	*m*-NO_2	*m*-Cl	-99.03	-8.57
2.21	*m*-NO_2	*o,p*-di CH_3	-93.04	-8.95
2.22	*o*-NO_2	H	-66.10	-2.13

2.23	*o*-NO_2	*p*-Cl	-74.88	-6.94
2.24	*o*-NO_2	*m*-Cl	-95.69	-7.58
2.25	*o*-NO_2	*o,p*-di CH_3	-95.41	-3.50
2.26	*p*-NO_2	H	-87.50	-6.18
2.27	*p*-NO_2	*p*-Cl	-65.86	-5.14
2.28	*p*-NO_2	*m*-Cl	-110.50	-6.06
2.29	*p*-NO_2	*o,p*-di CH_3	-97.45	-5.18
2.30	*p*-OCH_3	H	-88.96	-6.48
2.31	*p*-OCH_3	*p*-Cl	-91.70	-5.42
2.32	*p*-OCH_3	*m*-Cl	-76.64	-5.37
2.33	*p*-OCH_3	*o,p*-di CH_3	-87.89	-7.51

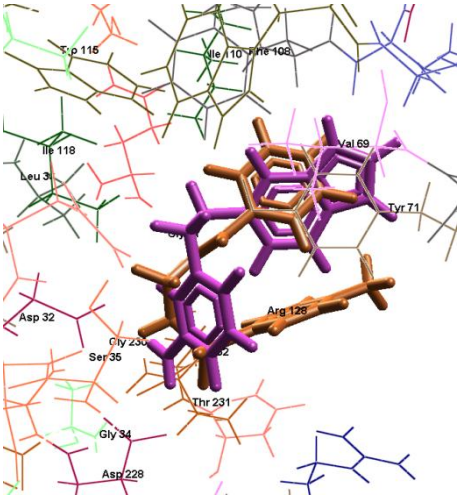

i. **Superimposed docked pose of 6IP-389 (purple) and 2.1 (brown)**

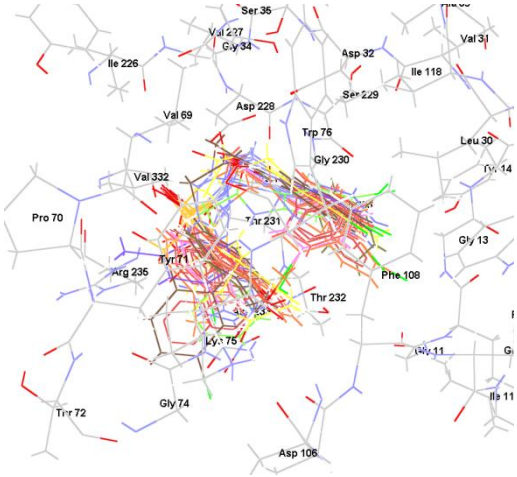

ii. Superimposed docked pose of all compounds (2.1-2.33)

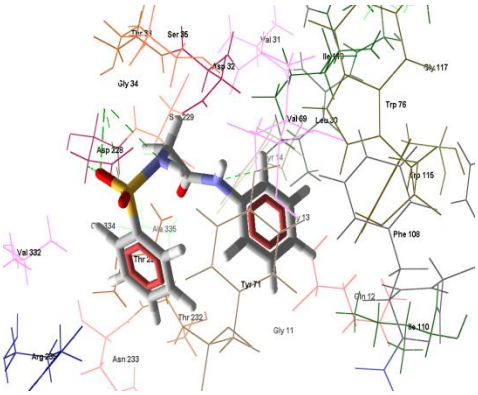

iii. Docking pose of 2.5

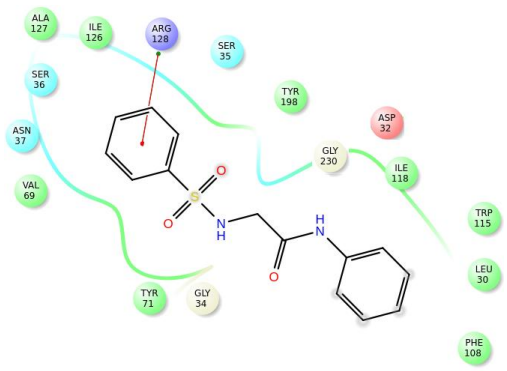

iv. 2D Ligplot of 2.5

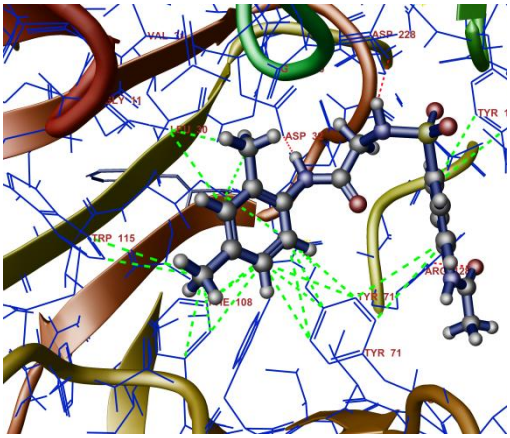

v. Docking pose of 2.17

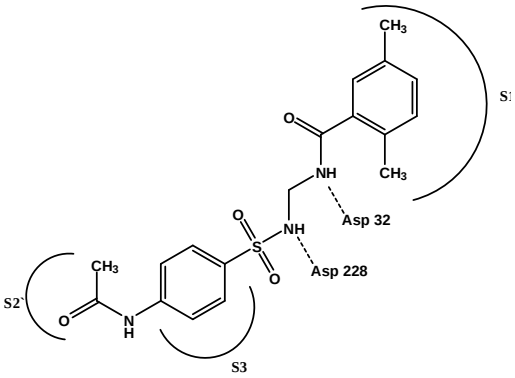

vi. 2D interaction plot of 2.17

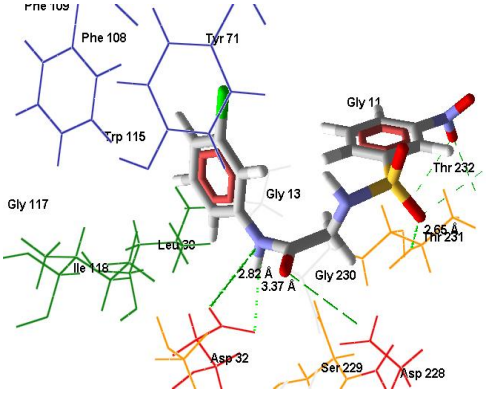

vii. Docking pose of 2.20

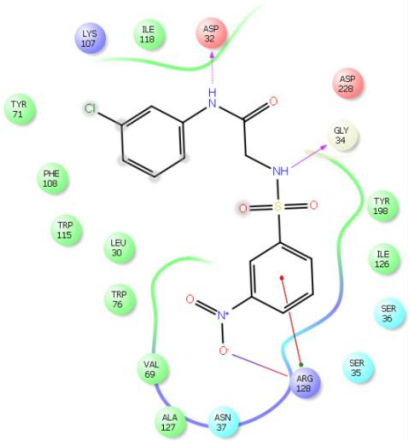

viii. 2D Ligplot of 2.20

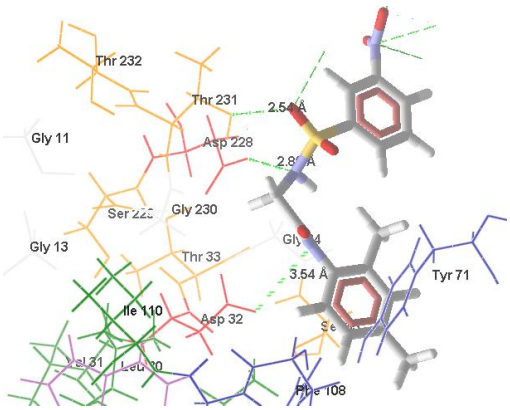

ix. Docking pose of 2.21

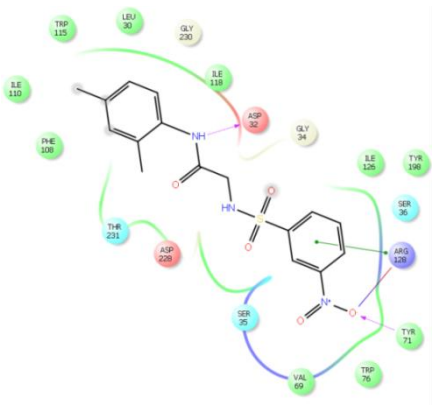

x. 2D Ligplot of 2.21

Figure 4.6: Docking poses of few *N*-Phenyl-2-[(phenylsulfonyl)amino]acetamide derivatives

4.4.2 Oral bioavailability and toxicity prediction

The designed molecules display compliance with Lipinski rule of five. The Log P values for all compounds were within specified range. Number of hydrogen bond donors ranged between

2 to 3 and hydrogen bond acceptors between 3 to 5. The molecular weight for all designed compound was well within criteria of being less than 500. The polar surface area was found to be between 75.27- 118.41Å^2. It shows that except few compounds, all other ligands have optimum value of polar surface area needed for brain permeation.

It was observed that (table 4.4) except few compounds, all the compounds were safe in terms of mutagenicity, tumorigenecity, irritant and reproductive effects. Those compounds that have been substituted with *m*-Cl or *o,p*-dimethyl group on ring B showed undesirable effects of irritancy and tumorigenicity. The compounds 1 to 8 did not display good drug likeliness, probably due to unsubstituted ring A or presence of 4-methyl substitution on ring A. Placing nitro substitution on any position on ring A also reduces drug likeliness of any compound. *p*-chloro, *p*-methoxy and *p*-acetamido favour the compounds to possess drug like nature. On the whole, the drug score ranged from good to medium.

Table 4.4: Physicochemical properties of *N*-Phenyl-2-[(phenylsulfonyl)amino]acetamide derivatives

Code	MW	HBA	HBD	PSA	LogP	M	T	I	RE	Drug likeliness	Drug score	BBB Score
2.1	304.08	3	2	75.27	2.22	G	G	G	G	-5.61	0.46	0.171
2.2	324.03	3	2	75.27	2.31	G	G	G	G	-3.04	0.45	0.145
2.3	324.03	3	2	75.27	2.31	G	G	R	G	-3.94	0.26	0.145
2.4	318.10	3	2	75.27	2.74	G	R	Y	G	-7.14	0.21	0.136
2.5	290.07	3	2	75.27	1.71	G	G	G	G	-4.53	0.45	0.177
2.6	338.04	3	2	75.27	2.83	G	G	G	G	-2.06	0.45	0.139
2.7	338.04	3	2	75.27	2.83	G	G	G	G	-2.86	0.26	0.139
2.8	332.11	3	2	75.27	3.25	G	R	Y	G	-6.02	0.20	0.119
2.9	304.08	3	2	75.27	2.22	G	G	G	G	1.62	0.80	0.171
2.10	324.03	3	2	75.27	2.31	G	G	G	G	2.78	0.83	0.145
2.11	357.99	3	2	75.27	2.92	G	G	G	G	4.83	0.76	0.145
2.12	374.02	3	2	75.27	2.83	G	G	R	G	4.83	0.46	0.145
2.13	352.06	3	2	75.27	3.34	G	R	G	G	1.26	0.33	0.105
2.14	347.09	4	3	104.37	0.95	G	G	G	G	4.69	0.87	0.143
2.15	361.10	4	3	104.37	1.46	G	G	G	G	6.74	0.80	0.111
2.16	381.05	4	3	104.37	1.55	G	G	R	G	6.31	0.48	0.111

2.17	375.12	4	3	104.37	1.97	G	R	Y	G	3.20	0.63	0.107
2.18	335.05	5	2	118.41	1.65	G	G	G	G	-7.06	0.44	0.131
2.19	369.01	5	2	118.41	2.25	G	G	G	G	-4.45	0.41	0.100
2.20	369.01	5	2	118.41	2.25	G	G	R	G	-5.34	0.24	0.100
2.21	363.08	5	2	118.41	2.68	G	R	Y	G	-8.55	0.20	0.092
2.22	335.05	5	2	118.41	1.65	G	G	G	G	-5.35	0.44	0.083
2.23	369.06	5	2	118.41	2.25	G	G	G	G	-2.77	0.43	0.050
2.24	369.01	5	2	118.41	2.25	G	G	R	G	-3.66	0.25	0.050
2.25	363.08	5	2	118.41	2.68	G	R	Y	G	-6.84	0.20	0.066
2.26	335.05	5	2	118.41	1.65	G	G	G	G	-6.97	0.44	0.131
2.27	369.01	5	2	118.41	2.25	G	G	G	G	-4.48	0.41	0.100
2.28	369.01	5	2	118.41	2.25	G	G	R	G	-5.29	0.24	0.100
2.29	363.08	5	2	118.41	2.68	G	R	Y	G	-8.46	0.20	0.092
2.30	320.08	4	2	84.50	1.55	G	G	G	G	2.14	0.85	0.085
2.31	354.04	4	2	84.50	2.16	G	G	G	G	4.60	0.83	0.058
2.32	354.04	4	2	84.50	2.16	G	G	R	G	3.81	0.50	0.058
2.33	348.11	4	2	84.50	2.58	G	R	O	G	0.64	0.33	0.045

M=mutagenicity, T= tumorigenic, I= Irritant, RE= reproductive effect. Alphabets in column representing M, T, I and RE imply G= no indication, Y = medium risk and R = high risk.

4.5 Substituted pyrimidine derivatives as BACE-1 inhibitors

N-Phenyl-2-[(phenylsulfonyl)amino]acetamide series, discussed in previous section, displayed key interactions with aspartate dyad and also occupied the S1 region well. Further, these derivatives showed few interactions with S3 region amino acids like Thr231 and Thr232. However, it was observed that these compounds were oriented more towards S2′ region than S3 pocket. The aim was therefore to occupy the S3 cavity along with S1 cavity retaining the desired interactions.

Gianpaolo *et al* have reported substituted 2-aminoimidazole derivatives as BACE-1 inhibitors [128]. These compounds have shown good *in vitro* inhibition as well as docking in the active site. These compounds had large structure with 2-aminoimidazole nucleus substituted with N-aromatic and C4 aromatic groups. Since it was noticed that, due to the flexibility of 5-atom chain linker separating two phenyl rings, N-Phenyl-2-[(phenylsulfonyl)amino]acetamides formed 'U' shape, flipping the orientation towards S2′ cavity than S3. The aim of occupying the S3 cavity along with S1 cavity could be achieved by reducing linker size and inducing

rigidity in the linker separating aromatic rings on both sides. Therefore, it was considered to induce rigidity by having a 6 member ring substituted with aromatic groups on both sides. Among the possible scaffolds, 2-aminopyrimidine appeared to be a very attractive moiety because, the 2-substitution was expected to interact with aspartic dyad and aromatic rings at 4th and 6th position would occupy targeted S1 and S3 pockets. The pyrimidine ring would provide 3-atom rigid linker to prevent flipping of the phenyl rings and orient the substitution at 2nd position in the centre of catalytic aspartate dyad.

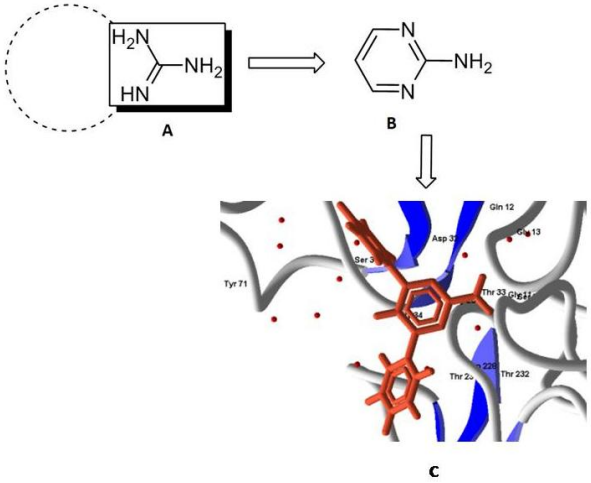

Figure 4.7: Rationale for designing 2-amino pyrimidines. (A) The guanidinium function present in reported 2-aminoimidazoles; (B) 2-aminopyrimidine moiety having similar functionality; (C) 2-aminopyrimidine oriented towards the catalytic dyad.

As a prototype, 2-aminopyrimidine with *m*-nitrophenyl (ring A, at C4) and unsubstituted phenyl ring (ring B, at C6), compound 2.1G, was considered. As expected, 2-aminopyrimidine moiety turned out to be oriented in the center of the rather large BACE-1 binding pocket by interacting with both catalytic aspartic acids, Asp32 and Asp228 *via* H-bond interactions (Figure 4.9). The binding mode of 2.1G at BACE-1 binding pocket showed following interactions:

i. The guanidinium moiety of 2.1G interacted with both aspartic acids (Asp32 and Asp228) with length of 3.45Å and 2.8Å; 2.8Å and 2.1Å respectively.

ii. Ring B formed hydrophobic interactions with Phe108, Leu30 and Ile110 in S1 cavity.

iii. Ring B also formed π-π stacking with Phe108 and Trp115 in S1 cavity.

iv. Ring A established hydrophobic interactions with Thr231, Gly230 in S3 cavity.

v. Nitro group was found to interact with Trp76 *via* hydrogen bonding interactions and with Arg128 through salt bridge (S2' cavity).

vi. Ring A also showed π-π stacking with Tyr71.

Thus, it was noticed that the prototype compound 2.1G occupied S1 as well as S2' and S3 active site region. Considering the promising docking data, we hypothesized that electron withdrawing substitution on ring A and changing the substituents on ring B would result in compounds with good BACE-1 inhibition. While 2-amino pyrimidines with various substituents were designed, it was also thought to replace the 2-amino group of pyrimidine with -hydroxyl and -thiol groups. Since –amino group can be bioisosterically replaced with –hydroxyl and –thiol, it was expected that these will retain or enhance the desired interactions.

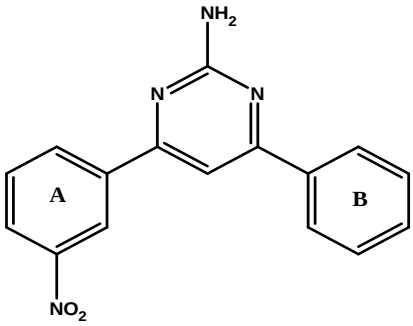

Structure of 2.1G

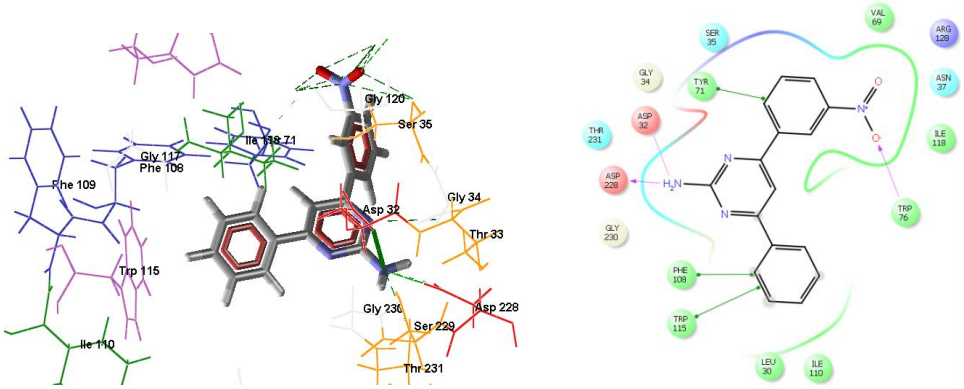

A **B**

Figure 4.8: Binding mode of compound 2.1G to 2OHP. (A) The compound 2.1G is represented as sticks and protein is represented as wireframe with shapely residue scheme. (B) 2D ligplot of compound 2.1G in active site.

4.5.1.1 2-aminopyrimidine derivatives as BACE-1 inhibitors

Since in compound 2.1G, it was observed that electron withdrawing substituent like –nitro gives good positioning in S3 cavity, for designing library, various other electron withdrawing groups were substituted. It was noticed that *meta* substitution on the ring A tends to favour overall interactions and increase binding affinity. Substitution of benzyloxy group at meta position of ring A (compound 2.13G) with *o,p*-dichloro on ring B enhanced the docking score

and had the best docking score. It was observed that benzyl ring accommodated the S3 pocket more deeply as compared to other groups. The amino group also formed key interactions with aspartate dyad and ring B occupied S1 and S2' cavities. Substitution at para position on ring A did not favour the interactions. It was observed that compounds 2.7G (*p*-chloro on ring A and unsubstituted ring B), 2.8G (*p*-chloro on ring A and *p*-methyl on ring B), 2.9G (*p*-chloro on ring A and *o,p*-dimethoxy on ring B) and 2.10G (*p*-*N*,*N*-dimethyl on ring A and *p*-nitro on ring B) displayed low docking scores and could not occupy the S3 region completely. Substitution of electronegative groups or deactivating groups at *ortho* or *para* position of ring B with *meta* substitution at ring A (2.3G having *m*-nitro on ring A and *p*-methoxy on ring B and 2.6G having *m*-nitro on ring A and o,*p*-dichloro on ring B) increased the interactions with S1 pocket and hence displayed relatively higher docking scores. It was also seen that dimethoxy group substitution over ring A (compound 2.11G substituted with *2,5*-dimethoxy on ring A and *m*-nitro on ring B and compound 2.12G substituted with *2,5*-dimethoxy on ring A *and o,p*-dichloro on ring B) gave low docking scores. Replacing phenyl ring with anthraldehyde (2.14G) as ring A and unsubstituted ring B reduced the interaction.

Table 4.5: *In silico* docking results of 2-amino pyrimidine derivatives

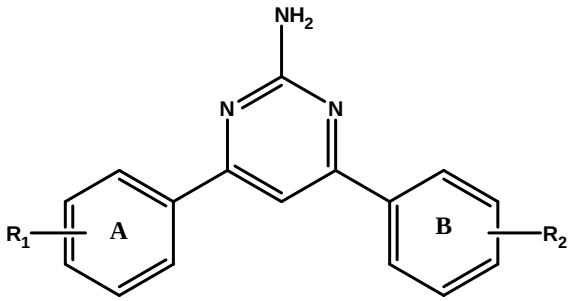

Code	R_1	R_2	Moldock score	Glide score
2.1G	*m*-NO_2	H	-78.90	-5.46
2.2G	*p*- NO_2	H	-73.39	-3.18
2.3G	*m*- NO_2	*p*-OCH_3	-104.30	-8.42
2.4G	*m*-NO_2	*p*-NH_2	-99.77	-5.49
2.5G	*m*-NO_2	*m*-Br	-71.20	-2.45
2.6G	*m*-NO_2	*o,p*-di Cl	-99.49	-6.43
2.7G	*p*-Cl	H	-63.75	-2.32

2.8G	*p*-Cl	*p*-CH_3	-65.43	-2.45
2.9G	*p*-Cl	*o,p*-di OCH_3	-73.23	-5.91
2.10G	*p*-NMe_2	*p*-NO_2	-84.36	-3.42
2.11G	2,5-di OCH_3	*m*-NO_2	-88.49	-6.57
2.12G	2,5-di OCH_3	*o,p*-di Cl	-79.40	-7.84
2.13G	*m*-O-Bn	*o,p*-di Cl	-111.09	-8.37
2.14G	Anthraldehye*	H	-75.16	-3.26

* Anthraldehyde has been used in place of substituted benzaldehyde.

4.5.1.2 2-thiopyrimidine derivatives as BACE-1 inhibitors

It was observed that the binding affinity is not much affected by bioisosteric replacement of 2-amino group with –thiol. Compound 2.2T having *m*-nitro on ring A and *p*-methoxy on ring B also displayed significant interactions. The thiol group aligns between the catalytic aspartates forming hydrogen bonding interactions. -SH acts as donor to the two oxygen atoms of Asp 32 and Asp 228 with lengths of 2.52Å, 3.39Å; 3.09Å, 2.75Å respectively. Both the pyrimidine nitrogens tend to form hydrogen bond (3.17Å and 2.27Å) with water molecules and nitrogen of *m*-nitro group acts as a proton acceptor for Thr232 (3.35Å, S3 cavity). Ring A occupied the S3 region while ring B occupied S1 cavity. It was observed that *m*-nitro substitution on ring A with *ortho* or *para* substitution on ring B (compound 2.5T with *o,p*-dichloro on ring B) was beneficial for activity while *meta* substitution on ring B (compound 2.4T having *m*-nitro on ring B) reduced the docking scores. Similar to 2-amino series, compound 2.9T having ring A was substituted with *m*-benzyloxy group and ring B with *o,p*-dichloro group showed best docking score. It displayed strong interactions with catalytic aspartate dyad. Further, S1 and S3 active site regions were accommodated by ring B and ring A respectively. Substitution at *ortho* and *para* position on ring A did not favour the activity. Substitution of electron donating groups on ring A also reduced the docking score as in compounds 2.6T (*p-N,N*-dimethyl on ring A and *p*-nitro on ring B*)*, 2.7T (*m,p*-dimethoxy on ring A *and p*-chloro on ring B) and 2.8T (*2,5*-dimethoxy on ring A *and o,p*-dichloro on ring B). Further, replacing phenyl ring with furan-2-aldehyde as ring A diminished the interaction with S3 cavity.

Table 4.6: *In silico* docking results of 2-thio pyrimidine derivatives

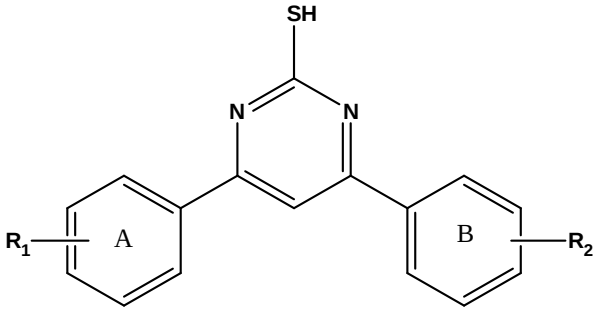

Code	R_1	R_2	Moldock score	Glide XP score
2.1T	*m*-NO_2	H	-100.03	-6.42
2.2T	*m*-NO_2	*p*-OCH_3	-84.90	-6.14
2.3T	*m*-NO_2	*m,p*-di OCH_3	-86.63	-5.72
2.4T	*m*-NO_2	*m*-NO_2	-98.68	-4.16
2.5T	m-NO_2	*o,p*-di Cl	-97.46	-8.02
2.6T	*p*-NMe_2	*p*-NO_2	-87.38	-5.94
2.7T	*m,p*-di OCH_3	*p*-Cl	-86.04	-5.67
2.8T	2,5-di OCH_3	*o,p*-di Cl	-81.58	-4.36
2.9T	*m*-O-Bn	*o,p*-di Cl	-108.40	-8.19
2.10T	Furan-2-aldehyde*	*m*-Br	-76.55	-3.48

* Furan-2-aldehyde has been used in place of substituted benzaldehyde.

4.5.1.3 2-hydroxypyrimidine derivatives as BACE-1 inhibitors

Binding affinity was reduced by bioisosteric replacement of 2-amino group with –hydroxy, in general. Overall, m-nitro substitution on ring A in compounds 2.1U (*m*-nitro on ring A and unsubstituted ring B), 2.3U (*m*-nitro on ring A and *p*-methoxy on ring B), 2.4U (*m*-nitro on ring a and *m*-nitro on ring B) and 2.5U (*m*-nitro on ring A and *o,p*-dichloro on ring B) revealed moderate docking score and fair interactions as compared to *ortho* and *para* substitution on ring A. Substitution at *para* position on ring A with electron withdrawing or electron donating groups (2.7U having *p*-*N*,*N*-dimethyl on ring A and p-nitro on ring B, 2.2U having *p*-nitro on ring A and unsubstituted ring B) reduced the docking score. Replacing phenyl ring with furan-2-aldehyde as ring A and *m*-Br on ring B reduced the interaction. In compound

2.11U, ring A has *m*-benzyloxy substitution and ring B has *o,p*-dichloro substitution. As in above two series, it was the most active compound with respect to docking scores.

Table 4.7: *In-silico* docking results of 2-hydroxy pyrimidine derivatives

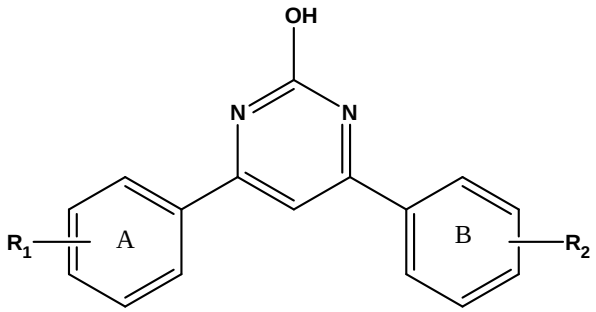

Code	R_1	R_2	Moldock score	Glide XP score
2.1U	*m*-NO_2	H	-94.45	-5.31
2.2U	*p*-NO_2	H	-74.01	-2.14
2.3U	*m*-NO_2	*p*-OCH_3	-84.56	-6.41
2.4U	*m*-NO_2	*m*-NO_2	-98.64	-6.64
2.5U	*m*-NO_2	*o,p*-di Cl	-104.28	-6.13
2.6U	*p*-Cl	*p*-CH_3	-81.41	-4.85
2.7U	*p*-NMe_2	*p*-NO_2	-72.31	-2.74
2.8U	*m,p*-di OCH_3	*m*-NO_2	-71.89	-2.67
2.9U	*m,p*-di OCH_3	*p*-Cl	-68.16	-2.87
2.10U	2,5-di OCH_3	*o,p*-di Cl	-65.37	-4.75
2.11U	*m*-O-Bn	*o,p*-di Cl	-98.94	-6.91
2.12U	Furan-2-aldehyde*	*m*-Br	-72.41	-2.63

* Furan-2-aldehyde has been used in place of substituted benzaldehyde.

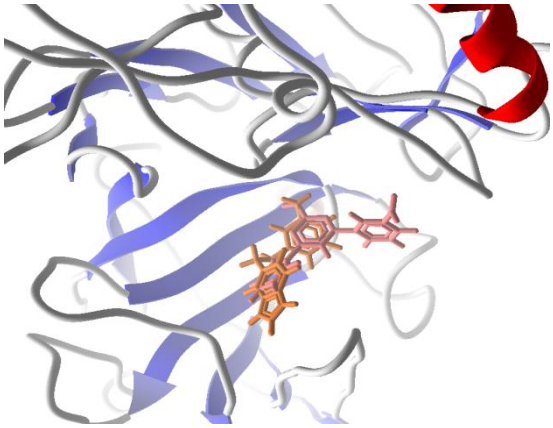

i. Superimposed docked view of 6IP-389(orange) and 2.1G(pink)

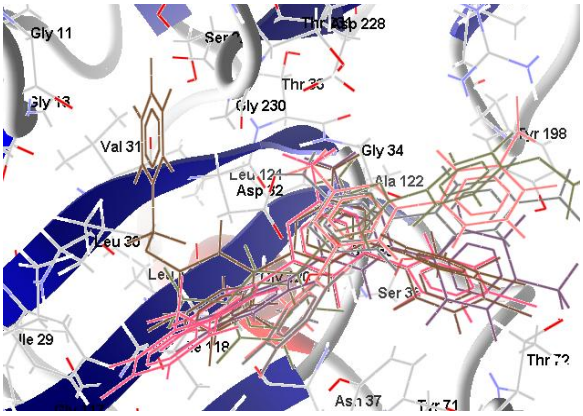

ii. Superimposed docked view of 2-amino pyrimidine derivatives

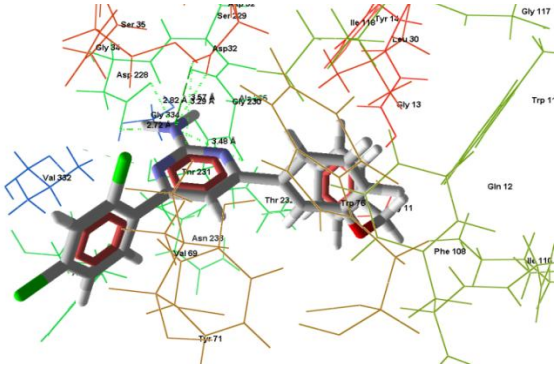

iii. Docking pose of 2.13G

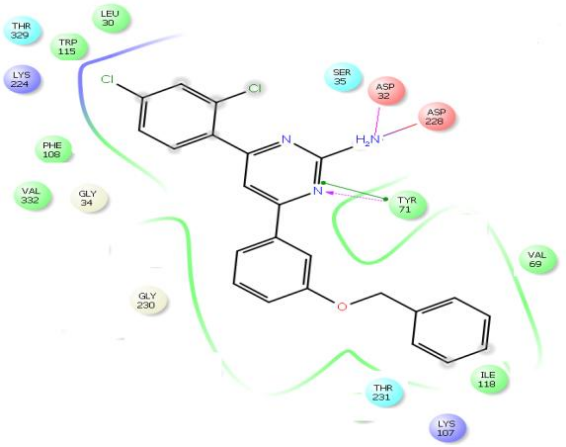

iv. 2D Ligplot of 2.13G

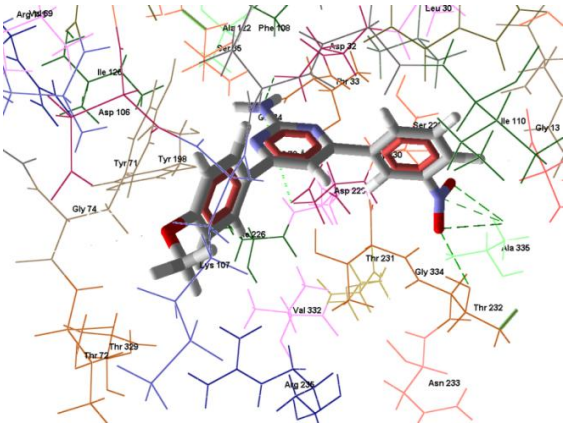

v.Docking pose of 2.3G

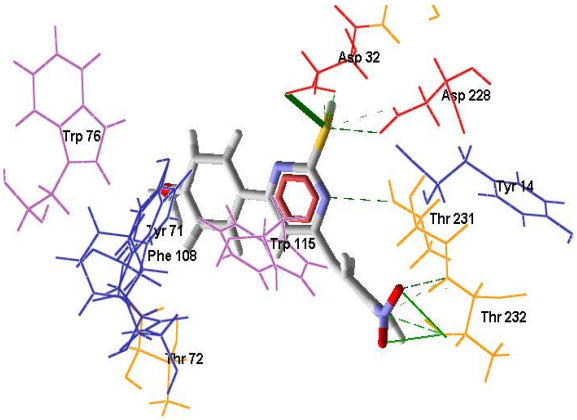

vi. Docking pose of 2.2T

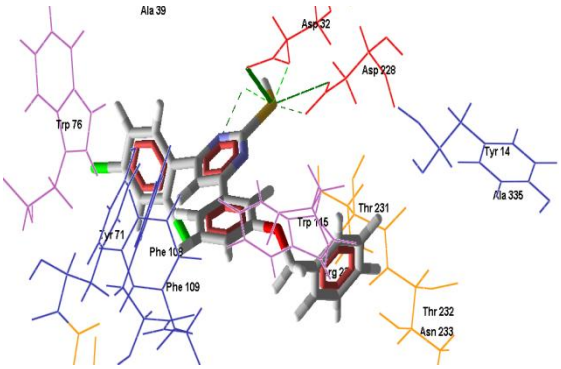

vii. Docking pose of 2.9T

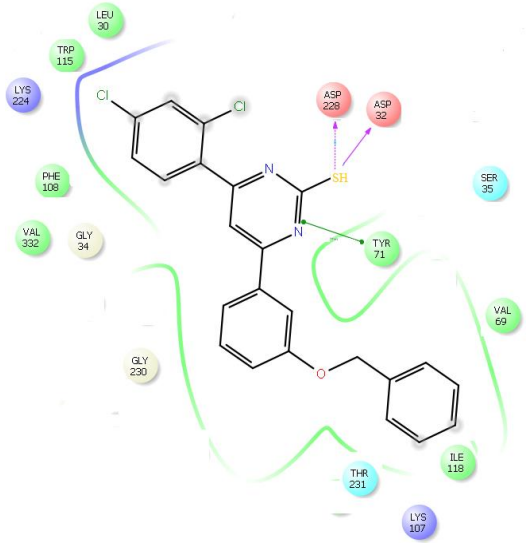

viii. 2D Ligplot of 2.9T

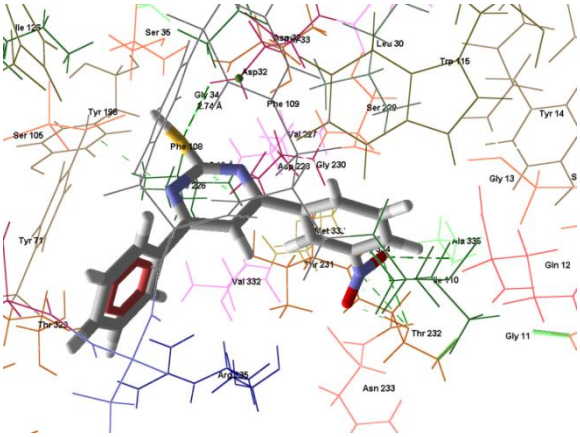

ix. Docking pose of 2.1T

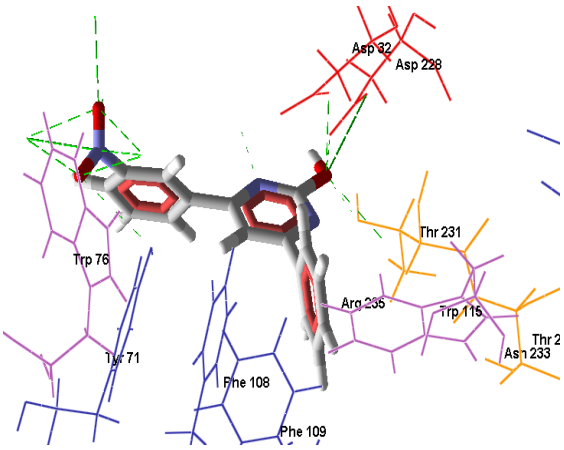

x. Docking pose of 2.1U

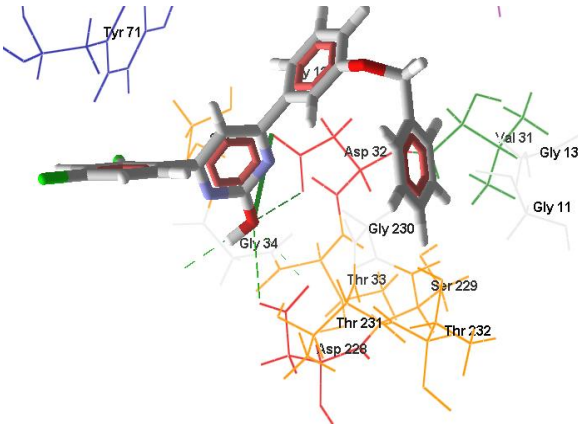

xi. Docking pose of 2.11U

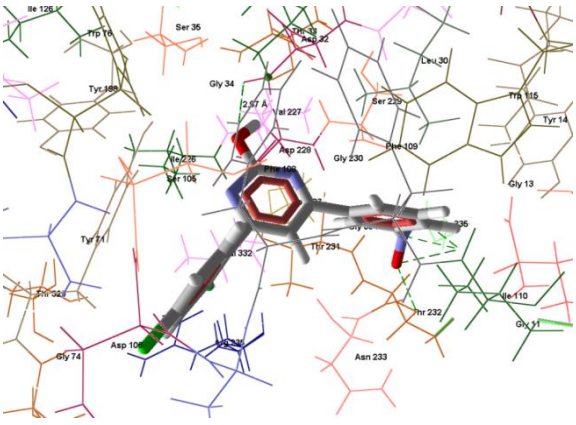

xii. Docking pose of 2.5U

Figure 4.9: Docking poses of representative substituted pyrimidine derivatives

4.5.2 Oral bioavailability and toxicity prediction

Designed molecules of 2-amino-, 2-thio- and 2-hydroxy- pyrimidines were subjected to *in-silico* oral bioavailability and toxicity prediction. The descriptors used for prediction are given in Table 4.8. All the compounds from 2- substituted pyrimidine series fulfilled the criteria for Lipinski rule of five. LogP of these derivatives varied from 1.69 to 6.34. As per the literature [129], there is only modest correlation between lipophilicity and brain permeability. Therefore, even if some compounds have higher LogP, they may show brain penetration via carrier transport. The number of hydrogen bond donors ranged between 1 to 2 and hydrogen bond acceptors between 3 to 7. The polar surface area was found to be in range of 35.01 $Å^2$ to 120.96 $Å^2$. The molecular weight for all designed compound fitted well within criteria of being less than 500. All these parameters indicate that the compounds would be orally bioavailable and also cross blood brain barrier. To further confirm, BBB permeability was predicted using online BBB permeation prediction software, according to which a compound having SVM_MACCSFP BBB score of more than 0.02 is said to cross BBB. It was observed that except two compounds (2.11G and 2.10U), all compounds scored above 0.02 and hence were predicted to be BBB penetrant.

Toxicity risk assessment was carried using OSIRIS property explorer and given in Table 4.8. It was observed that most of the compounds were safe as no indication of mutagenicity, tumorigenecity, irritant and reproductive effects were seen. Compounds having dimethylamino and anthraldehyde groups showed tumorigenicity as these groups have been reported to impart tumorigenicity as well as mutagenicity.

The pyrimidine series did not show favourable drug likeliness score for most of the compounds but the drug scores were moderate to medium. The unfavourable drug scores can be attributed to many factors such as mutagenecity, tumorigenecity, irritability and high ClogP values along with very low solubility. Overall, the drug score for all the compounds was a positive value. This indicates that the designed ligands have potential to serve as drug.

Table 4.8: Physicochemical properties of substituted pyrimidine derivatives

Code	MW	HBA	HBD	PSA	LogP	M	T	I	RE	Drug Likeliness	Drug score	BBB Score
2.1G	292.29	5	1	94.94	2.37	G	G	G	G	-6.85	0.35	0.110
2.2G	292.29	5	1	94.94	2.37	G	G	G	G	-6.85	0.35	0.110
2.3G	291.35	6	1	104.17	2.30	G	G	G	G	-6.05	0.35	0.082
2.4G	307.31	6	2	120.96	1.69	G	G	G	G	-6.29	0.35	0.091

2.5G	371.19	5	1	94.94	3.09	G	G	G	G	-8.66	0.28	0.075
2.6G	361.18	5	1	94.94	3.58	G	G	G	G	-4.83	0.25	0.053
2.7G	281.74	3	1	51.80	3.89	G	G	G	G	0.17	0.47	0.089
2.8G	295.77	3	1	51.80	2.24	G	G	G	G	-1.37	0.33	0.081
2.9G	341.80	5	1	70.26	3.75	G	G	G	G	-0.84	0.39	0.042
2.10G	335.36	6	1	98.18	2.26	G	R	G	G	-11.8	0.20	0.062
2.11G	352.35	7	1	113.40	2.23	G	G	G	G	-5.52	0.34	0.014
2.12G	376.24	5	1	70.26	4.36	G	G	G	G	1.25	0.42	0.050
2.13G	422.31	4	1	61.03	5.85	G	G	G	G	-5.00	0.15	0.081
2.14G	262.31	4	2	77.82	5.68	R	R	R	G	-3.57	0.04	0.110
2.1T	309.34	4	1	68.92	2.86	G	G	G	G	-9.10	0.31	0.136
2.2T	339.37	5	1	78.15	2.79	G	G	G	G	-8.30	0.31	0.108
2.3T	369.07	6	1	87.38	2.72	G	G	G	G	-5.55	0.37	0.049
2.4T	354.04	6	1	112.06	1.94	G	G	G	G	-9.32	0.29	0.110
2.5T	378.23	4	1	68.92	4.07	G	G	G	G	-7.09	0.22	0.077
2.6T	352.09	5	1	72.16	2.75	G	R	G	G	-14.06	0.18	0.083
2.7T	358.04	4	1	44.24	4.25	G	G	G	G	0.62	0.42	0.080
2.8T	392.01	4	1	44.24	4.85	G	G	G	G	0.80	0.34	0.037
2.9T	439.35	3	1	35.01	6.34	G	G	G	G	-7.25	0.13	0.130
2.10T	331.96	2	1	38.92	3.73	G	G	G	G	-6.80	0.30	0.145
2.1U	293.28	5	1	89.15	2.70	G	G	G	G	-6.85	0.35	0.093
2.2U	293.08	5	1	89.15	2.76	G	G	G	G	-11.66	0.37	0.093
2.3U	323.30	6	1	98.38	2.63	G	G	G	G	-6.01	0.36	0.061
2.4U	338.06	7	1	132.29	1.78	G	G	G	G	-7.02	0.34	0.069
2.5U	362.17	5	1	89.15	3.91	G	G	G	G	-4.80	0.25	0.045
2.6U	296.75	3	1	46.01	4.57	G	G	G	G	-6.81	0.37	0.132
2.7U	336.12	6	1	92.39	2.60	G	R	G	G	-11.77	0.21	0.039
2.8U	353.10	7	1	107.61	2.56	G	G	G	G	-3.27	0.37	0.028
2.9U	342.07	5	1	64.47	4.09	G	G	G	G	2.91	0.59	0.060
2.10U	376.03	5	1	64.47	4.69	G	G	G	G	3.09	0.47	0.015
2.11U	423.29	4	1	55.24	6.18	G	G	G	G	-4.96	0.15	0.129
2.12T	315.98	3	1	59.15	3.57	G	G	G	G	-4.19	0.36	0.102

M=mutagenicity, T= tumorigenic, I= Irritant, RE= reproductive effect. Alphabets in column representing M, T, I and RE imply G= no indication and R = high risk.

4.6 Substituted allylidene hydrazinecarboximidamide derivatives as BACE-1 inhibitors

4.6.1 *Design and In-silico study*

In (sulfonylamino)acetamide series, the linker for separating two aromatic rings was 5 atom long and it was noticed that ring A occupies S2' cavity and ring B is oriented towards S1 cavity. Thus, it did not occupy S3 cavity as due to flexibility, it formed 'U' shape in active site. In substituted pyrimidine series, having guanidinyl moiety present in pyrimidine ring to impart rigidity, it was observed that 5 atom linker is not essential and the substitution at 2 position is essential for binding with aspartate dyad. Therefore, another series of allylidene hydrazinecarboximidamide derivatives was envisaged, which had aminoguanidine substitution on a short 3 atom linker to bind with aspartate dyad and the two aromatic groups on either side of linker to bind S1 and S3 cavity. Thus, it had limited flexibility as compared to [sulfonyl)amino]acetamide series and had guanidinyl moiety of substituted pyrimidine series separated from linker by an amino group.

As prototype, two unsubstituted phenyl rings on either side of the allylidene hydrazinecarboximidamide linker were placed to see the binding pattern in BACE-1 active site. Compound C1A, ((Z)-2-((E)-1,3-diphenylallylidene)hydrazinecarboximidamide), in Moldock docking simulation, displayed the following interactions (Figure 4.11):

i. –NH- of hydrazide formed hydrogen bond interaction with Asp32 (3.33Å)

ii. $–NH_2$ group displayed hydrogen bonding interactions with Asp32 (3.17Å, 2.57Å) and Asp228 (2.25Å, 3.10Å)

iii. Ring A was seen to occupy S3 cavity

iv. Ring B was seen to occupy S1 cavity

Similar interactions were observed in Schrodinger, Glide docking algorithm.

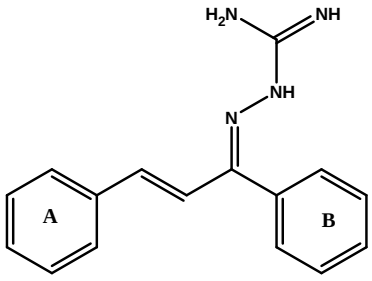

C1A

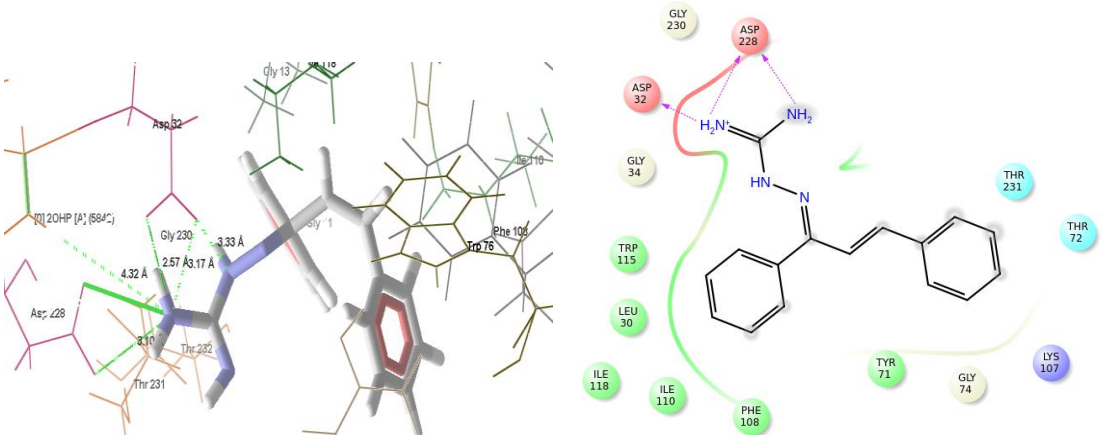

A **B**

Figure 4.10: Docking pose and 2D interaction plot of compound C1A (A: Binding mode of compound C1A to 2OHP, B: 2D Ligplot of compound C1A in the active site of 2OHP)

Exploring the same structure with different substituents on ring A and ring B revealed the occupance of substrate binding cavities and interactions with active site amino acids. It was seen that Compound C2A bearing a *m*-nitro group at on ring A and unsubstituted ring B had increased docking score over C1A and along with occupance of S1 cavity, its nitro group helped accommodate the S3 pocket better. Compared to these, Compound C4A (*m*-nitro on ring A and *p*-nitro on ring B) revealed excellent docking score and favourable interactions (table 4.9). Its guanidinium moiety formed strong hydrogen bonding interactions with the key aspartate dyad (Asp228: 2.99Å, 3.16Å, Asp 32:2.75Å, 2.99Å) and also with Gly230 (3.52Å and 3.23Å). Further, as compared to C2A and C3A, it covered S1 as well as S3 substrate binding pocket. The *para* nitro bearing ring B protruded well within the S1 cavity as nitro group helped in extending towards depth of the pocket and also formed π-π stacking with Tyr71. Another nitro group substituted at *meta* position of ring A was seen to accommodate well in the S3 pocket with enhanced hydrogen bonding interactions of the nitro group with Thr232 (3.16Å, 3.23Å, 2.23Å). It also formed hydrogen bond with water molecule since it was solvent exposed. Unsubstituted ring A with different substitutions on ring B displayed poor interactions (C6A- *m*-hydroxy on ring B, C9A-*m*-nitro on ring B, C11A-*p*-chloro on ring B, C19A- *p*-hydroxy on ring B). This reveals that substitution on ring A is important for activity. Substitution of *N,N*-dimethyl group (electron donating group) at *para* position on ring A did not show preference for the activity. Compounds C8A (*p*-methyl on ring B), C12A (*p*-nitro on ring B), C13A (unsubstituted ring B) and C16A (*m*-nitro on ring B) substituted with *N,N*-dimethyl group (electron donating group) at *para* position on ring A displayed low docking scores and weak interactions.

Substituting ring A with *m,p*-dimethoxy group and ring B with different substitutents was observed to favour the activity. When compared to the compound C22A (unsubstiuted ring B), C23A had better score and interactions. Compound C23A was substituted with *p*-nitro group on ring B which was seen to accommodate S1 cavity while *m,p*-dimethoxy group on ring A occupied S3 cavity through hydrogen bonding interactions of methoxy oxygen with Thr232. The guanidinium group formed hydrogen bonding interaction with Asp32 and Asp228 and also formed salt bridge with Asp228 (imine being positive charged as amine). In the same series, compound C24A having *p*-chloro on ring B also revealed favourable interactions. The guanidinium group formed hydrogen bonding interaction with Asp32 and Asp228 (2.83A^0, 3.19A^0 and 2.80A^0, 3.48A^0 respectively). The imine nitrogen also formed hydrogen bonding interaction with Gly34 (3.21A^0). Ring B displayed π-π stacking with Tyr71 and occupied the S1 active site while ring A occupied S1 region. Compound C25A with *m*-nitro group on ring B was observed to move the molecule away from S1 pocket orienting the methoxy group towards Gly11 and Thr232 while the nitro formed hydrogen bonds with water. Compound C38A with *m*- bromo group on ring B also revealed favourable interactions with aspartate 32 and 228. Ring B formed π-π stacking with Tyr71 and ring A was deeply engulfed in S3 substrate binding pocket. Substitution of halogen at *meta* position of ring B favoured the activity (C38A) while nitro substitution at *meta* position on ring B did not (C25A). Compounds substituted with 2,5-dimethoxy group on ring A (C5A: unsubstituted ring B, C30A: *m*-bromo on ring B and C31A: *p*-methoxy group on ring B) formed hydrogen bonding interactions with desired aspartates but failed to occupy S1 cavity though S3 cavity was well occupied with strong hydrophobic interactions. Replacing the phenyl ring with other heteroaromatic rings as ring A (C7A: Anthraldehyde as ring A and unsubstituted ring B; C18A: Anthraldehyde as ring A and *p*-chloro group on ring B; C21A: Indole-3-carboxaldehyde as ring A and unsubstituted ring B) reduced the activity as these compounds did not occupy S3 cavity.

Table 4.9: *In-silico* docking results of substituted allylidene hydrazinecarboximidamide derivatives

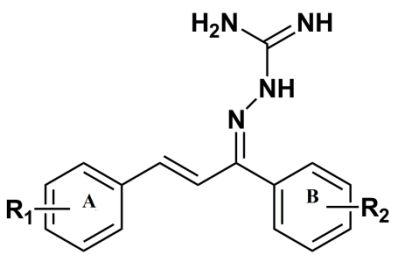

Code no.	R_1	R_2	Moldock score	Glide XP score
C1A	H	H	-92.06	-5.62
C2A	*m*-NO_2	H	-107.86	-6.41
C3A	H	*p*-NO_2	-109.70	-6.12
C4A	*m*-NO_2	*p*-NO_2	-107.35	-7.85
C5A	2,5 di OCH_3	H	-97.73	-5.18
C6A	H	*m*-OH	-94.60	-8.47
C7A	Anthraldehyde	H	-73.32	-4.19
C8A	*p*-NMe_2	*p*-CH_3	-88.40	-6.16
C9A	H	*m*-NO_2	-75.91	-4.93
C11A	H	*p*-Cl	-91.23	-4.18
C12A	*p*-NMe_2	*p*-NO_2	-80.06	-3.48
C13A	*p*-NMe_2	H	-73.29	-4.14
C16A	*p*-NMe_2	*m*-NO2	-78.74	-5.21
C17A	*p*-NMe_2	*p*-Cl	-84.19	-5.94
C18A	Anthraldehyde	*p*-Cl	-73.80	-6.07
C19A	H	*p*-OH	-100.16	-4.74
C20A	*p*-OCH_3	*p*-OH	-112.74	-4.91
C21A	Indole 3-carboxaldehyde	H	-78.50	-6.02
C22A	*m,p*- di OCH_3	H	-96.47	-8.94
C23A	*m,p*- di OCH_3	*p*-NO_2	-123.06	-10.53
C24A	*m,p*- di OCH_3	*p*-Cl	-105.65	-10.38
C25A	*m,p*- di OCH_3	*m*-NO_2	-95.04	-7.38
C28A	*m*-NO_2	*p*- OCH_3	-112.00	-9.59
C29A	*m*-NO_2	*o,p*-di Cl	-105.64	-9.17
C30A	2,5 di OCH_3	*m*-Br	-117.11	-10.09
C31A	2,5 di OCH_3	*p*-OCH_3	-118.49	-10.25
C33A	*m*-NO_2	*m*-Br	-104.62	-7.43
C35A	*m*-Br	*p*-NO_2	-104.38	-5.42
C36A	*o*-Cl	*m*-Br	-103.67	-6.70
C37A	*m,p*- di OCH_3	*o,p*-di Cl	-97.75	-6.03
C38A	*m,p*- di OCH_3	*m*-Br	-111.90	-9.58

* Anthraldehyde and indole-3-carboxaldehyde have been used in place of substituted benzaldehyde.

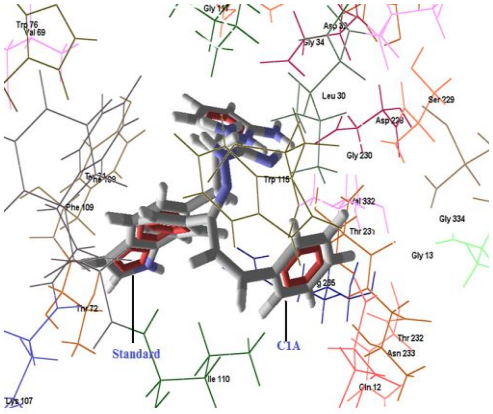

i. Superimposed docked view of standard (6IP-389) and C1A

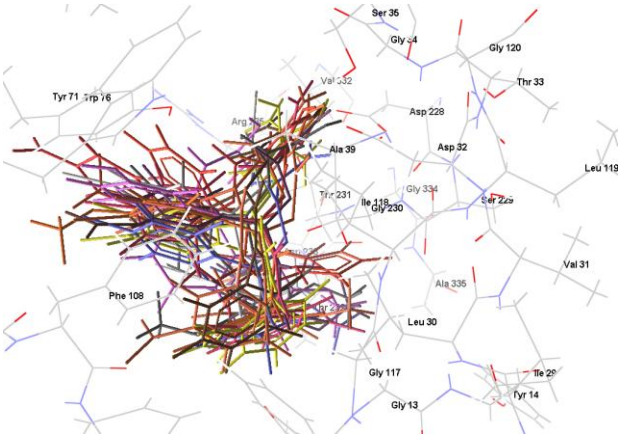

ii. Superimposed dock view of all compounds (C1A -C38A)

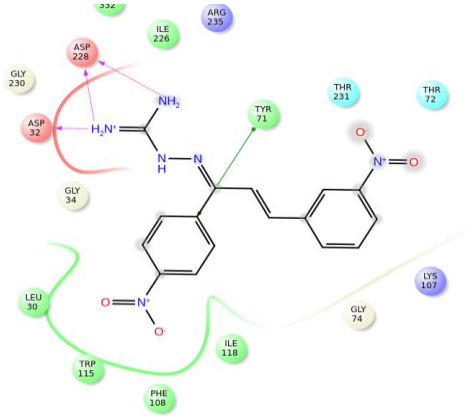

iii: 2D interaction plot of C4A

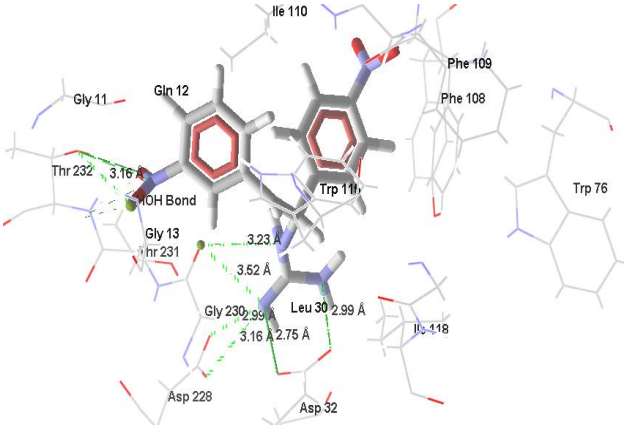

iv: Docking pose of C4A

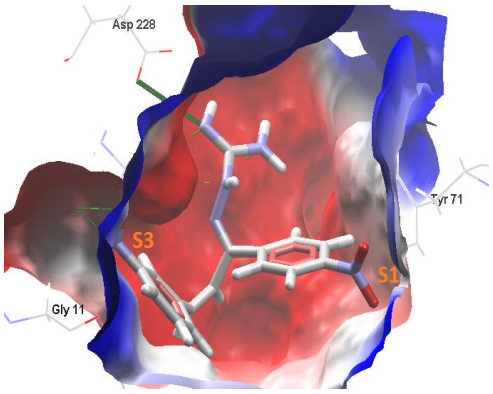

v. Electrostatic view of C4A

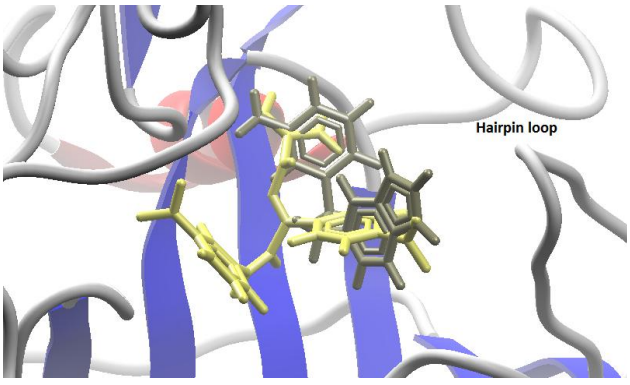

vi: Superimposed pose of C4A with standard: grey-std, buff: C4A

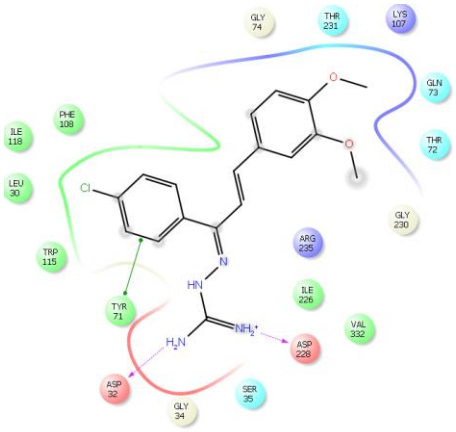

vii: 2D interaction plot of C24A

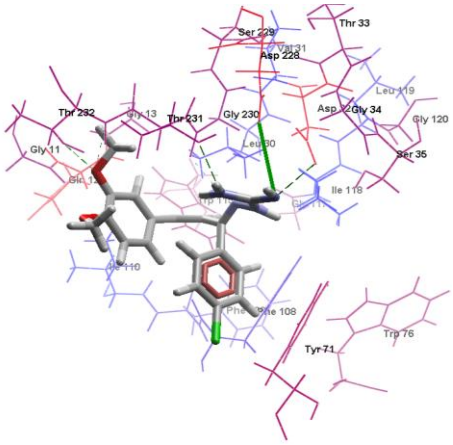

viii: Docking pose of C24A

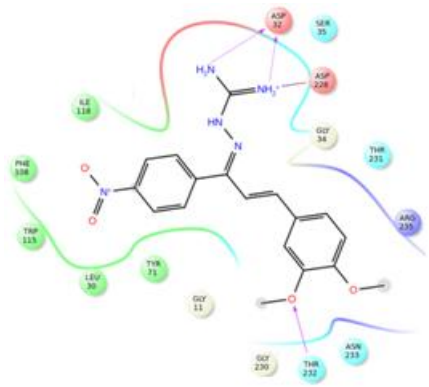

ix: 2D interaction plot of C23A

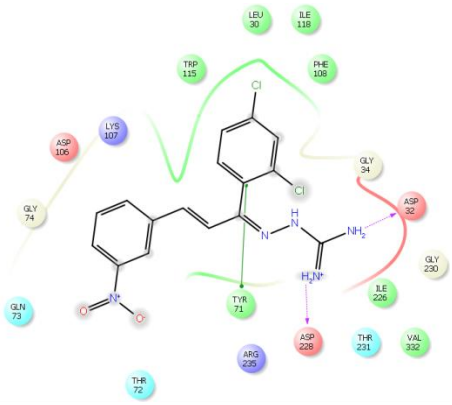

x: 2D interaction plot of C29A

Figure 4.11: Docking poses of representative substituted allylidene hydrazinecarboximidamide derivatives

4.6.2 Oral Bioavailability and toxicity prediction

Designed molecules were subjected to *in-silico* oral bioavailability and toxicity prediction. The descriptors used for prediction are given in Table 4.10. All the (1, 3 diphenylallylidene) hydrazinecarboximidamide derivatives fulfilled the criteria for Lipinski rule of five. LogP value for these derivatives varied from 1.45 to 5.15 which are considered optimal for brain permeation. The number of hydrogen bond donors ranged between 3 to 5 and hydrogen bond acceptors between 4 to 8. The total polar surface area was found to range from 74 to 126A^{02}. The molecular weight for all the designed compounds was less than 500 Da. Most of the compounds showed SVM_MACCSFP BBB Score more than 0.02 and hence would penetrate the BBB.

Toxicity risk assessment was performed using OSIRIS property explorer and given in Table 4.10. Majority of the compounds did not display any indication of mutagenicity, tumorigenecity, irritant and reproductive effects. Compound C7A and C12A displayed toxic

effects which correlates with its toxicity observed in 2-substituted pyrimidine series as well. These compounds had anthraldehyde as ring A and *p*-N,N-dimethyl substitution on ring A, respectively. The overall drug score of the series was better than 2-substituted pyrimidine derivatives.

Table 4.10: Physicochemical properties of substituted allylidene hydrazinecarboximidamide derivatives

Code	MW	HBA	HBD	PSA	LogP	M	T	I	RE	Drug likeliness	Drug score	BBB Score
C1A	264.33	4	3	76.00	3.17	G	G	G	G	2.41	0.79	0.100
C2A	309.32	6	3	119.07	2.32	G	G	G	G	-1.57	0.46	0.097
C3A	309.32	6	3	119.14	3.11	G	G	G	G	-7.85	0.39	0.097
C4A	354.32	8	3	177.88	2.28	G	G	G	G	-6.77	0.36	0.052
C5A	324.16	6	3	92.72	2.93	G	G	G	G	4.91	0.79	0.056
C6A	280.33	5	4	96.23	2.71	G	G	G	G	2.07	0.80	0.068
C7A	364.45	4	3	74.26	5.15	R	R	R	Y	1.65	0.08	0.109
C8A	321.20	4	4	77.50	3.45	G	G	G	G	-4.19	0.63	0.018
C9A	309.32	6	3	119.14	3.11	G	G	G	G	-3.29	0.40	0.097
C11A	298.77	3	4	74.27	3.74	G	G	G	G	-3.82	0.58	0.052
C12A	352.39	7	3	122.38	3.21	G	R	G	G	-5.28	0.36	0.033
C13A	307.39	4	4	77.50	3.46	G	R	G	G	-0.73	0.27	0.035
C16A	352.39	7	4	123.33	3.15	G	R	G	G	-0.82	0.19	0.033
C17A	341.85	4	4	77.50	4.39	G	G	G	G	-10.6	0.27	0.016
C18A	398.90	4	4	74.27	5.17	R	R	G	G	-6.44	0.14	0.102
C19A	280.32	4	5	94.49	2.79	G	G	G	G	2.07	0.80	0.068
C20A	310.35	5	5	103.73	2.66	G	G	G	G	3.47	0.82	0.047
C21A	253.30	5	4	86.63	0.98	G	G	G	G	4.76	0.82	0.118
C22A	324.38	5	4	92.73	2.93	G	G	G	G	5.63	0.80	0.050
C23A	369.38	8	3	135.86	2.79	G	G	G	G	-4.56	0.38	0.015
C24A	358.83	6	3	94.46	3.46	G	G	G	G	6.65	0.69	0.050
C25A	369.38	8	3	135.86	2.79	G	G	G	G	0.10	0.57	0.015
C28A	341.37	8	5	128.93	1.45	G	G	G	G	2.20	0.42	0.046
C29A	378.21	6	3	120.08	4.31	G	G	G	G	-0.56	0.38	0.044

C30A	403.28	6	3	94.46	3.62	G	G	G	G	0.47	0.42	0.049
C31A	354.41	7	3	103.69	2.69	G	G	G	G	4.12	0.78	0.043
C33A	390.24	7	5	119.70	2.37	G	G	G	G	-5.30	0.32	0.060
C35A	390.24	7	5	119.70	2.37	G	G	G	G	-9.91	0.32	0.067
C36A	377.67	4	3	76.00	4.54	G	G	G	G	0.53	0.27	0.073
C37A	393.27	6	3	94.46	4.06	G	G	G	G	6.43	0.57	0.050
C38A	403.28	6	3	94.46	3.62	G	G	G	G	1.97	0.61	0.047

M=mutagenicity, T= tumorigenic, I= Irritant, RE= reproductive effect. Alphabets in column representing M, T, I and RE imply G= no indication, Y=low risk and R = high risk.

Chapter 5

SYNTHESIS AND CHARACTERIZATION

5. Synthesis and characterization

In chapter 4, using structure based drug design, four libraries were designed and docked on 2OHP to get an indication of binding interactions in active site. It gave fair idea about probable activity; however, reports suggest that there is moderate correlation between *in silico* and *in vitro* activity data. Considering this, it was decided to synthesize all designed compounds. The synthesized compounds were characterized by standard methods of spectroscopy such as FTIR, NMR and Mass.

General chemical methods

Reaction progress was monitored by TLC using precoated silica gel plates (Keiselgel 60F254, Merck) and visualized using UV light. Melting points were measured with Buchi 530 melting point apparatus and were uncorrected. ^{1}H NMR spectra were recorded on a Bruker, Avance-400MHz system using $CDCl_3$ or DMSO as the solvent. Chemical shifts (δ) are reported in parts per millions (ppm) relative to TMS as internal standard. FTIR spectra were performed on IR Prestige 21 Shimadzu using KBr as standard. Mass spectra were recorded on Waters-Acquity instrument in electrospray mode. Unless otherwise stated, all reagents were obtained from commercial suppliers and used without further purification. Compounds were named as per Chem-draw Ultra 11.0 software.

5.1 Synthesis of Acridin-9-yl hydrazide derivatives

5.1.1 Synthesis

A dataset of 12 acridin-9-yl hydrazide compounds was designed. To synthesize, following scheme was followed:

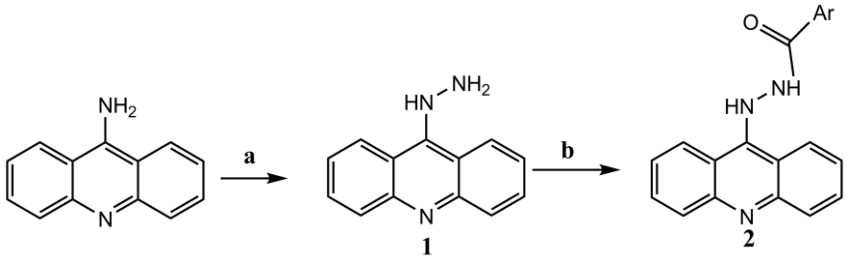

Scheme 1: Reagents and conditions: (a) $NaNO_2$, HCl, -5 to 0^0C , 1h; $SnCl_2$, HCl (b) HOBt, EDC-HCl, THF, TEA, substituted carboxylic acids, 0^0C , 12 h.

Synthesis of 1: 9-aminoacridine was dissolved in concentrated hydrochloric acid (HCl) and cooled to about 0^0 C. Cooled solution of sodium nitrite in water (1.1 equivalent) was slowly added to the above maintaining temperature to about 0^0 C for about 1 hour till the reaction was over. To the diazotized product, acidified stannous chloride was slowly added till completion of the reaction. The reduced product was then worked up with Sodium

hydroxide (NaOH) and extracted with ethyl acetate. The solvent was distilled under reduced pressure and crude compound was crystallized to get pure 9-hydrazinyl acridine.

Synthesis of 2: 1.5 equivalents of substituted carboxylic acids was added to tetrahydrofuran (THF) and allowed to stir till complete dissolution. To it was added, 1.5 equivalents of Hydroxy-O-benztriazole (HOBt) and N-(3-Dimethylaminopropyl)-N'ethylcarbidiimde.HCl (EDC.HCl) and stirred for 15-20 min at ice cold condition. To this solution was added, triethylamine (TEA) and 1.5 equivalent of 9-hydrazinyl acridine. The reaction was run at ice cold condition till completion and worked up with dichloromethane (DCM), washed with dil HCl and sodium biocarbonate ($NaHCO_3$). DCM layer was collected and solvent was evaporated under reduced pressure. The final solid product was crystallized.

5.1.2 Mechanism

Formation of compound 1 is a diazotization reaction (Griess reaction). The diazotized product was further reduced to form hydrazine. Synthesis of compound 2 is amide formation reaction from carboxylic acid and amine using HOBT-EDC.HCl as coupling reagent. The acid reacts with carbodiimide so as to form the key intermediate O-acyl isourea, which then reacts with amine to produce the desired amide and substituted urea as byproduct.

Mechanism step 1:

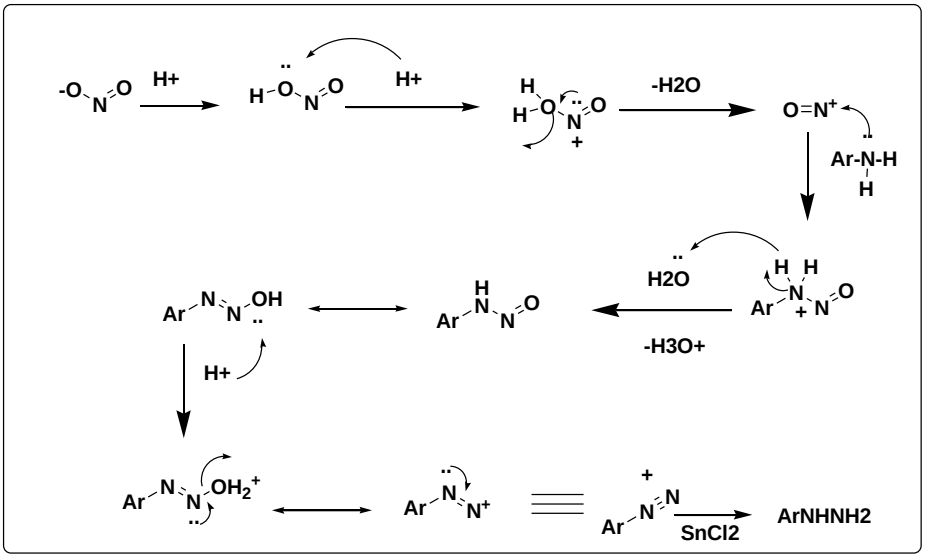

Mechanism step 2:

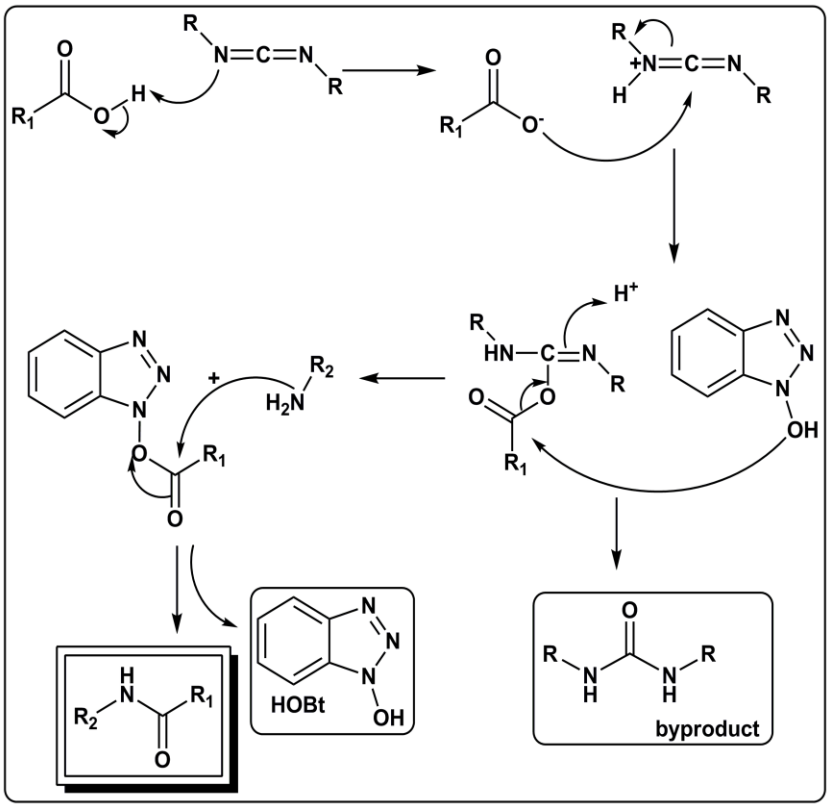

5.1.3 Spectral data of synthesized compounds

9-hydrazinylacridine (1): IR (cm^{-1}): 3410.58 (sec. N-H stretching), 3319.49 (sec. N-H stretching), 3217.31 (Aromatic C-H stretching), 2864.29 (Aliphatic C-H stretching), 1716.65 (C=O), 1587.42- 1438.90 (aromatic C=C stretch); 1H NMR (400 MHz, DMSO, δppm): 1.91 (s, $-NH_2$), 3.60 (br, 1H, -NH), 7.27 (dd, 2H, Ar-H), 7.60 (dd, 2H, Ar-H), 7.82 (d, 2H, Ar-H), 8.37 (d, 2H, Ar-H)

***N*'-(acridin-9-yl)-2-nitrobenzohydrazide (AA-11):** yield: 59.74%, mp 279^0C; IR (cm-1): 3331.07 (sec. N-H stretching), 3275.13 (Amide N-H stretch), 1641.42 (C=O stretching), 1588.42-1504.48 (aromatic C=C stretch), ^{1}H NMR (400 MHz, DMSO, δppm): 4.11 (s, 1H, -NH), 7.02 – 8.10 (m, 13H, 12Ar-H and 1 -NH)

***N*'-(acridin-9-yl)-3-fluorobenzohydrazide (AA-12):** yield: 72.42%, mp 290^0C; IR (cm^{-1}): 3390.49 (sec. N-H stretching), 3235.14 (Amide N-H stretch), 1631.78 (C=O stretching), 1588.42-1516.07 (aromatic C=C stretch), ^{1}H NMR (400 MHz, DMSO, δppm): 4.18 (s, 1H, -NH), 7.22 – 8.02 (m, 13H, 12Ar-H and 1 -NH)

***N*'-(acridin-9-yl)-2-fluorobenzohydrazide (AA-13):** yield: 80.40%, mp 270^0C; IR (cm^{-1}): 3275.13 (Amide N-H stretch), 3028.24 (Aromatic C-H stretching), 1680.00 (C=O stretching), 1641.42- 1504.48 (aromatic C=C stretch), ^{1}H NMR (400 MHz, DMSO, δppm): 4.09 (s, 1H, -NH), 7.15 – 8.06 (m, 13H, 12Ar-H and 1 -NH)

***N*'-(acridin-9-yl)-4-fluorobenzohydrazide (AA-14):** yield: 52.35%, mp 310^{0}C; IR (cm^{-1}): 3361.49 (sec. N-H stretching), 3292.31 (Amide N-H stretch), 3097.68 (Aromatic C-H stretching), 1692.65 (C=O stretching), 1587.42- 1438.90 (aromatic C=C stretch), ^{1}H NMR (400 MHz, DMSO, δppm): 4.06 (s, 1H, -NH), 7.11 – 8.10 (m, 13H, 12Ar-H and 1 -NH)

***N*'-(acridin-9-yl)-4-chlorobenzohydrazide (AA-15):** yield: 79.89%, mp 298^{0}C; IR (cm-1): 3415.93 (sec. N-H stretching), 1651.07 (C=O stretching), 1562.65-1497.01 (aromatic C=C stretch), ^{1}H NMR (400 MHz, DMSO, δppm): 4.06 (s, 1H, -NH), 7.15 – 8.18 (m, 13H, 12Ar-H and 1 -NH)

***N*'-(acridin-9-yl)-2-bromobenzohydrazide (AA-16):** yield: 68.97%, mp 277^{0}C, IR (cm-1): 3361.49 (sec. N-H stretching), 3292.31 (Amide N-H stretch), 3097.68 (Aromatic C-H stretching), 1692.65 (C=O stretching), 1587.42- 1438.90 (aromatic C=C stretch); 1H NMR (400 MHz,: DMSO, δppm): 3.63 (br, 1H, -NH), 7.09 – 8.58 (m, 13H, 12 Ar-H and 1 -NH)

***N*'-(acridin-9-yl)-2,4-dichlorobenzohydrazide (AA-17):** yield: 76.29%, mp 288^{0}C; IR (cm^{-1}): 3372.20 (sec. N-H stretching), 3102-3010 (Aromatic C-H stretching), 1648.27 (C=O stretching), 1525.06-1412.64 (aromatic C=C stretch), ^{1}H NMR (400 MHz, DMSO, δppm): 4.15 (s, 1H, -NH), 7.42 – 8.15 (m, 12H, 11Ar-H and 1 -NH)

***N*'-(4-(2-(acridin-9-yl)hydrazinecarbonyl)phenyl)acetamide (AA-18):** yield: 68.92%, mp 285^{0}C; ; IR (cm-1): 3356.14 (sec. N-H stretching), 3251.98 (Amide N-H stretch), 1645.28 (C=O), 1588.42- 1427.42 (aromatic C=C stretch), ^{1}H NMR (400 MHz, DMSO, δppm): 2.04 (s, 3H, -CH3), 4.10 (s, 1H, -NH), 7.46 – 8.12 (m, 14H, 12Ar-H and 2 -NH)

***N*'-(acridin-9-yl)-3-methoxybenzohydrazide (AA-19):** yield: 65.40%, mp 285^{0}C, IR (cm^{-1}): 3390.49 (sec. N-H stretching), 3235.55 (Amide N-H stretch), 3040-3018 (Aromatic C-H stretching), 2894 (Aliphatic C-H stretching), 1621.45 (C=O stretching), 1582.42-1518.05 (aromatic C=C stretch), ^{1}H NMR (400 MHz, DMSO, δppm): 3.86 (s, 3H, OCH_3), 4.13 (s, 1H, -NH), 6.95 – 8.28 (m, 13H, 12 Ar-H and 1 -NH)

***N*'-(acridin-9-yl)-3,4-dimethoxybenzohydrazide (AA-110):** yield: 83.26%, mp 286^{0}C; ; IR (cm-1): 3390.49 (sec. N-H stretching), 3277.06 (Amide N-H stretch), 1639.49 (C=O stretching), 1591.27- 1516.05 (aromatic C=C stretch), ^{1}H NMR (400 MHz, DMSO, δppm): 3.73-3.78 (s, 6H, $2OCH_3$), 4.15 (s, 1H, -NH), 6.84 – 8.12 (m, 12H, 11Ar-H and 1 -NH)

***N*'-(acridin-9-yl)-3-amino-4-methylbenzohydrazide (AA-111):** yield: 57.24%, mp 275^{0}C; IR (cm^{-1}): 3334.92 (sec. N-H stretching), 2925 (Aliphatic C-H stretching), 1639.49 (C=O stretching), 1586.39-1516.30 (aromatic C=C stretch), ^{1}H NMR (400 MHz, DMSO, δppm): 2.35 (s, 3H, $-CH_3$), 4.05-4.61 (hump, 3H), 6.99 – 7.98 (m, 12H, 11 Ar-H and 1 -NH)

***N*'-(acridin-9-yl)isonicotinohydrazide (AA-112):** yield: 74.57%, mp 301^{0}C; ; IR (cm-1): 3277.06 (Amide N-H stretch), 3026.31 (Aromatic C-H stretch), 1641.42 (C=O stretching), 1565.42- 1504.05 (aromatic C=C stretch), ^{1}H NMR (400 MHz, DMSO, δppm): 3.98 (s, 1H, -NH), 7.42 – 9.06 (m, 13H, 12Ar-H and 1 -NH)

5.2 Synthesis of *N*-Phenyl-2-[(phenylsulfonyl)amino]acetamide derivatives

5.2.1 Synthesis

To synthesize *N*-Phenyl-2-[(phenylsulfonyl)amino]acetamide derivaties, following scheme was used. Total of 33 compounds were synthesized.

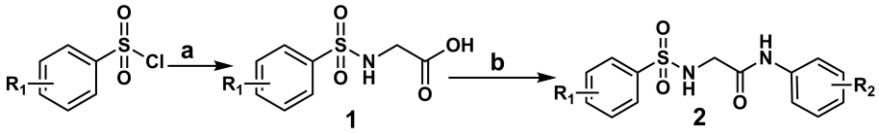

Scheme 2: Reagents and conditions: (a) $NaHCO_3$, glycine, 80^{0}C, 2-3 h (b) HOBt, EDC-HCl, DCM, TEA, substituted aniline, 0^{0}C, 12 h.

Synthesis of 1: To approximately 2.5 equivalent of sodium bicarbonate in water, was added 1 equivalent of glycine. The solution was stirred at 80^0 C till complete dissolution. It was cooled to around 50^0 C and then 1 equivalent of substituted phenyl sulfonyl chloride was added. The solution was stirred for 2-3 hours at 80^{0}C. The reaction completion was monitord by TLC. The solution was cooled to 10^0 C, neutralized with 1M HCl and kept for 30 min for precipitation. The solid compound was filtered out using vacuum and dried.

Synthesis of 2: To 1 equivalent of compound 1, was added 2.2 equivalent of HOBt and 2.2 equivalent of EDC.HCl. About 20 ml dichloromethane was added and stirred. To this, was added triethylamine and 2.5 equivalent of substituted aniline derivative. The reaction was allowed to stir at 0^{0}C overnight. The completion of the reaction was monitored by TLC and then worked up with DCM, dil. HCl and saturated sodium bicarbonate solution.

5.2.2 Mechanism

Formation of compound 1 is a nucleophilic substitution reaction which involves the reaction between halide and an amine thereby liberating halogen acid. Synthesis of compound 2 is amide formation reaction from carboxylic acid and amine using HOBT-EDC.HCl as coupling reagent. The acid reacts with carbodiimide so as to form the key intermediate; O-acyl isourea which then reacts with amine to produce the desired amide and substituted urea as byproduct. The mechanism is given in previous section 5.1.2

5.1.3 Spectral data

2-(4-methylphenylsulfonamido)-*N*-phenylacetamide (2.1): Off –white solid, yield: 89%, mp 150-152 ^{0}C IR (cm^{-1}, KBr): 3363.86 (sec. N-H stretching), 3253.91 (sec. N-H stretching), 3100.5 (Aromatic C-H stretching), 2967 (Aliphatic C-H stretching), 1093.64 (S=O), ^{1}H NMR (400 MHz, DMSO-d_6, δ ppm): 2.34 (s, 3H, methyl), 3.62 (d, 2H, CH_2), 6.90- 7.75 (m, 9H, Ar-H), 7.80 (t, 1H, -NH), 9.78 (s, 1H, -NH); ESI-MS m/z: 305.16 $[M+H]^+$, 327.10 $[M+Na]^+$

***N*-(4-chlorophenyl)-2-(phenylsulfonamido)acetamide (2.2):**Light brown solid, yield: 78%, mp: 164-166^{0}C, IR (cm^{-1}, KBr): 3471.87(sec. N-H stretching), 3379.29 (sec. N-H stretching), 3026.31 (Aromatic C-H stretching), 2985.81 (Aliphatic C-H stretching), 1684.01 (C=O), 1598.20-1535.67 (aromatic C=C bend) , ^{1}H NMR (400 MHz, DMSO-d_6, δ ppm): 3.69 (d, 2H, CH_2), 7.00- 7.77 (m, 9H, Ar-H), 7.85 (t, 1H, -NH), 9.46 (s, 1H, -NH); ESI-MS m/z: 325.14 $[M+H]^+$

***N*-(3-chlorophenyl)-2-(phenylsulfonamido)acetamide (2.3):** Light brown solid, yield: 81%%, mp: 162-164^{0}C, IR (cm^{-1}, KBr): 3471.83(sec. N-H stretching), 3379.12 (sec. N-H stretching), 3024.51 (Aromatic C-H stretching), 2985.81 (Aliphatic C-H stretching), 1684.01 (C=O), 1598.20-1535.67 (aromatic C=C bend), ^{1}H NMR (400 MHz, DMSO-d_6, δ ppm): 3.65 (d, 2H, CH_2), 7.05- 7.82 (m, 9H, Ar-H), 7.89 (t, 1H, -NH), 9.72 (s, 1H, -NH); ESI-MS m/z: 325.14 $[M+H]^+$

N*-(2,4-dimethylphenyl)-2-(phenylsulfonamido)acetamide (2.4*: Off-white solid, yield: 82%, mp: 180-182^{0}C, IR (cm^{-1}, KBr): 3481.83(sec. N-H stretching), 3359.42 (sec. N-H stretching), 3025.81 (Aromatic C-H stretching), 2985.81 (Aliphatic C-H stretching), 2965.51 (Aliphatic C-H stretching), 1688.01 (C=O), 1598.20-1535.67 (aromatic C=C bend), ^{1}H NMR (400 MHz, DMSO-d_6, δ ppm): 2.39 (s, 3H, *o*-CH_3), 2.59 (s, 3H, *p*-CH_3), 3.59 (d, 2H, CH_2), 7.10- 7.95 (m, 8H, Ar-H), 7.99 (t, 1H, -NH), 9.88 (s, 1H, -NH)

***N*-phenyl-2-(phenylsulfonamido)acetamide (2.5):** Dark yellow powder, yield: 82%, mp: 180-182 ^{0}C, IR (cm^{-1}, KBr): 3327.21 (sec. N-H stretching), 3234.62 (sec. N-H stretching), 3132.52 (Aromatic C-H stretching), 2910.58 (Aliphatic C-H stretching), 1691.57 (C=O), 1604.77-1522.67 (aromatic C=C bend), ^{1}H NMR (400 MHz, DMSO-d_6, δ ppm): 3.65 (d, 2H, -CH_2), 7.00-7.99 (m, 10H, Ar-H), 8.17 (t, 1H, -NH), 9.81 (s, 1H, –NH)

***N*-(4-chlorophenyl)-2-(4-methylphenylsulfonamido)acetamide (2.6):** Off-white powder, yield: 79%, mp 187-190 ^{0}C, IR (cm^{-1}, KBr): 3363.86 (sec. N-H stretching), 3253.91 (sec. N-H stretching), 3043.5 (Aromatic C-H stretching), 2978 (Aliphatic C-H stretching), 1093.64 (S=O); ^{1}H NMR (400 MHz, DMSO-d_6, δ ppm): 2.36 (s, 3H, *p*-CH_3), 3.62 (d, 2H, CH_2), 7.25 (d, 2H, Ar-H), 7.31 (d, 2H, Ar-H), 7.49-7.68 (m, 4H, Ar-H), 7.99 (t, 1H, -NH), 9.94 (s, 1H, -NH)

***N*-(3-chlorophenyl)-2-(4-methylphenylsulfonamido)acetamide (2.7):** Light brown solid, yield: 78%, mp 178-180 ^{0}C, IR (cm^{-1}, KBr): 3332.96 (sec. N-H stretching), 3263.86 (sec. N-H

stretching), 3078.35 (Aromatic C-H stretching), 2897 (Aliphatic C-H stretching), 1697.36 (C=O), 1595.13- 1444.68 (aromatic C=C stretch), ^{1}H NMR (400 MHz,

***N*-(2,4-dimethylphenyl)-2-(4-methylphenylsulfonamido)acetamide (2.8):** Light yellow solid, yield 83%, mp: 184-186^{0}C, IR (cm^{-1}, KBr): 3311.78 (sec. N-H stretching), 3277.06 (sec. N-H stretching), 3026.31 (Aromatic C-H stretching), 2939 (Aliphatic C-H stretching), 1651.07 (C=O), 1593.20 (aromatic C=C stretch); ^{1}H NMR (400 MHz, $CDCl_3$, δ ppm): 2.17 (s, 3H, *p*-CH_3), 2.27 (s, 3H, *o*-CH_3), 2.42 (s, 3H, *p*-CH_3), 3.69 (d, 2H, CH_2), 5.29 (t, 1H, -NH), 6.96-7.88 (m , 7H, Ar-H), 7.98 (s, 1H, -NH)

2-(2-methylphenylsulfonamido)-*N*-phenylacetamide (2.9): Light yellow solid, yield 79%, mp 183-184 ^{0}C, IR (cm^{-1}, KBr): 3340.71 (sec. N-H stretching), 3275.15 (sec. N-H stretching), 3024.38 (Aromatic C-H stretching), 2962.66 (Aliphatic C-H stretching), 1651.07 (C=O), 1537.27 (aromatic C=C stretch);^{1}H NMR (400 MHz, DMSO-d_6, δ ppm): 2.62 (s, 3H, CH_3), 3.68 (d, 2,H CH_2), 6.99-7.89 (m, 9H, Ar-H), 7.94 (t, 1H, -NH), 9.78 (s, 1H, -NH)

2-(4-chlorophenylsulfonamido)-*N*-phenylacetamide (2.10): Yellow solid, yield 78%, mp: 173-175^{0}C, IR (cm^{-1}, KBr): 3330.78 (sec. N-H stretching), 3265.15 (sec. N-H stretching), 3034.38 (Aromatic C-H stretching), 1641.07 (C=O), 1527.27 (aromatic C=C stretch); ^{1}H NMR (400 MHz, $CDCl_3$, δ ppm): 3.49 (d, 2H, CH_2), 7.16-7.78 (m , 9H, Ar-H), 8.04 (t, 1H, -NH), 9.62 (s, 1H, -NH)

3*N*-(4-chlorophenyl)-2-(4-chlorophenylsulfonamido)acetamide (2.11)*:*** Off-white solid, yield: 83%, mp 125-127 ^{0}C, IR (cm^{-1}, KBr): 3353.78 (sec. N-H stretching), 3281.27 (sec. N-H stretching), 3156.25 (Aromatic C-H stretching), 1730.15 (C=O), 1597.20-1473.43 (aromatic C=C stretch); ^{1}H NMR (400 MHz, $CDCl_3$, δ ppm): 3.59 (d, 2H, CH_2), 7.36-7.78 (m , 8H, Ar-H), 7.95 (t, 1H, -NH), 8.92 (s, 1H, -NH)

***N*-(3-chlorophenyl)-2-(4-chlorophenylsulfonamido)acetamide (2.12):** Off-white solid, yield: 89%, mp 115-117 ^{0}C, IR (cm^{-1}, KBr): 3343.58 (sec. N-H stretching), 3261.27 (sec. N-H stretching), 3136.25 (Aromatic C-H stretching), 1720.15 (C=O), 1567.20-1479.43 (aromatic C=C stretch); ^{1}H NMR (400 MHz, $CDCl_3$, δ ppm): 3.39 (d, 2H, CH_2), 7.26-8.38 (m , 8H, Ar-H), 8.42 (t, 1H, -NH), 8.98 (s, 1H, -NH)

2-(4-chlorophenylsulfonamido)-*N*-(2,4-dimethylphenyl)acetamide (2.13): Off-white to light yellow solid, yield: 81%, mp 142-146 ^{0}C, IR (cm^{-1}, KBr): 3319.78 (sec. N-H stretching), 3263.56 (sec. N-H stretching), 3124.68 (Aromatic C-H stretching), 2939 (Aliphatic C-H stretching), 2969 (Aliphatic C-H stretching), 1681.93 (C=O), 1593.20- 1500.62 (aromatic C=C stretch); ^{1}H NMR (400 MHz, $CDCl_3$, δ ppm): 2.65 (s, 3H, *o*-CH_3), 2.68 (s, 3H, *p*-CH_3), 3.64 (d, 2H, CH_2), 7.16-7.78 (m , 7H, Ar-H), 7.86 (t, 1H, -NH), 8.92 (s, 1H, -NH)

2-(4-acetamidophenylsulfonamido)-*N*-phenylacetamide (2.14): Off-white solid, yield:85%, mp 98-100^{0}C, IR (cm^{-1}, KBr): 3410.58 (sec. N-H stretching), 3319.49 (sec. N-H stretching), 3217.31 (Aromatic C-H stretching), 2864.29 (Aliphatic C-H stretching), 1716.65 (C=O), 1587.42- 1438.90 (aromatic C=C stretch); ^{1}H NMR (400 MHz, DMSO-d_6, δ ppm): 2.49 (s, 3H, -$COCH_3$), 3.61 (s, 2H, -CH_2), 5.89 (s, 1H, -NHCO), 7.02-7.84 (m, 9H, Ar-H), 7.92(t, 1H, -NH), 8.83 (s, 1H, -NH)

2-(4-acetamidophenylsulfonamido)-*N*-(4-chlorophenyl)acetamide (2.15): Off-white solid, yield: 82%, mp 155-160 ^{0}C, IR (cm^{-1}, KBr): 3388.98 (sec. N-H stretching), 3300.20, 3275.13 (sec. N-H stretching), 3054.31 (Aromatic C-H stretching), 2939 (Aliphatic C-H stretching), 1693.50 (C=O), 1670-1535.34 (aromatic C=C stretch), ^{1}H NMR (400 MHz, DMSO-d_6, δ ppm): 2.67 (s, 3H, -$COCH_3$), 3.81 (s, 2H, -CH_2), 5.54 (s, 1H, -NHCO), 7.12-7.52 (m, 8H, Ar-H), 7.63 (t, 1H, -NH), 9.21 (s, 1H, -NH), ESI-MS m/z: 382.12 $[M+H]^+$

2-(4-acetamidophenylsulfonamido)-*N*-(3-chlorophenyl)acetamide (2.16): Off-white solid, yield: 91%, mp 164-168^{0}C, IR (cm^{-1}, KBr): 3435.78 (sec. N-H stretching), 3277.06 (sec. N-H stretching), 3026.31 (Aromatic C-H stretching), 2971 (Aliphatic C-H stretching), 1678.07 (C=O), 1598.20-1535.67 (aromatic C=C stretch), ^{1}H NMR (400 MHz, DMSO-d_6, δ ppm): 2.73 (s, 3H, -$COCH_3$), 3.24 (s, 2H, -CH_2), 5.21 (s, 1H, -NHCO), 7.05-7.84 (m, 8H, Ar-H), 7.95 (t, 1H, -NH), 9.28 (s, 1H, -NH)

2-(4-acetamidophenylsulfonamido)-*N*-(2,4-dimethylphenyl)acetamide (2.17): Off-white solid; yield: 88%, mp 152-154^{0}C, IR (cm^{-1}, KBr): 3465.78 (sec. N-H stretching), 3237.06 (sec. N-H stretching), 3006.31 (Aromatic C-H stretching), 2977 (Aliphatic C-H stretching), 1688.07 (C=O), 1588.70-1535.67 (aromatic C=C stretch), ^{1}H NMR (400 MHz, DMSO-d_6, δ ppm): 2.46 (s, 3H, *o*-CH_3), 2.52 (s, 3H, *p*-CH_3), 2.89 (s, 3H, -$COCH_3$), 4.22 (s, 2H, -CH_2), 5.51 (s, 1H, -NHCO), 7.22-7.96 (m, 7H, Ar-H), 8.1 (t, 1H, -NH), 8.99 (s, 1H, -NH)

2-(3-nitrophenylsulfonamido)-*N*-phenylacetamide (2.18): Off-white solid, yied:79%, mp 172-176 ^{0}C, IR (cm^{-1}, KBr): 3435.78 (sec. N-H stretching), 3290.56 (sec. N-H stretching), 3026.31 (Aromatic C-H stretching), 1647.21 (C=O), 2985.84 (Aliphatic C-H stretching), 1620.97-1532.81 (aromatic C=C stretch), ^{1}H NMR (400 MHz, DMSO-d_6, δ ppm): 3.82 (s, 2H, -CH_2), 7.32-7.95 (m, 9H, Ar-H), 8.14 (t, 1H, -NH), 9.08 (s, 1H, -NH); ESI-MS m/z: 336.11 $[M+H]^+$, 358.10 $[M+Na]^+$

***N*-(4-chlorophenyl)-2-(3-nitrophenylsulfonamido)acetamide (2.19):** Off-white solid, yield: 72%, mp 185-187 ^{0}C, IR (cm^{-1}, KBr): 3350.35 (sec. N-H stretching), 3277.06 (sec. N-H stretching), 3070.68 (Aromatic C-H stretching), 2975.84 (Aliphatic C-H stretching), 1670.35

(C=O), 1598.20-1535.67 (aromatic C=C bend), ^{1}H NMR (400 MHz, DMSO-d_6, δ ppm): 3.62 (s, 2H, -CH_2), 7.22-7.99 (m, 8H, Ar-H), 8.13 (t, 1H, -NH), 9.27 (s, 1H, -NH)

***N*-(3-chlorophenyl)-2-(3-nitrophenylsulfonamido)acetamide (2.20):** Light brown powder, yield: 75%, mp 150-154 ^{0}C, IR (cm^{-1}, KBr): 3367.71 (sec. N-H stretching), 3219.19 (sec. N-H stretching), 3101.54 (Aromatic C-H stretching), 1697.36 (Amide C=O), 1593.20-1415.75 (aromatic C=C bend), ^{1}H NMR (400 MHz, DMSO-d_6, δ ppm): 3.51 (s, 2H, -CH_2), 7.05-7.81 (m, 8H, Ar-H), 7.99 (t, 1H, -NH), 8.47 (s, 1H, -NH); ESI-MS m/z: 370.08 $[M+H]^+$

***N*-(2,4-dimethylphenyl)-2-(3-nitrophenylsulfonamido)acetamide (2.21):** Light brown powder; yield: 71%, mp 158-160^{0}C, IR (cm^{-1}, KBr): 3465.78 (sec. N-H stretching), 3237.06 (sec. N-H stretching), 3006.31 (Aromatic C-H stretching), 2977 (Aliphatic C-H stretching), 1688.07 (C=O), 1588.70-1535.67 (aromatic C=C stretch), ^{1}H NMR (400 MHz, DMSO-d_6, δ ppm): 2.43 (s, 3H, *o*-CH_3), 2.51 (s, 3H, *p*-CH_3), 3.52 (s, 2H, -CH_2), 7.22-7.96 (m, 7H, Ar-H), 8.98 (s, 1H, -NH)

2-(2-nitrophenylsulfonamido)-*N*-phenylacetamide (2.22): Dark brown solid, yield: 73%, mp 160-161 ^{0}C; IR (cm^{-1}, KBr): 3445.28 (sec. N-H stretching), 3280.76 (sec. N-H stretching), 3036.37 (Aromatic C-H stretching), 1645.11 (C=O), 2988.84 (Aliphatic C-H stretching), 1622.97-1530.81 (aromatic C=C stretch), ^{1}H NMR (400 MHz, DMSO-d_6, δ ppm): 3.80 (s, 2H, -CH_2), 7.12-7.85 (m, 9H, Ar-H), 8.01 (t, 1H, -NH), 9.25 (s, 1H, -NH)

***N*-(4-chlorophenyl)-2-(2-nitrophenylsulfonamido)acetamide (2.23):** Brown solid, yield: 69%, mp 141-144^{0}C, IR (cm^{-1}, KBr): 3369.64 (sec. N-H stretching), 3217.27 (sec. N-H stretching), 3099.31 (Aromatic C-H stretching), 2873.94 (Aliphatic C-H stretching), 1703.14 (C=O), 1614-1531.48 (aromatic C=C stretch), ^{1}H NMR (400 MHz, DMSO-d_6, δ ppm): 3.62 (s, 2H, -CH_2), 6.95-7.72 (m, 8H, Ar-H), 7.91 (t, 1H, -NH), 8.95 (s, 1H, -NH)

***N*-(3-chlorophenyl)-2-(2-nitrophenylsulfonamido)acetamide (2.24):** Brown solid; yield: 74%, mp 182-184^{0}C, IR (cm^{-1}, KBr): 3357.41 (sec. N-H stretching), 3229.19 (sec. N-H stretching), 3121.54 (Aromatic C-H stretching), 1687.36 (Amide C=O), 1597.10-1415.75 (aromatic C=C bend), ^{1}H NMR (400 MHz, DMSO-d_6, δ ppm): 3.57 (s, 2H, -CH_2), 6.87-7.82 (m, 8H, Ar-H), 7.90 (t, 1H, -NH), 9.01 (s, 1H, -NH)

***N*-(2,4-dimethylphenyl)-2-(2-nitrophenylsulfonamido)acetamide (2.25):** Light yellow solid, yield: 73%, mp 165-167 ^{0}C, IR (cm^{-1}, KBr): 3370.64 (sec. N-H stretching), 3255.84 (sec. N-H stretching), 3043.67 (Aromatic C-H stretching), 2945.30 (Aliphatic C-H stretching), 1616.35 (C=O), 1598.53-1465.87 (aromatic C=C bend), ^{1}H NMR (400 MHz, DMSO-d_6, δ ppm): 2.35(s, 3H, *o*-CH_3), 2.57 (s, 3H, *p*-CH_3), 3.46 (s, 2H, -CH_2), 7.05-7.76 (m, 7H, Ar-H), 7.95 (t, 1H, -NH), 9.12 (s, 1H, -NH)

2-(4-nitrophenylsulfonamido)-*N*-phenylacetamide (2.26): Light yellow powder; yield: 83%, mp 175-177^{0}C, IR (cm^{-1}, KBr): 3465.28 (sec. N-H stretching), 3260.76 (sec. N-H stretching), 3056.37 (Aromatic C-H stretching), 1655.11 (C=O), 2978.84 (Aliphatic C-H stretching), 1632.97-1530.81 (aromatic C=C stretch), ^{1}H NMR (400 MHz, DMSO-d_6, δ ppm): 3.65 (s, 2H, -CH_2), 7.22-7.85 (m, 9H, Ar-H), 8.79 (s, 1H, -NH)

***N*-(4-chlorophenyl)-2-(4-nitrophenylsulfonamido)acetamide (2.27):** White solid, yield: 79%, mp 90-92^{0}C, IR (cm^{-1}, KBr): 3435.78 (sec. N-H stretching), 3277.06 (sec. N-H stretching), 3026.31 (Aromatic C-H stretching), 2971 (Aliphatic C-H stretching), 1678.07 (C=O), 1598.20-1535.67 (aromatic C=C stretch), ^{1}H NMR (400 MHz, DMSO-d_6, δ ppm): 3.41 (s, 2H, -CH_2), 6.91-7.54 (m, 8H, Ar-H), 7.98 (t, 1H, -NH), 8.87 (s, 1H, -NH)

***N*-(3-chlorophenyl)-2-(4-nitrophenylsulfonamido)acetamide (2.28):** Off-white solid; yield: 72%, mp 120-122^{0}C, IR (cm^{-1}, KBr): 3357.41 (sec. N-H stretching), 3229.19 (sec. N-H stretching), 3121.54 (Aromatic C-H stretching), 1687.36 (Amide C=O), 1597.10-1415.75 (aromatic C=C bend), ^{1}H NMR (400 MHz, DMSO-d_6, δ ppm): 3.42 (s, 2H, -CH_2), 7.05-8.10 (m, 8H, Ar-H), 8.25 (t, 1H, -NH), 9.45 (s, 1H, -NH)

***N*-(2,4-dimethylphenyl)-2-(4-nitrophenylsulfonamido)acetamide (2.29):** Off-white solid; yield: 84%, mp 111-113^{0}C , IR (cm^{-1}, KBr): 3370.64 (sec. N-H stretching), 3255.84 (sec. N-H stretching), 3043.67 (Aromatic C-H stretching), 2945.30 (Aliphatic C-H stretching), 1616.35 (C=O), 1598.53-1465.87 (aromatic C=C bend), ^{1}H NMR (400 MHz, DMSO-d_6, δ ppm): 2.52 (s, 3H, *o*-CH_3), 2.65 (s, 3H, *p*-CH_3), 3.97 (s, 2H, -CH_2), 6.98-7.96 (m, 7H, Ar-H), 8.01 (t, 1H, -NH), 9.65 (s, 1H, -NH)

2-(4-methoxyphenylsulfonamido)-*N*-phenylacetamide (2.30): Dark yellow solid, yield: 83%, mp 158-160 ^{0}C, IR (cm^{-1}, KBr): 3369.64 (sec. N-H stretching), 3292.49 (sec. N-H stretching), 3097.68 (Aromatic C-H stretching), 2883.58 (Aliphatic C-H stretching), 1673.86(C=O), 1598.20-1535.67 (aromatic C=C stretch), ^{1}H NMR (400 MHz, DMSO-d_6, δ ppm): 3.49 (s, 3H, -OCH_3), 3.54 (s, 2H, -CH_2), 7.05-7.94 (m, 9Ar-H, 1-NH), 9.98 (s, 1H, -NH)

***N*-(4-chlorophenyl)-2-(4-methoxyphenylsulfonamido)acetamide (2.31):** Light brown powder, yield: 68%, mp 156-158^{0}C, IR (cm^{-1}, KBr): 3327.21 (sec. N-H stretching), 3234.62 (sec. N-H stretching), 3076.46 (Aromatic C-H stretching), 2910.68 (Aliphatic C-H stretching), 1691.57 (C=O), 16-4.77-1552.70 (aromatic C=C bend), ^{1}H NMR (400 MHz, DMSO-d_6, δ ppm): 3.55 (s, 3H, -OCH_3), 3.84 (s, 2H, -CH_2), 7.15-7.95 (m, 8H, Ar-H), 8.05 (t, 1H, -NH), 9.54 (s, 1H, -NH)

***N*-(3-chlorophenyl)-2-(4-methoxyphenylsulfonamido)acetamide (2.32):** Yellow solid, yield: 74%, mp 128-130^{0}C, IR (cm^{-1}, KBr): 3350.35 (sec. N-H stretching), 3277.06 (sec. N-H

stretching), 3072.31 (Aromatic C-H stretching), 2877.79 (Aliphatic C-H stretching), 1670.35 (C=O), 1597.06- 1492.90 (aromatic C=C stretch), 1348.24 (C-O stretch), ^{1}H NMR (400 MHz, DMSO-d_6, δ ppm): 3.65 (s, 3H, -OCH_3), 3.86 (s, 2H, -CH_2), 7.12-7.96 (m, 8H, Ar-H), 8.11 (t, 1H, -NH), 9.28 (s, 1H, -NH)

***N*-(2,4-dimethylphenyl)-2-(4-methoxyphenylsulfonamido)acetamide (2.33):** Light brown solid, yield: 79%, mp 123-125^{0}C , IR (cm^{-1}, KBr): 3350.35 (sec. N-H stretching), 3277.06 (sec. N-H stretching), 3072.60 (Aromatic C-H stretching), 2877.79 (Aliphatic C-H stretching), 1670.35 (C=O), 1597.06- 1492.90 (aromatic C=C stretch), 1348.24 (C-O stretch), ^{1}H NMR (400 MHz, DMSO-d_6, δ ppm): 2.49 (s, 3H, *o*-CH_3), 2.55 (s, 3H, *p*-CH_3), 3.55 (s, 3H, -OCH_3), 3.41 (s, 2H, -CH_2), 7.22-7.96 (m, 8H, Ar-H, -NH), 9.98 (s, 1H, -NH)

5.3 Synthesis of substituted pyrimidine derivatives

5.3.1 Synthesis

Based upon the computational studies, the substituted pyrimidine derivatives were synthesized as given in the Scheme 3.

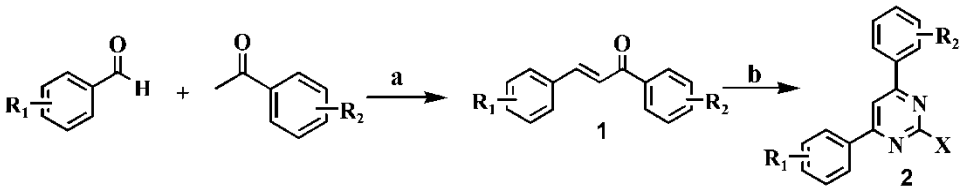

Scheme 3: Reagents and conditions: (a) NaOH, EtOH, rt, 4-6 h (b) NaOH, urea/thiourea/guanidine-HCl, EtOH, 70^{0}C, 2-8 h.

Synthesis of 1: An equimolar mixture of substituted benzaldehyde and acetophenone were dissolved in 15 ml ethanol. Then 10ml NaOH solution (6g in 10ml H_2O) was added drop wise to the reaction mixture with continuous stirring. The reaction temperature was maintained between 20-25˚ C using a cold water bath. The progress of the reaction was monitored by TLC. After vigorous stirring for 4-5 hours the reaction mixture was kept overnight. It was then neutralized by acidified cold water to precipitate the solid product. On filtering off, the crude chalcone was dried in air and recrystallized using ethanol.

Synthesis of 2: 1 equivalent of compound 1 and 2 equivalents of urea/thiourea/guanidine-HCl were dissolved in ethanol. 4 equivalents of ethanolic Sodium hydroxide was added to above mixture and refluxed for 2 to 8 hours. TLC of the reaction mixture was carried out to confirm the completion of the reaction. After completion of reaction, reaction mixture was poured in ice cooled water. Precipitate obtained was filtered, dried and recrystallized.

5.3.2 Mechanism

Benzylidene acetophenones were prepared by Claisen-Schmidt reaction [19] between substituted benzaldehyde and acetophenone in the presence of base. The reaction commences with formation of enolate ion by removal of α-hydrogen in presence of hydroxide. The nucleophilic enolate then attacks the carbonyl carbon of aromatic aldehyde to form an intermediate alkoxide (nucleophilic addition reaction). The alkoxide then deprotonates water producing hydroxide ion and β-hydroxyketone, the aldol product. Finally, the hydroxide acts as a base and removes an acidic β-hydrogen giving the reactive enolates. The electrons associated with a negative charge of the enolate are used to form a carbon-carbon double bond (C=C) and displace a leaving group, regenerating the hydroxide giving the final product, the conjugated ketone.

The plausible mechanism for the formation of compounds in the second step involves addition of urea/thiourea/guanidine-HCl nitrogen to the double bond to give aminoalcohol, which then undergoes intramolecular cyclization and subsequent aromatization via elimination water molecules under the reaction conditions.

Mechanism Step 1

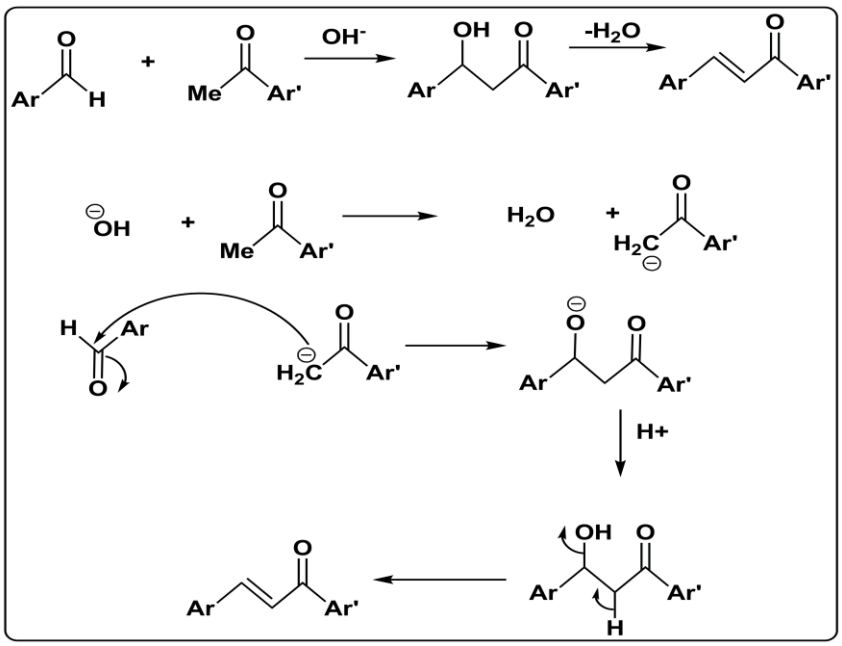

Mechanism Step 2:

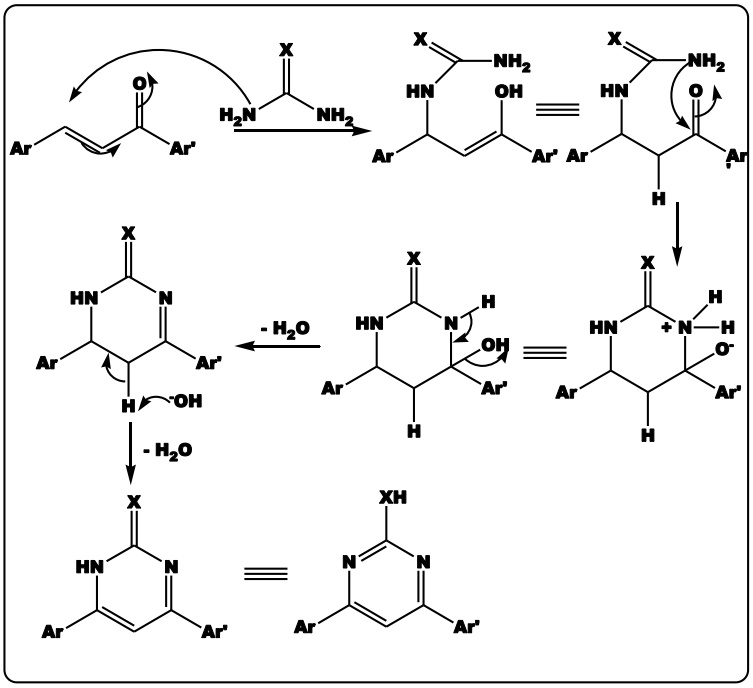

5.3.3 Spectral data

4-(3-nitrophenyl)-6-phenylpyrimidin-2-amine (2.1G): Yield 21.72%, mp: 128-130^{0}C, IR (cm^{-1}, KBr): 3502.73, 3386.30 (sharp, NH_2 Primary amine, N-H stretching), 3058.10 (Aromatic C-H stretching), 1592.00, 1522.67, 1437.29 (aromatic C=C stretching), 1347.24 (C-N stretch); ^{1}H-NMR (400 MHz, CDCl3, δ ppm): 5.25 (s, 2H, NH_2), 7.53-7.58 (m, 4H, ArH), 7.66-7.72 (dd, 1H, ArH), 8.09-8.13 (m, 2H, ArH), 8.34 (d, 1H, Ar-H), 8.42 (d, 1H, Ar-H), 8.96 (s, 1H, Ar-H). ESI-MS (m/z): 293.16 ($C_{16}H_{12}N_3O_2$, $[M+H]^+$)

4-(4-nitrophenyl)-6-phenylpyrimidin-2-amine (2.2G): Yield 56.09%, mp:112-115^{0}C, IR (cm^{-1}, KBr): 3506.58, 3387.30 (sharp, NH_2 Primary amine, N-H stretching), 3070.11 (Aromatic C-H stretching), 1588.00, 1524.69, 1449.47 (aromatic C=C stretching), 1354.14 (C-N stretch); ^{1}H-NMR (400 MHz, CDCl3, δ ppm): 5.60 (s, 2H, NH_2), 6.75-6.79 (d, 2H, Ar-H), 7.32 (s, 1H, pyrimidine-H_5), 7.44- 7.49 (m, 3H, Ar-H), 7.92-7.95 (d, 2H, Ar-H), 8.02-8.04 (dd, 2H, Ar-H). ESI-MS (m/z): 293.17 ($C_{16}H_{12}N_3O_2$, $[M+H]^+$)

4-(4-methoxyphenyl)-6-m-tolylpyrimidin-2-amine (2.3G): Yield 68.23%, mp 95-100^{0}C, IR (cm^{-1}, KBr): 3495.11, 3393.39 (NH_2 Primary amine, N-H stretching), 3081.32 (Aromatic C-H stretching), 2931.39 (Aliphatic C-H stretching for OCH_3), 1669.47 (C=N stretch), 1594.21, 1523.64, 1453.28 (aromatic C=C stretching), 1351.17 (C-N stretch); ^{1}H-NMR (400 MHz, CDCl3, δ ppm): 2.36 (s, 3H, CH_3), 3.88 (s, 3H, OCH_3), 5.74 (s, 2H, NH_2), 7.23-7.28 (d, 2H, Ar-

H), 7.56 (s, 1H, Ar-H), 7.67 (s, 1H, pyrimidine-H_5), 7.77- 7.89 (m, 4H, Ar-H), 7.96 (m, 1H, Ar-H). ESI-MS (m/z): 292.17 ($C_{18}H_{17}N_3O$, $[M+H]^+$)

4-(4-aminophenyl)-6-(3-nitrophenyl)pyrimidin-2-amine (2.4G): Yield 53.28%, mp:122-125^{0}C, IR (cm^{-1}, KBr): 3508.58, 3382.30 (s, sharp, NH_2 Primary amine, N-H stretching), 3077.11 (Aromatic C-H stretching), 1593.00, 1529.69, 1452.47 (aromatic C=C stretching), 1356.44 (C-N stretch); ^{1}H-NMR (400 MHz, CDCl3, δ ppm): 5.16 (s, 2H, NH_2), 6.27 (s, 2H, NH_2), 7.21-7.27 (d, 2H, Ar-H), 7.61 (s, 1H, pyrimidine-H_5), 7.81-8.11 (m, 4H, Ar-H) 8.36 (t, 1H, Ar-H), 8.58 (s, 1H, Ar-H). ESI-MS (m/z): 308.31 ($C_{16}H_{13}N_5O_2$, $[M+H]^+$)

4-(3-bromophenyl)-6-(3-nitrophenyl)pyrimidin-2-amine (2.5G): Yield 78.56%, mp 136-138^{0}C IR (cm^{-1}, KBr): 3516.23, 3311.78 (s, NH_2 Primary amine, N-H stretching), 3066.82 (Aromatic C-H stretching), 1660.35 (C=N stretch), 1589.34- 1471.69 (aromatic C=C stretching); ^{1}H-NMR (400 MHz, CDCl3, δ ppm): 5.73 (s, 2H, NH_2), 6.71-6.76 (d, 2H, Ar-H), 7.47 (s, 1H, Ar-H), 7.57 (s, 1H, pyrimidine-H_5), 7.62- 7.65 (m, 2H, Ar-H), 7.83 (s, 1H, Ar-H), 7.96-8.08 (d, 2H, Ar-H). ESI-MS (m/z): 372.18 ($C_{16}H_{11}BrN_4O_2$, $[M+H]^+$)

4-(2,4-dichlorophenyl)-6-(3-nitrophenyl)pyrimidin-2-amine (2.6G): Yield 78.15%, mp 110-112^{0}C, IR (cm^{-1} KBr): 3320.61, 3176.50 (NH_2 Primary amine, N-H stretching), 3084.29 (Aromatic C-H stretching), 1655.35 (C=N stretch), 1571.87, 1517.77, 1428.94 (aromatic C=C stretching), 1260.90 (C-N stretch); ^{1}H-NMR (400 MHz, CDCl3, δ ppm): 5.89 (s, 2H, NH_2), 7.02-7.13 (d, 2H, Ar-H), 7.60 (s, 1H, pyrimidine-H_5), 7.88 (s, 1H, Ar-H), 8.15- 8.23 (m, 4H, Ar-H). ESI-MS (m/z): 362.08 ($C_{16}H_{10}Cl_2N_4O_2$, $[M+H]^+$)

4-(4-chlorophenyl)-6-phenylpyrimidin-2-amine (2.7G): Yield 85.43%, mp: 125-127^{0}C, IR (cm^{-1}, KBr): 3492.54, 3366.71 (NH_2 Primary amine, N-H stretching), 3082.27 (Aromatic C-H stretching), 2937.29 (Aliphatic C-H stretching for OCH_3), 1671.35 (C=N stretch), 1596.69, 1526.69, 1451.47 (aromatic C=C stretching), 1357.17 (C-N stretch), ^{1}H-NMR (400 MHz, CDCl3, δ ppm): 5.24 (s, 2H, NH_2), 7.43 (d, 2H, ArH), 7.45 (s, 1H, Ar-H), 7.46-7.50 (m, 4H, ArH), 7.93 (m, 1H, Ar-H), 8.00-8.03 (d, 2H, ArH). ESI-MS (m/z): 282.11 ($C_{16}H_{12}ClN_3$, $[M+H]^+$)

4-(4-chlorophenyl)-6-p-tolylpyrimidin-2-amine (2.8G): Yield 78.15%, mp: 146-150^{0}C, IR (cm^{-1}, KBr): 3496.94, 3392.79 (NH_2 Primary amine, N-H stretching), 3080.32 (Aromatic C-H stretching), 2938.46 (Aliphatic C-H stretching), 1670.35 (C=N stretch), 1598.99, 1525.69, 1442.57 (aromatic C=C stretching), 1350.17 (C-N stretch); ^{1}H-NMR (400 MHz, CDCl3, δ ppm): 2.39 (s, 3H, CH_3), 5.91 (s, 2H, NH_2), 7.26-7.34 (d, 2H, Ar-H), 7.62 (s, 1H, pyrimidine-H_5), 7.67-7.82 (m, 4H, Ar-H), 7.96-8.04 (d, 2H, Ar-H). ESI-MS (m/z): 296.13 ($C_{17}H_{14}ClN_3$, $[M+H]^+$)

4-(4-chlorophenyl)-6-(2,4-dimethoxyphenyl)pyrimidin-2-amine (2.9G): Yield 74.32%, mp 130-132^{0}C, IR (cm^{-1} KBr): 3493.42, 3398.05 (NH_2 Primary amine, N-H stretching), 3083.12

(Aromatic C-H stretching), 2936.19 (Aliphatic C-H stretching for OCH_3), 1679.25 (C=N stretch), 1582.69, 1537.69, 1448.43 (aromatic C=C stretching), 1349.67 (C-N stretch); ^{1}H-NMR (400 MHz, CDCl3, δ ppm): 3.92 (s, 6H, OCH_3), 5.11 (s, 2H, NH_2), 6.92-7.08 (d, 2H, Ar-H), 7.58 (s, 1H, pyrimidine-H_5), 7.69- 7.75 (m, 4H, Ar-H), 7.82 (s, 1H, Ar-H). ESI-MS (m/z): 342.09 ($C_{18}H_{16}ClN_3O_2$, $[M+H]^+$)

4-(4-(dimethylamino)phenyl)-6-(4-nitrophenyl)pyrimidin-2-amine (2.10G): Yield 48.52%, mp 114-116^{0}C, IR (cm^{-1}, KBr): 3395.18, 3296.35 (NH_2 Primary amine, N-H stretching), 3063.35 (Aromatic C-H stretching), 2940.18 (Aliphatic C-H stretching for CH_3), 1663.14 (C=N stretch), 1587.26, 1521.29, 1494.87 (aromatic C=C stretching), 1346.24 (C-N stretch); ^{1}H-NMR (400 MHz, CDCl3, δ ppm): 2.91 (s, 6H, CH_3), 5.71 (s, 2H, NH_2), 7.22-7.31 (d, 2H, Ar-H), 7.54 (s, 1H, pyrimidine-H_5), 7.59- 7.80 (m, 4H, Ar-H), 7.93-8.02 (d, 2H, Ar-H). ESI-MS (m/z): 336.15 ($C_{18}H_{17}N_5O_2$, $[M+H]^+$)

4-(2,5-dimethoxyphenyl)-6-(3-nitrophenyl)pyrimidin-2-amine (2.11G): Yield 54.31%, mp 130-132^{0}C IR (cm^{-1}, KBr): 3490.34, 3385.29 (s, NH_2 Primary amine, N-H stretching), 3072.69 (Aromatic C-H stretching), 2918.30, 2848.66 (Aliphatic C-H stretching for OCH_3), 1664.80 (C=N stretch), 1583.69, 1518.25, 1446.37 (aromatic C=C stretching), 1223.25 (C-N stretch); ^{1}H-NMR (400 MHz, CDCl3, δ ppm): 3.93 (s, 6H, OCH_3), 6.17 (s, 2H, NH_2), 7.41 (s, 1H, Ar-H), 7.53-7.59 (d, 2H, Ar-H), 7.76 (s, 1H, pyrimidine-H_5), 7.92 (s, 1H, Ar-H) 8.37- 8.52 (m, 3H, Ar-H). ESI-MS (m/z): 353.34 ($C_{18}H_{16}N_4O_4$, $[M+H]^+$)

4-(2,4-dichlorophenyl)-6-(2,5-dimethoxyphenyl)pyrimidin-2-amine (2.12G): Yield 55.18%, mp 121-124^{0}C IR (cm^{-1} KBr): 3321.28, 3172.90 (NH_2 Primary amine, N-H stretching), 3085.09 (Aromatic C-H stretching), 2994.91, 2954.67 (Aliphatic C-H stretching for OCH_3), 1659.05 (C=N stretch), 1586.62, 1525.69, 1450.47 (aromatic C=C stretching), 1265.30 (C-N stretch); ^{1}H-NMR (400 MHz, CDCl3, δ ppm): 3.96 (s, 6H, OCH_3), 5.97 (s, 2H, NH_2), 7.18-7.25 (d, 2H, Ar-H), 7.52 (s, 1H, Ar-H), 7.69 (s, 1H, pyrimidine-H_5), 7.86 (s, 1H, Ar-H) 8.03- 8.12 (m, 2H, Ar-H). ESI-MS (m/z): 377.04 ($C_{18}H_{15}Cl_2N_3O_2$, $[M+H]^+$)

4-(4-(benzyloxy)phenyl)-6-(2,4-dichlorophenyl)pyrimidin-2-amine (2.13G): Yield 28.05%, mp: 116-120^{0}C, IR (cm^{-1}, KBr): 3361.02 (NH_2 Primary amine, N-H stretching), 3062.96 (Aromatic C-H stretching), 2870.08 (Alipahtic C-H stretch of CH_2), 1662-1579 (Aromatic C=C stretch); ^{1}H-NMR (400 MHz, CDCl3, δ ppm): 4.93 (s, 2H, CH_2), 5.87 (s, 2H, NH_2), 7.30-7.35 (d, 2H, Ar-H), 7.51 (s, 1H, Ar-H), 7.65 (s, 1H, pyrimidine-H_5), 7.71- 7.84 (m, 4H, Ar-H), 7.91 (m, 1H, Ar-H), 7.99-8.14 (d, 4H, Ar-H). ESI-MS (m/z): 423.25 ($C_{23}H_{17}Cl_2N_3O$, $[M+H]^+$)

4-(anthracen-9-yl)-6-phenylpyrimidin-2-amine (2.14G): Yield 62.81%, mp 130-132^{0}C, IR (cm^{-1}, KBr): 3482.56, 3396.74 (s, NH_2 Primary amine, N-H stretching), 3178.51 (Aromatic C-H

stretching), 1670 (C=N stretch), 1598.99, 1513.77 (aromatic C=C stretching), 1350.17 (C-N stretch)); ^{1}H-NMR (400 MHz, CDCl3, δ ppm): 5.12 (s, 2H, NH_2), 6.92-8.53 (m, 15H, Ar-H). ESI-MS (m/z): 348.02 ($C_{24}H_{17}N_3$, $[M+H]^+$)

4-(3-nitrophenyl)-6-phenylpyrimidine-2-thiol (2.1T): Yield: 82.6%, mp 130-134^{0}C, 3336.8 (b, S-H stretching), 3057.17 (Aromatic C-H stretching), 1672-1606 (C=C aromatic stretching); ^{1}H-NMR (400 MHz, δ ppm $CDCl_3$): 3.18 (s, 1H, SH), 6.63-6.72 (m, 4H, Ar-H), 6.78 (s, 1H, pyrimidine-N_5), 7.13 (t, 1H, Ar-H), 7.40 (m, 3H, Ar-H), 7.85 (s, 1H, Ar-H). ESI-MS (m/z): 310.07 ($C_{16}H_{11}N_3O_2S$, $[M+H]^+$)

4-(4-methoxyphenyl)-6-(3-nitrophenyl)pyrimidine-2-thiol (2.2T): Yield: 96%, mp 166-172^{0}C, IR (cm^{-1}, KBr): 3298.48 (S-H stretching), 3127.17 (Aromatic C-H stretching), 2869.45 (Aliphatic C-H stretch), 1674-1608 (C=C aromatic stretching), 1167.09 (C-O stretch); ^{1}H-NMR (400 MHz, δ ppm DMSO): 2.58 (s,1H, SH), 3.85-3.87 (s, 3H, OCH_3), 6.94-6.97 (d, 2H, ArH), 7.03-7.06 (d, 2H, ArH), 7.5-7.9 (m, 5H, ArH). ESI-MS (m/z): 340.08 ($C_{17}H_{13}N_3O_3S$, $[M+H]^+$)

4-(3,4-dimethoxy-phenyl)-6-(3-nitro-phenyl)-pyrimidine-2-thiol (2.3T): Yield: 92%, mp 161-163^{0}C, IR (cm^{-1}, KBr): 3242.47 (S-H stretching), 3126.17 (Aromatic C-H stretching), 2858.41 (Aliphatic C-H stretch), 1685-1618 (C=C aromatic stretching), 1200.54 (C-O stretch); ^{1}H-NMR (400 MHz, δ ppm DMSO): 2.81 (s,1H, SH), 3.34 (s, 6H, OCH_3), 6.91-6.97 (d, 2H, ArH), 7.01(d, 2H, ArH), 7.42-7.81 (m, 4H, ArH). ESI-MS (m/z): 370.89 ($C_{18}H_{15}N_3O_4S$, $[M+H]^+$)

4-(3,nitro-phenyl)-6-(3-nitro-phenyl)-pyrimidine-2-thiol (2.4T): Yield: 86%, mp 168-170^{0}C, IR (cm^{-1}, KBr): 3242.47 (S-H stretching), 3126.17 (Aromatic C-H stretching), 2858.41 (Aliphatic C-H stretch), 1685-1618 (C=C aromatic stretching), 1200.54 (C-O stretch); ^{1}H-NMR (400 MHz, δ ppm DMSO): 2.54 (s,1H, SH), 6.82-6.94 (d, 2H, ArH), 7.01(d, 2H, ArH), 7.51-7.82 (m, 5H, ArH). ESI-MS (m/z): 355.81 ($C_{16}H_{10}N_4O_4S$, $[M+H]^+$)

4-(2,4-dichlorophenyl)-6-(3-nitrophenyl)pyrimidine-2-thiol (2.5T): Yield: 72%, mp 196-200 ^{0}C, IR (cm^{-1}, KBr): 3322.86 (b, S-H stretching), 3087.29 (Aromatic C-H stretching), 1653.75 (C=N stretch), 1590.77, 1519.29, 1412.64 (aromatic C=C stretching), 1270.80 (C-N stretch); ^{1}H-NMR (400 MHz, CDCl3, δ ppm): 2.62 (s, 1H, SH), 7.14-7.19 (d, 2H, ArH), 7.29-7.36 (d, 2H, ArH), 7.38 (s, 1H, ArH), 7.79 (m, 1H, ArH) 8.18 (s, 1H, ArH), 8.42 (s, 1H, ArH). ESI-MS (m/z): 379.05 ($C_{16}H_9Cl_2N_3O_2S$, $[M+H]^+$)

4-(4-(dimethylamino)phenyl)-6-(4-nitrophenyl)pyrimidine-2-thiol (2.6T): Yield: 36.8%, mp 113-115^{0}C, IR (cm^{-1}, KBr): 3359.48 (b, S-H stretching), 3138.42 (Aromatic C-H stretching), 2836.92 (Aliphatic C-H stretch), 1667-1623 (C=C aromatic stretching); ^{1}H-NMR (400 MHz, CDCl3, δ ppm): 2.72 (s, 1H, SH) 3.14 (s, 6H, CH_3), 7.24-7.29 (d, 2H, Ar-H), 7.55 (s, 1H,

pyrimidine-H_5), 7.63- 7.86 (m, 4H, Ar-H), 7.97-8.05 (d, 2H, Ar-H). ESI-MS (m/z): 353.11 ($C_{18}H_{16}N_4O_2S$, $[M+H]^+$)

4-(4-chlorophenyl)-6-(2,4-dimethoxyphenyl)pyrimidine-2-thiol (2.7T): Yield: 52.10%, mp 121-123^{0}C, IR (cm^{-1}, KBr): 3326.82 (S-H stretching), 3182.89 (Aromatic C-H stretching), 2947.26 (Aliphatic C-H stretch), 1642.88 (C=N stretch), 1580.17-1469.43 (aromatic C=C stretching), 1189.92 (C-N stretch); ^{1}H-NMR (400 MHz, CDCl3, δ ppm): 2.58 (s, 1H, SH), 3.88 (s, 6H, OCH_3), 6.89-7.09 (d, 2H, Ar-H), 7.37 (s, 1H, pyrimidine-H_5), 7.42 (s, 1H, Ar-H), 7.45-7.66 (m, 4H, Ar-H),. ESI-MS (m/z): 359.12 ($C_{18}H_{15}ClN_2O_2S$, $[M+H]^+$)

4-(2,4-dichlorophenyl)-6-(2,5-dimethoxyphenyl)pyrimidine-2-thiol (2.8T): Yield: 71.36%, mp 132-135^{0}C, IR (cm^{-1}, KBr): 3324.16 (s, b, S-H stretching), 3091.89 (Aromatic C-H stretching), 1658.75 (C=N stretch), 1578.91, 1520.19, 1447.50 (aromatic C=C stretching), 1274.80 (C-N stretch); ^{1}H-NMR (400 MHz, CDCl3, δ ppm): 2.71 (s, 1H, SH), 3.79 (s, 6H, OCH_3), 7.27-7.41 (d, 2H, Ar-H), 7.47 (s, 1H, Ar-H), 7.69 (s, 1H, pyrimidine-H_5), 7.87 (s, 1H, Ar-H) 8.17-8.30 (m, 2H, Ar-H). ESI-MS (m/z): 393.04 ($C_{18}H_{14}Cl_2N_2O_2S$, $[M+H]^+$)

4-(4-(benzyloxy)phenyl)-6-(2,4-dichlorophenyl)pyrimidin-2-thiol (2.9T): Yield: 60%, mp 106-110^{0}C, IR (cm^{-1}, KBr): 3325.18 (s, S-H stretching), 3187.16 (Aromatic C-H stretching), 2939.04 (Aliphatic C-H stretch), 1641.08 (C=N stretch), 1585.07-1458.04 (aromatic C=C stretching), 1284.96 (C-N stretch); ^{1}H-NMR (400 MHz, CDCl3, δ ppm): 2.43 (s, 1H, SH), 5.13 (s, 2H, CH_2), 7.26-7.34 (d, 2H, Ar-H), 7.52 (s, 1H, Ar-H), 7.61 (s, 1H, Ar-H), 7.64- 7.81 (m, 4H, Ar-H), 7.83 (m, 1H, Ar-H), 7.95-8.02 (d, 4H, Ar-H). ESI-MS (m/z): 440.10 ($C_{23}H_{16}Cl_2N_2OS$, $[M+H]^+$)

4-(3-bromophenyl)-6-(furan-2-yl)pyrimidine-2-thiol (2.10T): Yield 48.47%, mp 133-134^{0}C IR (cm^{-1}, KBr): 338292.73 (s, b, S-H stretching), 3071.32 (Aromatic C-H stretching), 1673.00 (C=N stretch), 1598.99, 1525.69, 1432.92 (aromatic C=C stretching), 1221.57 (C-N stretch); ^{1}H-NMR (400 MHz, CDCl3, δ ppm): 2.43 (s, 1H, SH), 7.10-8.21 (m, 8H, Ar-H); ESI-MS (m/z): 334.45 ($C_{14}H_9BrN_2OS$, $[M+H]^+$)

4-(3-nitrophenyl)-6-phenylpyrimidin-2-ol (2.1U): Yield 42.31%, mp 240-244^{0}C, IR (cm-1, KBr): 3360.00 (b, O-H stretching), 3061.03 (Aromatic C-H stretching), 1661-1577 (Aromatic C=C stretching), 1348.24 (C-O); ^{1}H-NMR (400 MHz, DMSO-*d_6*, δ ppm): 6.51 (broad, 1H, OH), 6.93-6.98 (d, 2H, ArH), 7.22-7.25 (d, 2H, ArH), 7.61 (s, 1H, ArH), 7.78 (s, 1H, pyrimidine-N_5), 8.23-8.31 (m, 4H, ArH). ESI-MS (m/z): 294.09 ($C_{16}H_{11}N_3O_3$, $[M+H]^+$)

4-(3-nitrophenyl)-6-phenylpyrimidin-2-ol (2.2U): Yield 81.75%, mp: 112-115^{0}C, IR (cm^{-1}, KBr): 3381.30 (s, b, O-H stretching), 3117.43 (Aromatic C-H stretching), 1574.09-1465.87 (aromatic C=C stretching), 1353.42 (C-N stretch); ^{1}H-NMR (400 MHz, DMSO-*d_6*, δ ppm): 6.11

(hump, 1H, OH), 7.24-7.36 (d, 2H, Ar-H), 7.62 (s, 1H, Ar-H), 7.91 (s, 1H, pyrimidine-H_5), 8.29-8.35 (m, 2H, Ar-H), 8.37- 8.52 (m, 4H, Ar-H). ESI-MS (m/z): 294.10 ($C_{16}H_{10}N_4O_5$, $[M+H]^+$)

4-(4-methoxyphenyl)-6-(3-nitrophenyl)pyrimidin-2-ol (2.3U): Yield 68.34%, mp MT280^{0}C, IR (cm-1, KBr): 3348.42 (s, b, O-H stretching), 3059.10 (Aromatic C-H stretching), 2924.09 (Aliphatic C-H stretching of OCH_3), 1678-1604 (Aromatic C=C stretching), 1355.96, 1288.16 (C-O stretching of OCH_3 and C-O of CH-OH); ^{1}H-NMR (400 MHz, DMSO-d_6, δ ppm): 3.83 (s, 3H OCH_3), 6.5 (hump, 1H, OH), 7.10-7.13 (d, 2H, ArH), 7.75-7.85 (d, t, 1H each, ArH), 8.16 (s, 1H, ArH, pyrimidine-N_5), 8.21-8.25 (d, 2H, ArH), 8.27 (d, 1H, ArH), 8.79 (s, 1H, ArH). ESI-MS (m/z): 324.51 ($C_{17}H_{13}N3O_4$, $[M+H]^+$)

4,6-bis(3-nitrophenyl)pyrimidin-2-ol (2.4U): Yield 78.09%, mp: 102-104^{0}C, IR (cm^{-1}, KBr): 3384.67 (s, b, O-H stretching), 3071.11 (Aromatic C-H stretching), 1597.00, 1534.29, 1456.97 (aromatic C=C stretching), 1352.44 (C-N stretch). ^{1}H-NMR (400 MHz, DMSO-d_6, δ ppm): 6.18 (hump, 1H, OH), 7.32-7.37 (d, 2H, Ar-H), 7.49 (s, 1H, Ar-H), , 7.71 (s, 1H, pyrimidine-H_5), 8.08-8.22 (m, 4H, Ar-H), 8.39 (s, 1H, Ar-H),. ESI-MS (m/z): 339.15 ($C_{16}H_{10}N_4O_5$, $[M+H]^+$)

4-(2,4-dichlorophenyl)-6-(3-nitrophenyl)pyrimidin-2-ol (2.5U): Yield 77.83%, mp 248-250^{0}C, IR (cm^{-1}, KBr): 3327.21 (s, b, O-H stretching), 3089.02 (Aromatic C-H stretching), 1657.95 (C=N stretch), 1576.91, 1512.25, 1443.67 (aromatic C=C stretching), 1259.65 (C-N stretch); ^{1}H-NMR (400 MHz, DMSO-d_6, δ ppm): 6.81 (broad, 1H, OH), 7.06-7.11 (d, 2H, ArH), 7.31-7.38 (d, 2H, ArH), 7.42 (s, 1H, pyrimidine-N_5), 7.53 (s, 1H, ArH), 7.92 (s, 1H, ArH), 8.15-8.17 (t, 1H, ArH). ESI-MS (m/z): 362.08 ($C_{16}H_9Cl_2N_3O_3$, $[M+H]^+$)

4-(4-chlorophenyl)-6-p-tolylpyrimidin-2-ol (2.6U): Yield 90.29%, mp 64-68 ^{0}C, IR (cm-1, KBr): 3367.00 (s, b, O-H stretching), 3161.03 (Aromatic C-H stretching), 2983.00 (Aliphatic C-H stretch), 1668-1595 (Aromatic C=C stretching); ^{1}H-NMR (400 MHz, DMSO-d_6, δ ppm): 2.28 (s, 3H, CH_3), 6.80 (broad, 1H, OH), 6.96-7.02 (d, 2H, ArH), 7.29-7.35 (d, 2H, ArH), 7.48 (s, 1H, pyrimidine-N_5), 8.30-8.41 (m, 4H, ArH). ESI-MS (m/z): 297.12 ($C_{17}H_{13}ClN_2O$, $[M+H]^+$)

4-(4-Dimethylamino-phenyl)-6-(3-nitro-phenyl)-pyrimidin-2-ol (2.7U): Yield 81.25%, mp 66-68 ^{0}C, IR (cm-1, KBr): 3358.00 (s, b, O-H stretching), 3161.09 (Aromatic C-H stretching), 2983.00 (Aliphatic C-H stretch), 1668-1595 (Aromatic C=C stretching); ^{1}H-NMR (400 MHz, DMSO-d_6, δ ppm): 2.28 (s, 6H, CH_3), 6.57 (broad, 1H, OH), 6.96-8.41 (m, 9H, ArH). ESI-MS (m/z): 337.82 ($C_{18}H_{16}N_4O_3$, $[M+H]^+$)

4-(3,4-Dimethoxy-phenyl)-6-(3-nitro-phenyl)-pyrimidin-2-ol (2.8U): Yield 58%, mp 81-84^{0}C, IR (cm^{-1}, KBr): 3345.27 (s, b, O-H stretching), 3189.86 (Aromatic C-H stretching), 1652.91 (C=N stretch), 1575.93-1455.44 (aromatic C=C stretching), 1272.21 (C-N stretch); ^{1}H-NMR

(400 MHz, DMSO-d_6, δ ppm): 3.32 (s, 6H, OCH_3), 6.87 (broad, 1H, OH), 7.28-7.8.24 (m, 8H, Ar-H). ESI-MS (m/z): 355.81 ($C_{18}H_{15}N_3O_5$, $[M+H]^+$)

4-(4-chlorophenyl)-6-(2,4-dimethoxyphenyl)pyrimidin-2-ol (2.9U): Yield 64%, mp 108-110^{0}C, IR (cm^{-1}, KBr): 3323.85, (s, b, O-H stretching), 3090.39 (Aromatic C-H stretching), 2999.31, 2956.67 (Aliphatic C-H stretching for OCH_3), 1673.26 (C=N stretch), 1573.97, 1532.59, 1439.67 (aromatic C=C stretching), 1261.76 (C-N stretch); ^{1}H-NMR (400 MHz, DMSO-d_6, δ ppm): 3.78 (s, 6H, OCH_3), 6.86-6.99 (d, 2H, Ar-H), 7.15 (s, 1H, Ar-H), 7.34 (s, 1H, pyrimidine-H_5), 7.41 (s, 1H, OH), 7.73- 7.93 (m, 4H, Ar-H). ESI-MS (m/z): 343.11 ($C_{18}H_{15}ClN_2O_3$, $[M+H]^+$)

4-(2,4-dichlorophenyl)-6-(2,5-dimethoxyphenyl)pyrimidin-2-ol (2.10U): Yield 56%, mp 114-116^{0}C IR (cm^{-1}, KBr): 3329.86, (s, b, O-H stretching), 3191.89 (Aromatic C-H stretching), 2993.71, 2952.69 (Aliphatic C-H stretching for OCH_3), 1654.95 (C=N stretch), 1591.27, 1531.83, 1456.50 (aromatic C=C stretching), 1263.90 (C-N stretch); ^{1}H-NMR (400 MHz, DMSO-d_6, δ ppm): 3.87 (s, 6H, OCH_3), 6.84 (hump, 1H, OH), 7.33-7.43 (d, 2H, Ar-H), 7.52 (s, 1H, Ar-H), 7.63 (s, 1H, pyrimidine-H_5), 8.06 (s, 1H, Ar-H), 8.18- 8.33 (m, 2H, Ar-H). ESI-MS (m/z): 377.04 ($C_{18}H_{14}Cl_2N_2O_3$, $[M+H]^+$)

4-(4-(benzyloxy)phenyl)-6-(2,4-dichlorophenyl)pyrimidin-2-ol (2.11U): Yield 52%, mp 80-84^{0}C, IR (cm^{-1}, KBr): 3345.27 (s, b, O-H stretching), 3189.86 (Aromatic C-H stretching), 1652.91 (C=N stretch), 1575.93-1455.44 (aromatic C=C stretching), 1272.21 (C-N stretch); ^{1}H-NMR (400 MHz, DMSO-d_6, δ ppm): 5.32 (s, 2H, CH_2), 6.87 (broad, 1H, OH), 7.28-7.39 (d, 2H, Ar-H), 7.47 (s, 1H, Ar-H), 7.70 (s, 1H, Ar-H), 7.64- 7.83 (m, 4H, Ar-H), 7.94-8.01 (d, 4H, Ar-H) 8.24 (m, 1H, Ar-H). ESI-MS (m/z): 424.81 ($C_{23}H_{16}Cl_2N_2O_2$, $[M+H]^+$)

4-(3-bromophenyl)-6-(furan-2-yl)pyrimidine-2-ol (2.12U): Yield 51.31%, mp 130-132^{0}C IR (cm^{-1}, KBr): 3392.79 (s, b, O-H stretching), 3078.39 (Aromatic C-H stretching), 1666.50 (C=N stretch), 1598.99, 1525.69, 1450.47 (aromatic C=C stretching), 1224.80 (C-N stretch); ^{1}H-NMR (400 MHz, CDCl3, δ ppm): 6.14 (broad, 1H, OH), 7.05-8.16 (m, 8H, Ar-H); ESI-MS (m/z): 318.22 ($C_{14}H_9BrN_2O_2$, $[M+H]^+$)

5.4 Synthesis of substituted allylidene hydrazinecarboximidamide derivatives

5.4.1 Synthesis

Allylidene hydrazinecarboximidamide derivatives were prepared using scheme 4 given below. Scheme 3 and scheme 4, both involve chalcone preparation in first step.

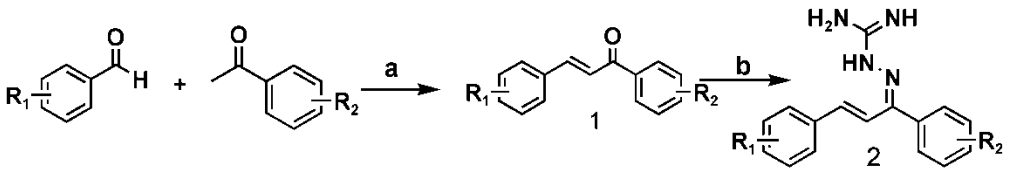

Scheme 4: Reagents and conditions: (a) NaOH, EtOH, rt, 4-6 h (b) Aminoguanidine-HCl, Conc. HCl, THF, Reflux 20-24 h.

Synthesis of 1: An equimolar mixture of substituted benzaldehyde and acetophenone were dissolved in 15 ml ethanol. Then 10ml NaOH solution (6g in 10ml H_2O) was added drop wise to the reaction mixture with continuous stirring. The reaction temperature was maintained between 20-25˚ C using a cold water bath. The progress of the reaction was monitored by TLC. After vigorous stirring for 4-5 hours the reaction mixture was kept overnight. It was then neutralized by acidified cold water to precipitate the solid product. On filtering off, the crude chalcone was dried in air and recrystallized using ethanol.

Synthesis of 2: To the equimolar mixture of 1 and aminoguanidine hydrochloride, 0.5 ml HCl and 10 ml THF were added and set for reflux for 20 to 24 hrs. Reaction was monitored by TLC for completion. The solvent was evaporated under reduced pressure. Residue was washed with water and then with diethylether. The compounds were finally purified by column chromatography.

5.4.2 Mechanism

Benzylidene acetophenone derivatives can be prepared by Claisen-Schmidt reaction between a substituted benzaldehyde and an acetophenone in the presence of a catalyst as described previously in section 5.3.2. It then reacts with aminoguanidine hydrochloride to form carbinolamine intermediate, which liberates a water molecule and ultimately results in the formation of allylidene hydrazinecarboxiimidamide.

Mechanism Step 2:

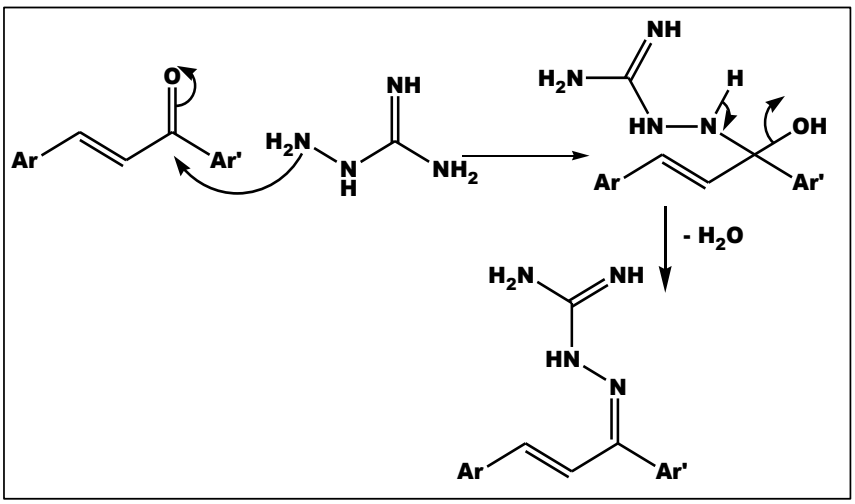

5.4.3 Spectral data

(*Z*)-2-((*E*)-1,3-diphenylallylidene)hydrazinecarboximidamide (C1A): Yield: 52%, mp: 68-70^{0}C, IR (cm^{-1}, KBr): 3412.08 (N-H stretching), 3062.963 (aromatic C-H stretching), 3001.24 (=C-H alkene stretch), 1668.43 (C=N stretch); ^{1}H NMR (300 MHz, $CDCl_3$, δppm): 1.96 (s, 2H, NH_2), 4.21 (d, 1H, *J*=16.2*Hz*, =C-H), 4.34 (d, 1H, *J*=16.2*Hz*, =C-H), 7.38-7.73 (m, 10H, Ar-H), 10.29 (s, 1H, =NH) ESI-MS (m/z): 265.18 ($C_{16}H_{16}N_4$, $[M+H]^+$)

(*Z*)-2-((*E*)-3-(3-nitrophenyl)-1-phenylallylidene)hydrazinecarboximidamide(C2A): Yield: 65.18%, mp: 105-107^{0}C, IR (cm^{-1}, KBr): 3317.08 (N-H stretching), 3032.93 (Aromatic C-H stretching), 3021.14 (=C-H alkene stretch), 1658.73 (C=N stretch); 1H NMR (400 MHz, DMSO, δppm): 3.96 (s, 2H, NH_2), 4.51 (d, 1H, *J*=15.3*Hz*, =C-H), 4.98 (d, 1H, *J*=15.3*Hz*, =C-H), 7.17-7.89 (m, 9H, Ar-H), 9.1 (s, 1H, =NH) ESI-MS: 310.30 ($C_{16}H_{15}N_5O_2$, $[M+H]^+$)

(*Z*)-2-((*E*)-1-(4-nitrophenyl)-3-phenylallylidene)hydrazinecarboximidamide(C3A): Yield: 62.72%, mp: 110-112^{0}C, IR (cm^{-1}, KBr): 3326.08 (N-H stretching), 3032.93 (Aromatic C-H stretching), 3041.14 (=C-H alkene stretch), 1668.73 (C=N stretch); ^{1}H NMR (400 MHz, DMSO, δppm): 3.46 (s, 2H, NH_2), 4.71 (d, 1H, *J*=16.1*Hz*, =C-H), 5.28 (d, 1H, *J*=16.1*Hz*, =C-H), 7.11-7.95 (m, 9H, Ar-H), 10.2 (s, 1H, =NH) ESI-MS (m/z): 310.52 ($C_{16}H_{15}N_5O_2$), $[M+H]^+$)

(*Z*)-2-((*E*)-3-(3-nitrophenyl)-1-(4-nitrophenyl)allylidene)hydrazinecarboximidamide(C4A): Yield: 61.10%, mp: 110-112^{0}C, IR (cm^{-1}, KBr): 3316.08 (N-H stretching), 3032.93 (Aromatic C-H stretching), 3021.14 (=C-H alkene stretch), 1658.73 (C=N stretch); ^{1}H NMR (400 MHz, DMSO, δppm): 4.8 (hump, 2H, NH_2), 4.51 (d, 1H, *J*=16.1*Hz,* =C-H), 4.98 (d, 1H, *J*=16.1*Hz,* =C-H), 7.28-7.81 (m, 8H, Ar-H) ESI-MS (m/z): 355.43 ($C_{16}H_{14}N_6O_4$, $[M+H]^+$)

(*Z*)-2-((*E*)-3-(2,5-dimethoxyphenyl)-1-phenylallylidene)hydrazinecarboximidamide(C5A): Yield: 42%, mp: 132-134^{0}C, IR (cm^{-1}, KBr): 3316.55 (N-H stretching), 3027.97 (Aromatic C-H stretching), 3021.14 (=C-H alkene stretch), 2908.85, 2833.83 (Aliphatic C-H stretching for OCH_3),1658.73 (C=N stretch); ^{1}H NMR (400 MHz, DMSO, δppm): 3.25 (s, 2H, OCH_3), 3.65 (s, 2H, OCH_3), 4.86 (s, 2H, NH_2), 6.51 (d, 1H, *J*=15.7*Hz,* =C-H), 6.88 (d, 1H, *J*=15.7*Hz,* =C-H), 7.48-8.03 (m, 8H, Ar-H) ESI-MS (m/z): 325.25 ($C_{18}H_{20}N_4O_2$, $[M+H]^+$)

(*Z*)-2-((*E*)-1-(3-hydroxyphenyl)-3-phenylallylidene)hydrazinecarboximidamide(C6A): Yield: 28.93%, mp: 124-126^{0}C, IR (cm^{-1}, KBr): 3400.52 (-OH stretching), 3318.21 (N-H stretching), 3032.93 (Aromatic C-H stretching), 3021.14 (=C-H alkene stretch), 1658.73 (C=N stretch); ^{1}H NMR (400 MHz, DMSO, δppm): 3.82 (hump, 1H, OH), 4.41 (s, 2H, NH_2), 4.59 (d, 1H, *J*=15.8*Hz*, =C-H), 4.96 (d, 1H, *J*=15.8*Hz*, =C-H), 6.99-7.84 (m, 9H, Ar-H), 9.3 (s, 1H, =NH) ESI-MS (m/z): 281.14 ($C_{16}H_{16}N_4O$, $[M+H]^+$)

(*Z*)-2-((*E*)-3-(anthracen-9-yl)-1-phenylallylidene) hydrazinecarboximidamide(C7A): Yield: 44%,mp: 135-137^{0}C, IR (cm^{-1}, KBr): 3346.78 (sec. N-H stretching), 3052.44 (Aromatic C-H stretching), 3022.54 (=C-H alkene stretch), 1669.42 (C=N stretch)ESI-MS: 365.26 ($C_{24}H_{20}N_4$, $[M+H]^+$)

(*Z*)-2-((*E*)-3-(4-(dimethylamino)phenyl)-1-(4-tolyl)allylidene)hydrazinecarboximidamide (C8A): Yield: 48%%, mp: 117-119^{0}C, IR (cm^{-1}, KBr): 3233.53 (N-H stretching), 3051.00 (Aromatic C-H stretching), 3024.18 (=C-H alkene stretch), 2945.13 (CH_3 stretching), 1658.73 (C=N stretch); ^{1}H NMR (400 MHz, DMSO, δppm): 3.45 (s, 6H, CH_3), 3.81 (s, 3H, CH_3), 3.2-3.8 (hump, 2H, NH_2), 6.8-7.9 (m, 2H, =C-H and 8H, Ar-H), 7-8 (hump, 1H, NH) ESI-MS (m/z): 322.18 ($C_{19}H_{23}N_5$, $[M+H]^+$)

(*Z*)-2-((*E*)-1-(3-nitrophenyl)-3-phenylallylidene)hydrazinecarboximidamide (C9A): Yield: 62%, mp: 110-112^{0}C, IR (cm^{-1}, KBr): 3326.12 (N-H stretching), 3032.94 (Aromatic C-H stretching), 3041.14 (=C-H alkene stretch), 1670.65 (C=N stretch); ^{1}H NMR (400 MHz, DMSO, δppm): 4.2 (s, 2H, NH_2), 4.74 (d, 1H, *J*=15.4*Hz*, =C-H), 5.35 (d, 1H, *J*=15.4*Hz,* =C-H), 7.20-7.94 (m, 9H, Ar-H) ESI-MS (m/z): 310.43 ($C_{16}H_{15}N_5O_2$), $[M+H]^+$)

(*Z*)-2-((*E*)-1-(4-chlorophenyl)-3-phenylallylidene)hydrazinecarboximidamide (C11A): Yield: 51.5%, mp: 121-123^{0}C, IR (cm^{-1}, KBr): 3346.78 (N-H stretching), 3052.44 (Aromatic C-H stretching), 3022.54 (=C-H alkene stretch), 1665.33 (C=N stretch); ^{1}H NMR (400 MHz, DMSO, δppm): 4.46 (s, 2H, NH_2), 4.61 (d, 1H, *J*=16.1*Hz,* =C-H), 5.10 (d, 1H, *J*=16.1*Hz,* =C-H), 7.15-8.13 (m, 9H, Ar-H), 10.4 (s, 1H, =NH) ESI-MS (m/z): 299.31 ($C_{16}H_{15}N_4Cl$, $[M+H]^+$)

(*Z*)-2-((*E*)-3-(4-(dimethylamino)phenyl)-1-(4-Nitrophenyl)allylidene)hydrazinecarboximidamide (C12A): Yield: 31%, mp: 120-122^{0}C, IR (cm^{-1}, KBr): 3219.15 (N-H stretching), 3042.00 (Aromatic C-H stretching), 3021.14 (=C-H alkene stretch), 2945.13 (CH_3 stretching), 1658.73 (C=N stretch); ^{1}H NMR (400 MHz, DMSO, δppm): 3.15 (s, 6H, CH_3), 4.98 (s, 2H, NH_2), 4.75 (d, 1H, *J*=15.6*Hz,* =C-H), 4.98 (d, 1H, *J*=15.6*Hz,* =C-H), 6.96-7.74 (m,8H,Ar-H), 10.6 (s, 1H, =NH) ESI-MS (m/z): 353.35 ($C_{18}H_{20}N_6O_2$, $[M+H]^+$)

(*Z*)-2-((*E*)-3-(4-(dimethylamino)phenyl)-1-phenylallylidene)hydrazinecarboximidamide (C13A): Yield: 30.53%, mp: 118-120^{0}C, IR (cm^{-1}, KBr): 3316.08 (N-H stretching), 3032.93 (Aromatic C-H stretching), 3021.14 (=C-H alkene stretch), 2945 (CH_3 stretching), 1658.73 (C=N stretch); ^{1}H NMR (400 MHz, DMSO, δppm): 2.25 (s, 6H, CH_3), 5.78 (s, 2H, NH_2), 5.67 (d, 1H, *J*=16.2*Hz,* =C-H), 5.88 (d, 1H, *J*=16.2*Hz,* =C-H), 7.27-7.87 (m, 9H, Ar-H), 9.8 (s, 1H, =NH) ESI-MS (m/z): 308.27 ($C_{18}H_{21}N_5$, $[M+H]^+$)

(*Z*)-2-((*E*)-3-(4-(dimethylamino)phenyl)-1-(3-nitrophenyl)allylidene)hydrazinecarboximidamide (C16A): Yield: 28%, mp: 120-122^{0}C, IR (cm^{-1}, KBr): 3316.08 (N-H stretching), 3032.93 (Aromatic C-H stretching), 3021.14 (=C-H alkene stretch), 2945 (CH_3 stretching), 1658.73 (C=N stretch); ^{1}H NMR (400 MHz, DMSO, δppm): 2.88 (s, 6H, CH_3), 6.30 (hump, NH_2), 6.58 (d, 1H, Ar-H), 6.61-6.67 (m, 2H, Ar-H), 7.38-7.41 (d,1H, *J*=16.5*Hz,* -CH=), 7.62-7.68 (m, 3H, Ar-H), 7.91-7.99 (d, 1H, *J*=16.5*Hz,* -CH=), 8.17-8.3 (m, 2H, Ar-H; ESI-MS (m/z): 353.25 ($C_{18}H_{20}N_6O_2$, $[M+H]^+$)

(*Z*)-2-((*E*)-3-(4-(benzyloxy)phenyl)-1-(4-nitrophenyl)allylidene)hydrazinecarboximidamide (C17A): Yield: 48.4%, mp: 135-137^{0}C, IR (cm^{-1}, KBr): 3412.08 (sec. N-H stretching), 3062.963 (Aromatic C-H stretching), 3001.24 (=C-H alkene stretch), 2908.85, 2833.83 (Aliphatic C-H stretching for OCH_2), 1668.43 (C=N stretch); ^{1}H NMR (400 MHz, $CDCl_3$, δppm): 4.50 (s, 2H, CH_2), 4.85 (d, 1H, =C-H), 5.05 (d, 1H, =C-H), 5.18 (s, 2H, NH_2), 7.38-8.28 (m,13H,Ar-H), 10.9 (s, 1H, =NH)

(*Z*)-2-((*E*)-3-(anthracen-9-yl)-1-(4-chlorophenyl)allylidene)hydrazinecarboximidamide (C18A): Yield: 32%,mp: 125-127^{0}C, IR (cm^{-1}, KBr): 3342.11 (sec. N-H stretching), 3042.46 (Aromatic C-H stretching), 3022.54 (=C-H alkene stretch), 1669.42 (C=N stretch); ^{1}H NMR (400 MHz, $CDCl_3$, δppm): 4.91 (d, 1H, =C-H), 5.54 (d, 1H, =C-H), 6.01 (s, 2H, NH_2), 7.38-8.28 (m, 13H, Ar-H), 10.41 (s, 1H, =NH); ESI-MS: 399.21 (C24H19ClN_4, $[M+H]^+$)

(*Z*)-2-((*E*)-1-(4-hydroxyphenyl)-3-phenylallylidene)hydrazinecarboximidamide(C19A): Yield: 28.98%, mp: 121-124^{0}C, IR (cm^{-1}, KBr): 3410.04 (-OH stretching), 3310.35 (N-H stretching), 3032.93 (Aromatic C-H stretching), 3021.14 (=C-H alkene stretch), 1658.73 (C=N stretch); ^{1}H NMR (400 MHz, DMSO, δppm): 3.75 (hump, 1H, OH), 4.46 (s, 2H, NH_2), 4.59 (d, 1H, *J*=15.8*Hz*, =C-H), 4.96 (d, 1H, *J*=15.8*Hz*, =C-H), 6.82-7.81 (m, 9H, Ar-H), 9.28 (s, 1H, =NH) ESI-MS (m/z): 281.42 ($C_{16}H_{16}N_4O$, $[M+H]^+$)

(*E*)-2-((*E*)-1-(4-hydroxyphenyl)-3-(4-methoxyphenyl)allylidene)hydrazinecarboximidamide (C20A): Yield: 31.72%, mp: 110-112^{0}C, IR (cm^{-1}, KBr): 3389.10 (-OH stretching), 3321.52 (N-H stretching), 3102.61 (Aromatic C-H stretching), 3029.11 (=C-H alkene stretch), 1634.15 (C=N stretch); ^{1}H NMR (400 MHz, DMSO, δppm): 3.24 (s, 3H, OCH_3), 3.94 (hump, 1H, OH), 4.81 (s, 2H, NH_2), 6.01 (d, 1H, *J=16Hz*, =C-H), 6.34 (d, 1H, *J*=16*Hz*, =C-H), 7.01-7.99 (m, 9H, Ar-H), 10.05 (s, 1H, =NH) ESI-MS (m/z): 311.34 ($C_{17}H_{18}N_4O_2$, $[M+H]^+$)

(*E*)-2-((*E*)-3-(1H-indol-3-yl)-1-phenylallylidene)hydrazinecarboximidamide (C21A): Yield: 25.14%, mp: 124-126^{0}C, IR (cm^{-1}, KBr): 3412.09 (-OH stretching), 3312.34 (N-H stretching), 3012.74 (Aromatic C-H stretching), 1634.21 (C=N stretch); ESI-MS (m/z): 320.42 ($C_{18}H_{17}N_5O$, $[M+H]^+$)

(*Z*)-2-((*E*)-3-(3,4-dimethoxyphenyl)-1-phenylallylidene)hydrazinecarboximidamide (C22A): Yield: 32%, mp: 128-130^{0}C, IR (cm^{-1}, KBr): 3452.68 (N-H stretching), 3082.93 (Aromatic C-H stretching), 3041.24 (=C-H alkene stretch), 2908.85, 2833.83 (Aliphatic C-H stretching for –OCH_3), 1668.43 (C=N stretch); ^{1}H NMR (400 MHz, DMSO, δppm): 3.52 (s, 3H, OCH_3), 3.58 (s, 3H, OCH_3), 6.75 (d, 1H, *J*=15.9*Hz,* =C-H), 7.15 (d, 1H, *J*=15.9*Hz,* =C-H), 7-8 (hump, 2H, NH_2), 7.05-8.95 (m, 8H, Ar-H), 11.59 (s, 1H, =NH) ESI-MS (m/z): 325.17 ($C_{18}H_{20}N_4O_2$, $[M+H]^+$)

(*Z*)-2-((*E*)-3-(3,4-dimethoxyphenyl)-1-(4-nitrophenyl)allylidene)hydrazinecarboximidamide (C23A): Yield: 21%, mp: 122-124^{0}C, IR (cm^{-1}, KBr): 3462.88 (N-H stretching), 3088.33 (Aromatic C-H stretching), 3044.64 (=C-H alkene stretch), 2918.85, 2853.83 (Aliphatic C-H stretching for –OCH_3), 1669.43 (C=N stretch); ^{1}H NMR (400 MHz, DMSO, δppm): 3.55 (s, 3H, OCH_3), 3.68 (s, 3H, OCH_3), 4.62 (s, 1H, -NH), 4.76 (d, 1H, *J*=16.2*Hz,* =C-H), 5.25 (d, 1H, *J*=16.2*Hz,* =C-H), 5.88 (s, 2H, NH_2), 7.10-8.18 (m, 7H, Ar-H) ESI-MS (m/z): 370.27 ($C_{18}H_{19}N_5O_4$, $[M+H]^+$)

(*Z*)-2-((*E*)-1-(4-chlorophenyl)-3-(3,4-dimethoxyphenyl)allylidene)hydrazinecarboximidamide (C24A): Yield: 34%, mp: 120-122^{0}C, IR (cm^{-1}, KBr): 3462.88 (N-H stretching), 3088.33 (Aromatic C-H stretching), 3044.64 (=C-H alkene stretch), 2918.85, 2853.83 (Aliphatic C-H stretching for –OCH_3), 1669.43 (C=N stretch); ^{1}H NMR (400 MHz, DMSO, δppm): 3.66 (s, 3H, OCH_3), 3.89 (s, 3H, OCH_3), 6.69 (d, 1H, Ar-H), 6.84 (d, 1H, *J*=16.0*Hz,* =C-H), 7.14 (d, 1H, *J*=16.0*Hz,* =C-H), 7.44-7.49 (m, 3H, Ar-H), 7.65 (d, 2H, Ar-H), 7.69 (s, 1H, Ar-H), 7.98 (s, 2H, NH_2), 12.25 (s, 1H, =NH) ESI-MS (m/z): 359.89 ($C_{18}H_{19}ClN_4O_2$, $[M+H]^+$)

(*Z*)-2-((*E*)-3-(3,4-dimethoxyphenyl)-1-(3-nitrophenyl)allylidene)hydrazinecarboximidamide (C25A): Yield: 42.83%, mp: 124-126^{0}C, IR (cm^{-1}, KBr): 3462.88 (N-H stretching), 3088.33 (Aromatic C-H stretching), 3044.64 (=C-H alkene stretch), 2918.85, 2853.83 (Aliphatic C-H stretching for –OCH_3), 1669.43 (C=N stretch); 1H NMR (400 MHz, DMSO, δppm): 3.55 (s, 3H, OCH_3), 3.69 (s, 3H, OCH_3), 4.78 (d, 1H, *J*=15.8*Hz,* =C-H), 5.25 (d, 1H, *J*=15.8*Hz,* =C-H), 5.88 (s, 2H, NH_2), 7.02-8.10 (m, 7H, Ar-H) ESI-MS (m/z): 370.41 ($C_{18}H_{19}N_5O_4$, $[M+H]^+$)

(*Z*)-2-((*E*)-1-(4-methoxyphenyl)-3-(3-nitrophenyl)allylidene)hydrazinecarboximidamide (C28A): Yield: 49%, mp: 121-123^{0}C, IR (cm^{-1}, KBr): 3466.88 (N-H stretching), 3098.33 (Aromatic C-H stretching), 3054.64 (=C-H alkene stretch), 2928.85, 2856.83 (Aliphatic C-H stretching for –OCH_3), 1668.43 (C=N stretch); ^{1}H NMR (400 MHz, DMSO, δppm): 4.05 (s, 3H, OCH_3), 4.62 (s, 1H, *J*=15.6*Hz,* -CH=), 4.86 (d, 1H, *J*=15.6*Hz,* =C-H), 5.55 (d, 1H, =C-H), 6.88 (s, 2H, NH_2), 7.10-8.18 (m, 8H, Ar-H), 10.7 (s, 1H, =NH) ESI-MS (m/z): 342.46 ($C_{17}H_{17}N_5O_3$, $[M+H]^+$)

(*Z*)-2-((*E*)-1-(2,4-dichlorophenyl)-3-(3-nitrophenyl)allylidene)hydrazinecarboximidamide (C29A): Yield: 67.34%, mp: 132-134^{0}C, IR (cm^{-1}, KBr): 3316.08 (N-H stretching), 3032.73 (Aromatic C-H stretching), 3021.14 (=C-H alkene stretch), 1658.73 (C=N stretch); ^{1}H NMR (400 MHz, DMSO, δppm): 4.51 (d, 1H, *J*=16.0*Hz,* =C-H), 4.98 (d, 1H, *J*=16.0*Hz,* =C-H), 7.28-7.83 (m,7H, Ar-H), 11.14 (s, 1H, =NH) ESI-MS (m/z): 379.26 ($C_{16}H_{13}Cl_2N_5O_2$, $[M+H]^+$)

(*Z*)-2-((*E*)-1-(3-bromophenyl)-3-(2,5-dimethoxyphenyl)allylidene)hydrazinecarboximidamide (C30A): Yield: 29%, mp: 128-130^{0}C, IR (cm^{-1}, KBr): 3454.51 (N-H stretching), 3432.55, 3307.92 (s, NH_2 Primary amine, N-H stretching), 3149. 76 (=C-H stretch), 3074.53 (Aromatic C-H stretching), 2960.73, 2926.01 (Aliphatic C-H stretching for OCH_3), 1701.64 (C=N stretch), 1612.49 (alkene C=C stretch), 1261.45 (C-O of methoxy); ^{1}H NMR (400 MHz, DMSO, δppm): 3.69 (s, 3H, OCH_3), 3.81 (s, 3H, OCH_3), 6.83 (d, 2H, Ar-H), 7.17 (d, 1H, *J*=15.1*Hz,* =C-H), 7.42-7.44 (m, 3H, Ar-H), 7.60-7.62 (m, 2H, Ar-H), 7.70 (d, 1H, *J*=15.1*Hz,* =C-H), 3.2-3.8 (hump, NH), 6.5-7.5 (hump, NH_2) ESI-MS (m/z): 404.51($C_{18}H_{19}BrN_4O_2$, $[M+H]^+$)

(*Z*)-2-((*E*)-3-(2,5-dimethoxyphenyl)-1-(4-methoxyphenyl)allylidene)hydrazinecarboximidamide (C31A): Yield: 29.45%, IR (cm^{-1}, KBr): 3487.30 (N-H stretching), 3452.58, 3307.92 (s, NH_2 Primary amine, N-H stretching), 3149. 76 (=C-H stretch), 3074.53 (Aromatic C-H stretching), 2899.01, 2831.29 (Aliphatic C-H stretching for OCH_3), 1701.35 (C=N stretch), 1610.56 (alkene C=C stretch), 1220.94 (C-O of methoxy); ^{1}H NMR (400 MHz, DMSO, δppm): 3.45 (s, 3H, OCH_3), 3.78 (s, 3H, OCH_3), 4.08 (s, 3H, OCH_3), 4.92 (s, 1H, -CH), 4.96 (d, 1H, *J*=15.8*Hz,* =C-H), 5.95 (d, 1H, *J*=15.8*Hz,* =C-H), 6.18 (s, 2H, NH_2), 7.25-8.58 (m, 7H, Ar-H), 10.4 (s, 1H, =NH) ESI-MS (m/z): 355.11 ($C_{19}H_{22}N_4O_3$, $[M+H]^+$)

(*Z*)-2-((*E*)-1-(3-bromophenyl)-3-(3-nitrophenyl)allylidene)hydrazinecarboximidamide (C33A): Yield: 74%, mp: 121-123^{0}C, IR (cm^{-1}, KBr): 3456.44 (N-H stretching), 3454.58, 3334.92 (s, NH_2 Primary amine, N-H stretching), 3082.25 (Aromatic C-H stretching), 1666.50 (C=N stretch), 1600.92 (alkene C=C stretch), 1529.56,1350.17 (s, N-O stretching for nitro group) ESI-MS (m/z): 391.05 ($C_{16}H_{14}BrN_5O_2$, $[M+H]^+$)

(*Z*)-2-((*E*)-3-(3-bromophenyl)-1-(4-nitrophenyl)allylidene)hydrazinecarboximidamide(C35A): Yield: 83%, mp: 120-122^{0}C, IR (cm^{-1}, KBr): 3446.48 (sec. N-H stretching), 3464.78, 3344.97 (s, NH_2 Primary amine, N-H stretching), 3086.25 (Aromatic C-H stretching), 1668.50 (C=N stretch), 1602.72 (alkene C=C stretch), 1529.56,1350.17 (s, N-O stretching for nitro group); ^{1}H NMR (400 MHz, $CDCl_3$, δppm): 5.18 (s, 1H, -CH), 5.29 (d, 1H, =C-H), 6.25 (d, 1H, =C-H), 6.78 (s, 2H, NH_2), 7.40-8.88 (m, 8H, Ar-H), 10.7 (s, 1H, =NH)

(*Z*)-2-((*E*)-1-(3-bromophenyl)-3-(2-chlorophenyl)allylidene)hydrazinecarboximidamide (C36A): Yield: 62.71%, mp: 132-134^{0}C, IR (cm^{-1}, KBr): 3454.51 (sec. N-H stretching), 3392.89, (s, NH_2 Primary amine, N-H stretching), 3062.96 (Aromatic C-H stretching), 1666.50 (C=N stretch), 1566.20 (alkene C=C stretch), 1359.82 (C-N stretch); ^{1}H NMR (400 MHz, $CDCl_3$, δppm): 5.01 (s, 1H, -CH), 5.19 (d, 1H, =C-H), 6.15 (d, 1H, =C-H), 6.72 (s, 2H, NH_2), 7.40-8.88 (m, 8H, Ar-H), 10.4 (s, 1H, =NH)

(*Z*)-2-((*E*)-1-(2,4-dichlorophenyl)-3-(3,4-dimethoxyphenyl)allylidene)hydrazinecarboximidamide (C37A): Yield: 47%, mp: 130-132^{0}C, IR (cm^{-1}, KBr): 3352.28 (sec. N-H stretching), 3041.53 (Aromatic C-H stretching), 2960.73, 2926.01 (Aliphatic C-H stretching for OCH_3), 1695.43 (C=N stretch), 1612.49 (alkene C=C stretch), 1261.45 (C-O of methoxy); ^{1}H NMR (400 MHz, DMSO, δppm): 3.98 (s, 3H, OCH_3), 4.28 (s, 3H, OCH_3), 4.99 (d, 1H, *J*=15.4*Hz,* =C-H), 6.05 (d, 1H, *J*=15.4*Hz,* =C-H), 6.68 (s, 2H, NH_2), 7.40-8.88 (m, 6H, Ar-H), 10.6 (s, 1H, =NH) ESI-MS (m/z): 394.27 ($C_{18}H_{18}Cl_2N_4O_2$, $[M+H]^+$)

(*Z*)-2-((*E*)-1-(3-bromophenyl)-3-(3,4-dimethoxyphenyl)allylidene)hydrazinecarboximidamide (C38A): Yield: 37%, mp: 128-130^{0}C, IR (cm^{-1}, KBr): 3390.86 (N-H stretching), 3313.71 (sec. N-H stretching), 3273.20, 3174.83 (s, NH_2 Primary amine, N-H stretching), 3080.32 (Aromatic C-H stretching), 2835.36 (Aliphatic C-H stretching of OCH3), 1668.43 (C=N stretch), 1591.27 (alkene C=C stretch); ^{1}H NMR (400 MHz, DMSO, δppm): 3.88 (s, 3H, OCH_3), 4.16 (s, 3H, OCH_3), 5.08 (s, 1H, -CH), 5.29 (d, 1H, *J*=15.1*Hz,* =C-H), 6.25 (d, 1H, *J*=15.1*Hz*, =C-H), 6.88 (s, 2H, NH_2), 7.40-8.88 (m, 7H, Ar-H), 9.7 (s, 1H, =NH) ESI-MS (m/z): 404.24 ($C_{18}H_{19}BrN_4O_2$, $[M+H]^+$)

Chapter 6

IN VITRO SCREENING AND *IN SILICO* - *IN VITRO* CORRELATION

6. *In vitro* screening of BACE-1 Inhibitors

For studying the BACE-1 inhibitory potency of all the synthesized compounds, *in vitro* enzyme inhibition assay was done. The concentration used was 10µM as the compounds used for designing library had been reported to have maximum inhibition at around 10µM concentration. From amongst designed compounds, those showing maximum inhibitory potential were also subjected to IC_{50} value determination. This section also describes the *in silico* - *in vitro* correlation.

6.1 *In vitro* BACE-1 inhibition assay

For this purpose, BACE-1 inhibition assay kit was purchased from Panvera (Madison, WI, U.S.A). The assay is based on Fluorescence resonance energy transfer (FRET) method.

6.1.1 Principle

The measure of inhibitory activity of compounds is based upon the reduction in fluorescence quantum yield due to inhibition of BACE-1 enzymatic activity. The given BACE-1 substrate consists of a fluorescence donor [a rhodamine (Rh) derivative] on one end and a proprietary quenching acceptor on the other. The distance between these two groups has been selected in such a way that upon light excitation, the donor fluorescence energy is significantly quenched by the acceptor through a quantum mechanical phenomenon known as resonance energy transfer. The intrinsic fluorescence of the intact substrate is dramatically reduced because of intramolecular resonance energy transfer to the quenching group. Upon enzymatic cleavage, the fluorophore is separated from the quenching group; the energy transfer is disrupted, restoring the full fluorescence yield of the donor. Enzyme activity is linearly related to the increase in fluorescence as weakly fluorescent peptide substrate becomes highly fluorescent upon enzymatic cleavage; the increase in fluorescence is proportional to the rate of proteolysis. FRET methods are widely used because they offer a homogenous and sensitive assay easily adapted for high-throughput screening (HTS) [151].

6.1.2 Methodology

Assay kit was purchased from Panvera (Madison, WI, U.S.A). DMSO was purchased from Sigma Aldrich. Purified water was used to prepare buffers and standard solutions. Spectrofluorimetric analyses were carried out on Tecan multiwell spectrofluorimeter (excitation: 545nm; emission: 590nm) using black microwell (96 wells) plates. Stock solutions of the tested compounds were prepared in DMSO and diluted with BACE-1 assay buffer (50mM sodium acetate buffer pH = 4.5). 3X BACE-1 enzyme was prepared using given 77units/ml of enzyme. For this 52µl of enzyme was diluted with buffer to make 4ml. Test

compounds were diluted with DMSO to prepare the stock solution of 10mM and further diluted with buffer to achieve desired concentration of 10µM.

10µL of substrate was added to 10µL of test compound and mixed gently. Then 10µL BACE-1 enzyme (25nM) was added and incubated for 60 minutes at room temperature. To stop the reaction, 10µL of BACE-1 stop solution (sodium acetate 2.5 M) was added to each well. The fluorescence signal was read at 590 nm. Assays were done with a blank containing all components except BACE-1 in order to account for non enzymatic reaction. Percentage inhibition due to the presence of test compounds was calculated. Each concentration was analyzed in triplicate. The percent inhibition of the enzyme activity due to the presence of increasing test compound concentration was calculated by the following expression: 100-(vi/vo × 100), where vi is the initial rate calculated in the presence of inhibitor and vo is the enzyme activity without inhibitor.

6.2 Results and discussion

6.2.1 Acridin-9-yl hydrazide derivatives

Overall, the acridin-9-yl hydrazide derivatives displayed consistent BACE-1 inhibition profile. Visual analysis of docking poses was done to correlate with % inhibition values. It was observed that compound AA-12 substituted with *m*-fluoro group on the phenyl ring displayed interaction with Asp32. The acridine nitrogen formed hydrogen bond with the main chain of Gly230. Acridine ring had π- π stacking with Trp115 covering the S2′ cavity and phenyl ring occupied the S1 pocket. Placing the fluoro group at *ortho* and *para* position (AA-13, AA-14) reduced the activity. Compound AA-12 showed 34.54% inhibition while AA-13 and AA-14 had 24.18% and 27.90% inhibition respectively. The *in vitro* results were supported by docking study where AA-12 scored higher than AA-13 and AA-14. It was observed that placing an *o*-fluoro or *p*-fluoro group (AA-13, AA-14) instead of *m*-fluoro, diminished the aspartate interactions though AA-13 formed key interaction with 10s loop amino acid Gly11. As compared to other deactivating groups like nitro (AA-11) and bromo (AA-16) at *ortho* position, fluorine was found to be least active. This can be explained from docking study whereby it is observed that fluorine being highly electronegative gets solvent exposed, changing the conformation in such a way that interaction of amide nitrogen with Asp32 does not occur. Since this is not the case with bromine and nitro substituted compounds, these compounds show interaction with Asp32. Placing *o,p*-dichloro (Compound AA-17) promoted interactions with Asp32, Tyr71, placed the acridine ring in S2′ cavity while phenyl ring occupied S1 pocket and had better docking score as compared to

other electron withdrawing substituted derivatives. However, it did not show any advantage in % inhibition studies.

Comparatively, compound AA-18 having *p*-acetamido substitution formed contacts with Asp32, showed π- π stacking with Tyr71 and Phe108, and had 52.72% BACE-1 inhibition. Compound AA-19 bearing *m*-methoxy substitution failed to interact with the aspartate dyad nevertheless it showed good inhibitory activity (43.54%). AA-110 with *m*,*p*-dimethoxy phenyl group also showed similar interactions viz: hydrogen bonding interaction with Asp32, amine group of phenyl ring formed interaction with Phe108 and π- π stacking of both the rings with Tyr71. It showed 53.27% BACE-1 inhibition *in vitro*. Most active compound AA-111, having *m*-amino and *p*-methyl phenyl group, showed that NH of hydrazine formed hydrogen bonding interaction with Asp32, amine group of phenyl ring formed interaction with Phe108 and π- π stacking of both the rings with Tyr71. The electron donating substitution appears to increase the potency but it also makes the compounds polar and may reduce brain permeation. Both, AA-18 and AA-111, displayed highest docking score in the series and this result was concurrent with BACE-1 inhibition (52.72 and 54.54% respectively). It was observed that replacing benzoyl on hydrazine with isonicotinoyl, as in compound AA-112, reduced the interactions as well as BACE-1 inhibition.

Table 6.1: *In vitro* assay data for Acridin-9-yl hydrazide derivatives

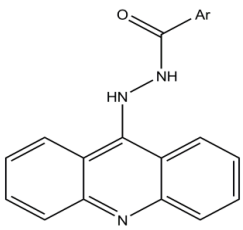

Code	R_1	Moldock score	Glide score	% Inhibition*
AA-11	*o*-NO_2-Ph	-84.34	-4.48	41.80 ± 0.71
AA-12	*m*-F-Ph	-85.30	-6.73	34.54 ± 0.80
AA-13	*o*-F-Ph	-74.64	-5.85	24.18 ± 0.04
AA-14	*p*-F-Ph	-78.82	-5.64	27.90 ± 0.02
AA-15	*p*-Cl-Ph	-78.24	-5.92	32.18 ± 0.25
AA-16	*o*-Br-Ph	-80.75	-6.45	31.45 ± 0.14
AA-17	(*o,p*-di Cl)-Ph	-86.95	-6.90	32.00 ± 0.12
AA-18	(*p*-$NHCOCH_3$)-Ph	-100.70	-7.95	52.72 ± 0.57
AA-19	*m*-OCH_3-Ph	-84.56	-5.68	43.54 ± 0.41

AA-110	(*m,p*-di OCH_3)-Ph	-104.57	-6.31	53.27 ± 0.22
AA-111	(*m*-NH_2, *p*-CH_3)-Ph	-87.48	-7.96	54.54 ± 0.09
AA-112	-C_5H_4N (Isonicotinic acid)	-77.84	-5.68	37.18 ± 0.81

* % inhibition at 10μM concentration, values are mean ± S.D. of triplicate experiment performed independently

6.2.2 *N*-Phenyl-2-[(phenylsulfonyl)amino]acetamide derivatives

Most of the compounds in this series revealed improved potency as compared to prototype compound A (2.1). It was observed that the compounds having unsubstituted ring A and B were almost inactive while the compounds having electron donating substituents on ring A and bulkier substitutents on ring B showed good inhibitory potential, in general. Among ring A substitutents, *p*-acetamido substitution was most favourable (compounds 2.15, 2.16 and 2.17). When ring B is substituted with *m*-chloro or *o,p*-dimethyl, showed enhanced potency as compared to *p*-chloro. 2-(4-acetamidophenylsulfonamido)-*N*-(2,4-dimethylphenyl)acetamide (compound 2.17) showed most potent activity with 61.90% inhibition at 10μM concentration. It was analyzed further for IC_{50} value calculations whereby it displayed IC_{50} of 7.90 μM.

Difference in potency of the synthesized compounds was assessed by exploring the binding modes through docking study. It was observed that when ring A is not substituted by any group (2.2, 2.3, 2.4, 2.5), it fails to occupy the S3 or S2' region properly and interacts with only one of the aspartates i.e. Asp32. The low percentage inhibition was consistent with low docking scores. Substitution of electron donating groups such as *p*-methyl, *p*-methoxy and *p*-acetamido groups on ring A with different substitutions on ring B showed higher % inhibition values probably because these groups favoured the interaction pattern in docking studies. Among the electron withdrawing substitutents, *p*-chloro and *m*-nitro groups displayed better percentage inhibition, which can possibly be attributed to the electron pull effect of these groups from electron rich aromatic residues like Trp115, Thr231, Thr232 and Trp76. *p*-Cl in ring A influences the binding pattern favourably with better docking score as well as % inhibition. Among these, compound 2.12 having *m*-chloro on ring B showed 48% inhibition. When ring A is substituted with nitro group, it was observed that *meta* substituted compounds show higher % inhibition than *ortho* or *para*. Possibly, *ortho* substitution brings sulfonyl and nitro group in close proximity and thus it does not occupy S3 or S2' cavity and *p*-nitro, being linear, does not fit in the active site; therefore, these compounds do not show appreciable inhibitory profile. Placing electron donating *p*-methoxy on ring A improves the

inhibition as compared to electron withdrawing nitro group. *In silico* studies reveal that the *p*-methoxy group does not bind S3 region.

On the other hand, among ring B substitutents, *meta* chloro substitution is preferred over *para* chloro substitution. All the *meta* chloro substituted compounds showed better % inhibition than *para* chloro substituted or unsubstituted ring B. It was observed in docking studies that *meta* chloro occupies the S1 region in better manner over *para* chloro. Further, it was observed that bulky group on ring B covers the S1 cavity through strong hydrophobic interactions with amino acids of S1 active site and hence *o*,*p*-dimethyl substituted compounds also showed good inhibitory potency. Therefore, as compared to *p*-chloro, *m*-chloro and *o*,*p*-dimethyl group substituted compounds showed better % inhibition values.

However, if complemented with acetamide on ring A, it shows highest % inhibition, it displayed key interactions with catalytic aspartate dyad. -NH group of acetamide moiety formed hydrogen bonding interaction with Asp32 while -NH of sulfonamide moiety formed hydrogen bond with Asp228. Ring A was seen to occupy S2´-S3 active site region through hydrophobic interactions with Gly230, Tyr71 and Tyr198. Further, the oxygen of substituted acetamide group displayed hydrogen bonding interaction with Arg128, which also is a key component of S2´ region. Ring B bearing *o*,*p*-dimethyl group revealed strong hydrophobic network with Leu30, Pro70, Tyr71, Phe108 and Trp115 confirming the occupancy of S1 active site. *p*-methyl group on ring B was oriented towards Phe108 and Trp115 while *o*-methyl was present near Leu30. π electron cloud of ring B interacted with Tyr71 and Pro70 through strong π-π stacking. These docking results were concurrent with in-vitro activity data as it showed 61.90% inhibition at 10µM concentration.

Overall, it was observed that substituents on ring A matter more than substituent on ring B. Further, it can be said that bulkier the ring substituent, better is the activity. Both the substituents complement each other and adjusting the bulkiness would improve BACE-1 inhibition.

Since compound 2.17 showed highest % inhibition, it was studied for IC_{50} determination. It showed IC_{50} of 7.90µM, indicating that it has comparable potency to the prototype compound reported by Gerritz *et al*. Advantage of this compound is that it is much smaller to reported prototype.

Table 6.2: *In vitro* assay data for *N*-Phenyl-2-[(phenylsulfonyl)amino]acetamide derivatives

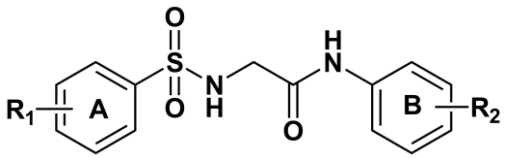

Code	R_1	R_2	Moldock score	Glide score	% Inhibition*
2.1	*p*-CH_3	H	-84.57	-6.39	21.94 ± 0.2
2.2	H	*p*-Cl	-76.82	-4.72	5.09 ± 0.1
2.3	H	*m*-Cl	-77.39	-5.30	4.83 ± 2.5
2.4	H	*o,p*-di CH_3	-64.21	-4.24	5.38 ± 1.3
2.5	H	H	-72.13	-4.28	8.72 ± 0.5
2.6	*p*-CH_3	*p*-Cl	-84.23	-6.51	25.31 ± 0.3
2.7	*p*-CH_3	*m*-Cl	-86.75	-5.94	31.75 ± 1.5
2.8	*p*-CH_3	*o,p*-di CH_3	-83.50	-7.21	35.02 ± 0.1
2.9	*o*-CH3	H	-79.51	-4.32	18.54 ± 0.6
2.10	*p*-Cl	H	-74.04	-4.93	22.75 ± 0.3
2.11	*p*-Cl	*p*-Cl	-90.75	-6.74	34.82 ± 1.2
2.12	*p*-Cl	*m*-Cl	-96.32	-8.91	48.63 ± 0.8
2.13	*p*-Cl	*o,p*-di CH_3	-101.02	-8.48	35.92 ± 0.2
2.14	*p*-$NHCOCH_3$	H	-101.55	-7.17	28.93 ± 0.1
2.15	*p*-$NHCOCH_3$	*p*-Cl	-97.40	-8.27	37.09 ± 1.8
2.16	*p*-$NHCOCH_3$	*m*-Cl	-102.09	-9.84	52.94 ± 0.6
2.17	*p*-$NHCOCH_3$	*o,p*-di CH_3	-111.74	-10.93	61.90 ± 0.9
2.18	*m*-NO_2	H	-79.19	-4.58	42.05 ± 1.2
2.19	*m*-NO_2	*p*-Cl	-90.00	-6.79	29.48 ± 1.1
2.20	*m*-NO_2	*m*-Cl	-99.03	-8.57	42.11 ± 0.4
2.21	*m*-NO_2	*o,p*-di CH_3	-93.04	-8.95	41.04 ± 0.2
2.22	*o*-NO_2	H	-66.10	-2.13	14.92 ± 0.2
2.23	*o*-NO_2	*p*-Cl	-74.88	-6.94	18.53 ± 1.1
2.24	*o*-NO_2	*m*-Cl	-95.69	-7.58	17.48 ± 1.5
2.25	*o*-NO_2	*o,p*-di CH_3	-95.41	-3.50	21.64 ± 0.6
2.26	*p*-NO_2	H	-87.50	-6.18	5.03 ± 0.1
2.27	*p*-NO_2	*p*-Cl	-65.86	-5.14	9.89 ± 0.4

2.28	*p*-NO_2	*m*-Cl	-110.50	-6.06	17.03 ± 1.1
2.29	*p*-NO_2	*o,p*-di CH_3	-97.45	-5.18	9.49 ± 0.2
2.30	*p*-OCH_3	H	-88.96	-6.48	28.59 ± 0.7
2.31	*p*-OCH_3	*p*-Cl	-91.70	-5.42	35.09 ± 2.3
2.32	*p*-OCH_3	*m*-Cl	-76.64	-5.37	38.26 ± 0.8
2.33	*p*-OCH_3	*o,p*-di CH_3	-87.89	-7.51	28.45 ± 0.4

* % inhibition at 10μM concentration, values are mean ± S.D. of triplicate experiment performed independently

6.2.3 Substituted pyrimidine derivatives

The % inhibition data for substituted pyrimidine derivatives is given in table 6.3. It was observed that *meta* substitution on the ring A (2.1G) favored overall interactions while substitution at *para* position (2.2G) reduced the docking score as well as percentage inhibition. It was observed that nitro group at para position interacts with Tyr198 and thereby pulls the molecule towards solvent and away from active site. This solvent exposure may be the probable reason for reduced activity of 2.2G. Therefore, we focused more on compounds with *m*-nitro on ring A and substituting ring B with different electron donating and withdrawing groups. Placing *p*-methoxy group on ring B (2.3G) increased the inhibitory potential (37.08%) which was concurrent to the docking score. This compound displayed hydrogen bonding interaction with aspartate dyad, *m*-nitro group showed interaction with Thr232 (S3 region) while ring B with *p*-methoxy group occupied S1 cavity. However, it did not show very good % inhibition. It was expected that replacing *p*-methoxy with *p*-amino (2.4G) will increase the interactions however; it decreased the docking score as well as the % inhibition indicating that electron donating substitution in ring B is not preferred. When substitution was done at *meta* position with bromine (2.5G), it reduced the docking score as well as % inhibition, implying that substitution at *meta* position on ring B is not suitable for activity. When ring B was substituted with *o,p*-dichloro (2.6G), it showed moderate docking score but significant increase in the activity (45.28%) indicating that *o,p*-disubstitution with electron withdrawing groups is favored in ring B. Introducing *p*-chloro on ring A with unsubstituted ring B (2.7G) or electron donating group like -methyl at *para* position on ring B (2.8G), reduced the docking score as well as % inhibition significantly. The reason may be attributed to less occupance of S1 active site. However, *o,p*-di-methoxy (2.9G) substitution showed better occupance of S1 site and hence docking score and % inhibition; indicating that *o,p*-disubstitution with bulky groups may favor the binding.

When electron donating group like *p*-dimethyl amino was positioned in ring A with *p*-nitro group on ring B (2.10G), the S3 cavity was seen to be occupied but failed to occupy S1 cleft, hence rendered the molecule low score and probably, low inhibition. This again attests that *para* substitution on ring A is not favored. On the other hand, introducing 2,5-dimethoxy (2.11G) on ring A with *meta* nitro on ring B improved the docking score which was concurrent to the % inhibition (50.98%). The amino group of 2.11A displayed hydrogen bonding interaction with Asp32 and Asp228 (2.78Å, 3.41Å; 2.73Å, 3.01Å respectively). The methoxy group at fifth position was also found to extend hydrogen bonding interaction with Arg128 (3.05Å). 2,5 disubstitution twisted the aromatic ring in such a way that ring B was pushed towards S2' region and thus occupied S2'-S3 region. When substituents of compound 2.6G and 2.11G were placed in a single compound (*o,p*-dichloro on ring B and 2,5-dimethoxy on ring A: compound 2.12G), it was observed that the % inhibition reduced though it revealed better docking score. Substitution of bulky benzyloxy group at *meta* position of ring A (compound 2.13G) with *o,p*-dichloro on ring B enhanced the docking score. It extended the ring A through ether linkage helping the benzyl moiety accommodate the S3 pocket more deeply as compared to other groups. It also enhanced the occupance of S1 and S2' cavities by ring B. The amino group formed key interactions with aspartate dyad (Asp32: 3.29Å, 3.57Å; Asp228: 2.72Å, 2.82Å). It also displayed hydrogen bonding with Gly230 (3.48Å). Further, π-π stacking was observed between Tyr71 and pyrimidine nucleus and nitrogen at pyrimidine ring also had interaction with Val332. Excellent interaction pattern observed for compound 2.13G was concomitant with BACE-1 inhibition where it displayed maximum inhibition of 73.91% at 10μM concentration. Therefore, it was tested further and was found to have IC_{50} of 6.92μM.

Further, bioisosteric replacement of amino group with thiol and hydroxy was done to find out the effect on activity. It was observed that placing thiol group, in general, did not enhance the binding affinity and the docking scores and % inhibition values obtained for this series were concurrent with conclusions drawn for 2-aminopyrimidine series. Compound 2.1T with *m*-nitro on ring A and unsubstituted ring B revealed desired interactions with catalytic sites of BACE-1 and also had moderate inhibition (32.8%). Compound 2.2T having *m*-nitro on ring A and *p*-methoxy on ring B also displayed significant interactions but low % inhibition as was the case with 2.3G. Compound 2.3T with *m*-nitro on ring A and *m,p*-dimethoxy on ring B revealed low docking score with moderate inhibitory potential (52%) augmenting the conclusion that ring B needs bulky substituents to occupy S1 cavity. If both rings have *meta* nitro substitution (Compound 2.4T) reduced the docking score as well as

potency indicating that *meta* substitution in ring B is not preferred. Keeping *m*-nitro substitution on ring A with *ortho* and *para* substitution on ring B (compound 2.5T: *o,p*-dichloro on ring B) was seen to be beneficial for activity (61.90% inhibition). Supplementing the conclusions drawn in above series, Compounds 2.6T (*p*-dimethylamino on ring A and *p*-nitro on ring B*)*, 2.7T (*m,p*-dimethoxy on ring A *and p*-chloro on ring B) and 2.8T (2,5-dimethoxy on ring A *and o,p*-dichloro on ring B) revealed low docking score with moderate inhibitory potential. Best interaction pattern with highest docking score was observed when ring A was substituted with *m*-benzyloxy group and ring B with *o,p*-dichloro group (Compound 2.9T) similar to that of 2-aminopyrimidine series (compound 2.13G). Its thiol group displayed strong interactions with catalytic aspartate dyad (Asp32: 2.76Å, 3.41Å; Asp228: 2.73Å, 3.07Å). Further, S1 cavity was well occupied by phenyl ring bearing *o,p*-di-chloro substitution which also formed π-π stacking with Tyr71 and S3 active site regions were accommodated by ring carrying benzyloxy linker. This compound also displayed best inhibition profile in this series (70.27%).

Bioisosteric replacement of 2-amino group with 2–hydroxy was seen to reduce the overall binding affinity as well as % inhibition values. Although the overall interactions of compounds of this series were similar to 2-amino and 2-thiol substituted derivatives, the inhibition was poor. In this series too, substitution at *meta* position on ring A with different substituents on ring B favoured the interaction pattern (eg. compounds 2.1U (*m*-nitro on ring A and unsubstituted ring B), 2.3U (*m*-nitro on ring A and *p*-methoxy on ring B), 2.4U (*m*-nitro on ring a and *m*-nitro on ring B) and 2.5U (*m*-nitro on ring A and *o,p*-dichloro on ring B) revealed moderate docking score and fair interactions as compared to *ortho* and *para* substitution on ring A. Further, the most active compound was 2.11U having *m*-benzyloxy substitution on ring A and *o,p*-dichloro on ring B showed highest docking score. The hydroxy group was present bridged between the two aspartates and -OH acts as donor to the two oxygen atoms of Asp32 and Asp228 with length of 2.91Å, 3.56Å; 3.11Å, 2.69Å respectively. It also had the proximity to Gly34 and also formed a hydrogen bond with water (HOH-478; 3.24Å). Ring A having *m*-benzyloxy substitution was seen to occupy the S3 region. Ring B bearing *o,p*-dichloro substitution was able to accommodate S1 cavity. However, the % inhibition values were not so encouraging.

Overall, it was also observed that replacing phenyl with heterocyclic ring as ring A, in general, weakens the activity. Taking into account the inhibition profile and interaction patterns of all these compounds, it can be proposed that 2-amino pyrimidines having substitution of electron withdrawing (such as –nitro) or moderately activating groups (such

as benzyloxy) at *meta* position on ring A with electron withdrawing substituents on ring B at *ortho and para* position are beneficial for BACE-1 inhibitory activity.

Table 6.3: *In-vitro* assay data for substituted pyrimidine derivatives

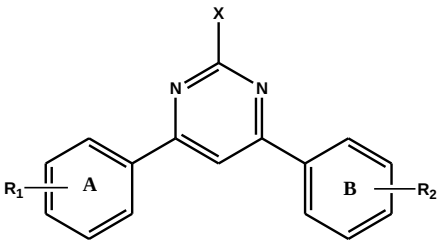

Code	R_1	R_2	X	Moldock score	Glide score	% Inhibition*
2.1G	*m*-NO_2	H	NH_2	-78.90	-5.46	30.09 ± 0.41
2.2G	H	*p*- NO_2	NH_2	-73.39	-3.18	10.85 ± 0.20
2.3G	*m*- NO_2	*p*-OCH_3	NH_2	-104.30	-8.42	37.08 ± 0.07
2.4G	*m*-NO_2	*p*-NH_2	NH_2	-99.77	-5.49	35.69 ± 0.24
2.5G	*m*-NO_2	*m*-Br	NH_2	-71.20	-2.45	21.45 ± 0.18
2.6G	*m*-NO_2	*o,p*-di Cl	NH_2	-99.49	-6.43	45.28 ± 0.44
2.7G	*p*-Cl	H	NH_2	-63.75	-2.32	10.54 ± 0.17
2.8G	*p*-Cl	*p*-CH_3	NH_2	-65.43	-2.45	3.63 ± 0.24
2.9G	*o,p*-di OCH_3	*p*-Cl	NH_2	-73.23	-5.91	41.20 ± 0.32
2.10G	*p*-NMe_2	*p*-NO_2	NH_2	-84.36	-3.42	15.75 ± 0.46
2.11G	2,5-di OCH_3	*m*-NO_2	NH_2	-88.49	-6.57	50.98 ± 0.17
2.12G	2,5-di OCH_3	*o,p*-di Cl	NH_2	-79.40	-7.84	31.89 ± 0.05
2.13G	*m*-O-Bn	*o,p*-di Cl	NH_2	-111.09	-8.37	73.91 ± 0.09
2.14G	Anthraldehye	H	NH_2	-75.16	-3.26	19.34 ± 0.09
2.1T	*m*-NO_2	H	SH	-100.03	-6.42	32.80 ± 0.40
2.2T	*m*-NO_2	*p*-OCH_3	SH	-84.90	-6.14	10.14 ± 0.08
2.3T	*m,p*-di OCH_3	*m*-NO_2	SH	-86.63	-6.72	52.00 ± 0.05
2.4T	*m*-NO_2	*m*-NO_2	SH	-98.68	-4.16	21.27 ± 0.01
2.5T	m-NO_2	*o,p*-di Cl	SH	-97.46	-8.02	61.90 ± 0.35
2.6T	*p*-NMe_2	*p*-NO_2	SH	-87.38	-5.94	32.18 ± 0.34
2.7T	*m,p*-di OCH_3	*p*-Cl	SH	-86.04	-5.67	34.90 ± 0.20
2.8T	2,5-di OCH_3	*o,p*-di Cl	SH	-81.58	-2.36	33.00 ± 0.41

2.9T	*m*-O-Bn	*o,p*-di Cl	SH	-108.40	-7.19	70.27 ± 0.55
2.10T	Furan-2-aldehyde*	*m*-Br	SH	-76.55	-3.48	IA
2.1U	*m*-NO_2	H	OH	-94.45	-5.31	8.13 ± 0.58
2.2U	*p*-NO_2	H	OH	-74.01	-5.14	44.36 ± 0.33
2.3U	*m*-NO_2	*p*-OCH_3	OH	-84.56	-6.41	6.45 ± 0.22
2.4U	*m*-NO_2	*m*-NO_2	OH	-98.64	-6.64	5.83 ± 0.31
2.5U	*m*-NO_2	*o,p*-di Cl	OH	-104.28	-6.13	24.63 ± 0.04
2.6U	*p*-Cl	*p*-CH_3	OH	-81.41	-6.85	14.61 ± 0.31
2.7U	*p*-NMe_2	*p*-NO_2	OH	-72.31	-2.74	IA
2.8U	*m,p*-di OCH_3	*m*-NO_2	OH	-71.89	-2.67	IA
2.9U	*m,p*-di OCH_3	*p*-Cl	OH	-68.16	-2.87	27.12 ± 0.54
2.10U	2,5-di OCH_3	*o,p*-di Cl	OH	-65.37	-4.75	25.29 ± 0.16
2.11U	*m*-O-Bn	*o,p*-di Cl	OH	-98.94	-6.91	33.54 ± 0.39
2.12U	Furan-2-aldehyde*	*m*-Br	OH	-72.41	-4.63	16.36 ± 0.24

* % inhibition at 10μM concentration, values are mean ± S.D. of triplicate experiment performed independently; IA: inactive

6.2.4 Allylidene hydrazinecarboximidamide derivatives

The *in vitro* inhibition data along with the docking scores for (1, 3 diphenylallylidene) hydrazinecarboxiidamide derivatives is given in table 6.4. For this series, the docking scores as well as % inhibition values are higher. This can be attributed to favourable interactions with the catalytic aspartates and cavity occupance. When ring A alone was substituted, it was observed that compound C2A with *m*-nitro had high docking score and high (48%) inhibition. The reason may be explained through strong interactions observed in docking simulation: i. ring A occupied S3 active site region with the nitro group hydrogen bonded to Gly11 and Thr232; ii. aminoguanidinium formed interactions with catalytic aspartate dyad; iii. imine formed hydrogen bond with Gly230 and; iv. guanidinium group also formed interaction with Thr231. Introducing 2,5-dimethoxy (C5A) and *p*-dimethylamino (C13A) on ring A with unsubstituted ring B gave less potent molecules probably due to weaker interactions with the enzymatic active site.

Substituting ring B alone with electron poor and electron rich moieties was not favourable for BACE-1 inhibition. Among ring B substituted compounds, C3A with *p*-nitro group had high

docking score compared to the compounds C6A, C9A, C11A and C19A. This may be because *p*-nitro group is engulfed deep in the S1 region while *m*-nitro group (C9A) was slightly solvent exposed. In the *in vitro* study, however, contrary to docking scores, compound C9A had higher inhibition as compared to others. Placing *p*-methoxy (C28A)*, o,p*-dichloro (C29A) or *m*-Br (C33A) on ring B and *m*-nitro on ring A, although showed good interactions in docking, were less active, which may be attributed to poor hydrophobic interactions in S1 region.

It was observed that placing *m*-nitro on ring A and *p*-nitro at ring B (compound C4A) displayed high potency with 62% inhibition. In docking studies, it displayed good interaction pattern. It was observed that both the nitro groups help orient the aromatic ring properly into S1 and S3 pockets. When *p*-dimethylamino group was substituted on ring A with alterations on ring B, it was observed that all three compounds (C8A, C12A, C16A and C17A) had low docking scores and weak activity. It can be proposed that polar nature of *p*-dimethylamino group having high electron density bars it from eliciting hydrophobic and van der Waal interactions and hence ring A fails to completely occupy S3 region. Another series with 2,5 di-methoxy group on ring A and *m*-bromo (C30A) and *p*-methoxy (C31A) on ring B also had poor inhibitory profile. It was observed that 2,5 di-methoxy group on ring A changes the conformation in such as way that ring B is pushed out of S1 active site. However, docking scores were good because the substitutents formed hydrogen bonds with amino acids outside the cavity.

Replacing the phenyl ring system of aldehyde with larger ring like anthraldehyde did not show any activity while indole-3-carboxaldehyde shows 38.50% inhibition and its activity may be attributed to hydrogen bonding interaction of indole nitrogen with Gly230.

When *m,p*-dimethoxy group was on ring A, favorable interaction pattern was seen with high docking scores and BACE-1 inhibitory potential (Compounds C23A, C24A, C25A, C37A and C38A). It was observed that *para* electron withdrawing substitution on ring B is preferred over *o,p*- or *meta*. Compound C23A (*p*-nitro on ring B) and C24A (*p*-chloro on ring B) had highest inhibition of 61.18% and 78.23% respectively, which is concurrent with docking interactions. Further, 2,5–dimethoxy substitution on ring A is less preferred over *m*,*p*-dimethoxy substitution. The reason for this can be better hydrogen bonding interaction observed in *m,p*-dimethoxy substitution with amino acid residues of S3 region (Thr232). In this series, maximum inhibition was displayed when *m,p*-dimethoxy group is present on ring A and *p*-Cl at ring B (C24A) and it displayed IC_{50} of 6.42µM.

Table 6.4: *In-vitro* assay data for substituted allylidene hydrazinecarboximidamide derivatives

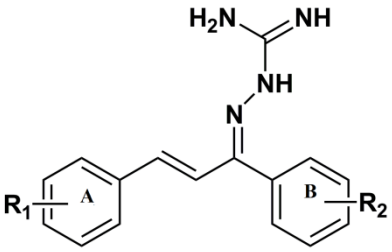

Code	R_1	R_2	Moldock score	Glide score	% Inhibition*
C1A	H	H	-92.06	-5.62	10.84 ± 0.03
C2A	*m*-NO_2	H	-107.86	-6.41	47.93 ± 0.05
C3A	H	*p*-NO_2	-109.70	-6.12	13.50 ± 0.01
C4A	*m*-NO_2	*p*-NO_2	-107.35	-7.85	62.14 ± 0.07
C5A	2,5 di OCH_3	H	-97.73	-5.18	32.58 ± 0.32
C6A	H	*m*-OH	-94.60	-8.47	NT
C7A	Anthraldehyde	H	-73.32	-4.19	IA
C8A	*p*-NMe_2	*p*-CH_3	-88.40	-6.16	10.83 ± 0.07
C9A	H	*m*-NO_2	-75.91	-4.93	23.40 ± 0.18
C11A	H	*p*-Cl	-91.23	-4.18	IA
C12A	*p*-NMe_2	*p*-NO_2	-80.06	-3.48	23.95 ± 0.40
C13A	*p*-NMe_2	H	-73.29	-4.14	IA
C16A	*p*-NMe_2	*m*-NO2	-78.74	-5.21	27.97 ± 0.21
C17A	*p*-NMe_2	*p*-Cl	-84.19	-5.94	35.70 ± 0.02
C18A	Anthraldehyde	*p*-Cl	-73.80	-6.07	27.89 ± 0.15
C19A	H	*p*-OH	-100.16	-4.74	NT
C20A	*p*-OCH_3	*p*-OH	-112.74	-4.91	NT
C21A	Indole 3-carboxaldehyde	H	-78.50	-6.02	38.50 ± 0.34
C22A	*m,p*- di OCH_3	H	-96.47	-8.94	42.13 ± 0.27
C23A	*m,p*- di OCH_3	*p*-NO_2	-123.06	-10.53	61.18 ± 0.04
C24A	*m,p*- di OCH_3	*p*-Cl	-105.65	-10.38	78.23 ± 0.09
C25A	*m,p*- di OCH_3	*m*-NO_2	-95.04	-7.38	45.83 ± 0.14
C28A	*m*-NO_2	*p*- OCH_3	-112.00	-9.59	11.04 ± 0.09

C29A	*m*-NO_2	*o,p*-di Cl	-105.64	-9.17	5.40 ± 0.56
C30A	2,5 di OCH_3	*m*-Br	-117.11	-10.09	23.94 ± 0.43
C31A	2,5 di OCH_3	*p*-OCH_3	-118.49	-10.25	10.33 ± 0.09
C33A	*m*-NO_2	*m*-Br	-104.62	-7.43	10.76 ± 0.55
C35A	*m*-Br	*p*-NO_2	-104.38	-5.42	NT
C36A	*o*-Cl	*m*-Br	-103.67	-6.70	NT
C37A	*m,p*- di OCH_3	*o,p*-di Cl	-97.75	-6.03	21.83 ± 0.52
C38A	*m,p*- di OCH_3	*m*-Br	-111.90	-9.58	25.94 ± 0.06

* IA: Inactive, NT: Not tested

Chapter 7

SUMMARY AND CONCLUSION

Alzheimer's disease (AD) is a progressive and fatal brain disorder, for which there is no cure. It leads to memory loss, steady deterioration of cognition, and dementia. Despite of large population suffering from AD, the number of therapeutic options in market remain few. At present, four drugs (tacrine, donepezil, rivastigmine and galantamine) have been approved for AD treatment. These drugs, however, are not able to alter or prevent disease progression. They are, instead, palliative in alleviating the symptoms of disease. No disease-modifying therapy is available yet.

One of the major characteristic and pathological hallmarks of AD is represented by the senile plaques chiefly composed of cytotoxic amyloid-β peptide (Aβ-42), of which production and deposition is the central event in the pathogenesis of Alzheimer's disease (AD). Aβ-42 is excised from the amyloid precursor protein (APP) through sequential actions of the BACE-1 (β-secretase), which cleaves at the β-site, and the γ-secretase, which cleaves at the γ-site of APP. Localization, activity, and regulation of BACE-1 have been well investigated and is recognized as one of the most promising targets in the treatment of AD.

The search for small molecule BACE-1 inhibitors has proven to be challenging. The aim was therefore; to design, synthesize and evaluate small molecular BACE-1 inhibitors using structure based drug design. From amongst the various crystal structures available for BACE-1, 2OHP (PDB id) was chosen after validating the crystal structure for docking simulation using co-crystallized ligand and extracted ligand. It was also cross-validated using external dataset of 20 standard molecules.

The design of these compounds involved docking study followed by oral bioavailability along with *in silico* toxicity prediction. Docking studies were performed on molegro virtual docker and Glide (Schrodinger). Chemaxon JChem for Excel was used for oral bioavailability prediction and OSIRIS property explorer for toxicity prediction. BBB permeation was predicted using online BBB permeation predictor software available at http://www.cbligand.org/BBB/.

To start with, the compounds reported to inhibit other aspartate proteases like Plasmepsin-II and Cathepsin-D were studied to find a suitable prototype. Using available information, acridin-9-yl hydrazide derivatives were designed. Docking studies revealed that these compounds, in general, occupy S1 active site region and formed hydrogen bonding interactions with Asp32. 12 derivatives were designed, synthesized and evaluated for *in vitro* BACE-1 inhibition. Overall this series displayed consistent BACE-1 inhibitory profile with compound AA-111 displaying maximum inhibition of 54.54% at 10μM concentration. It was observed that electron donating groups had better activity as compared to electron

withdrawing substitutents. These compounds followed Lipinski rule of five but were found to possess mutagenicity, toxicity and irritancy, rendering them a low drug score due to acridine ring system.

When the docking poses of library of acridin-9-yl hydrazide derivatives were analyzed, it was observed that these derivatives failed to occupy S3 active site region and interacted with only Asp32. None of these compounds could form hydrogen bond with Asp228, considered important component of aspartate dyad. Hence, it was aimed to design compounds that would interact with aspartate dyad and also occupy S1 as well as S3 region. To achieve this, *N*-Phenyl-2-[(phenylsulfonyl)amino]acetamide derivatives were designed through bioisosteric replacement of reported acyl guanidine derivatives. Docking studies revealed that these compounds interacted well with aspartate dyad. They were observed to occupy the S1 region, S2' region and also interacted with few S3 cavity amino acids. The compounds complied with criteria for oral bioavailability and also were mostly free of toxicity. From amongst 33 compounds designed and synthesized, compound 2.17 displayed maximum inhibition with IC_{50} of 7.90µM. The *in vitro* activity was concomitant with the docking scores.

It was noted that *N*-Phenyl-2-[(phenylsulfonyl)amino]acetamide derivatives showed good interactions but occupied more of S2' cavity than S3 region owing to the increased flexibility of sulfonylamino acetamide linker. To overcome this problem, heteroaromatic rings that could provide rigidity and maintain the desired interactions were designed. Report of aminoimidazole compounds showing BACE-1 inhibition were available. Hence, 2- amino pyrimidines were selected with a rationale that the guanidium moiety could interact with Asp32 and Asp228 and the two aromatic rings placed at fourth and sixth position of pyrimidine ring would occupy S1 and S3 cavity. Further, effect of bioisosterically replacing amino group with thiol and hydroxy was also considered. Therefore, a total of 37 compounds were designed having amino/thiol/hydroxy group at second position and substituted aromatic rings at fourth and sixth positions of the pyrimidine ring. These compounds occupied the S1 as well as S3 cavity and also formed hydrogen bonds with Asp32 and Asp228. It was observed that -amino and -thiol substituted compounds had comparable binding affinity but it was lower for hydroxy substituted derivatives as it gets charged and looses the ability to form hydrogen bond with aspartates. Compound 2.9G of 2-amino pyrimidine series displayed maximum inhibition (73.91%) in this series with IC_{50} value 6.92 µM. Compound 2.3T and 2.6T of 2-thioipyrimidines also displayed significant inhibition; 61.90% and 70.27% respectively at 10µM concentration. Further, the series complied well with Lipinski rule of five and overall did not display any toxicity in *in silico* prediction. It is

proposed that placing electron withdrawing group or weakly activating group on ring A and electron withdrawing group on ring B is favourable for BACE-1 inhibition which is concurrent with docking simulation study.

Docking and inhibition data obtained from above two series was encouraging and helped in drawing a conclusion that long linker of *N*-Phenyl-2-[(phenylsulfonyl)amino]acetamide was not required. Further, positioning aromatic groups on either side of pyrimidine nitrogen were occupying S1 and S3 cavity. Hence, it was envisioned to design a series having less flexibility using short linker, placing aminoguanidine substitution on linker to complement the aspartate dyad and placing two aromatic rings on either side of linker to occupy the S1 and S3 cavities. Keeping this in mind, a library of 31 allylidene hydrazinecarboximidamide derivatives was designed. All the compounds displayed higher docking score revealing strong hydrogen bonding interactions with catalytic aspartate dyad and the aromatic rings properly accommodated in S1 and S3 substrate binding clefts. Also, these compounds obeyed Lipinski rule of oral bioavailability and had better drug score than previous series indicating no sign of toxicity, better solubility and drug likeliness. Of all the compounds, compound C24A displayed maximum inhibition in this series as well as among all the four series. It had 78.23% BACE-1 inhibition at 10µM concentration and IC_{50} value of 6.42µM.

To conclude, the specific contribution of the present work can be given as:

1. It complements the understanding that structure-based design followed by computer aided drug discovery is helpful technique in achieving higher hit rates.
2. The study helps in identifying the potential binding modes for the design of BACE-1 inhibitors. It was observed that moderately rigid structure with groups for interacting with aspartate dyad, occupying S1 as well as S3 cavity is essential.
3. The most active compound, C24A displayed all the desired interactions and hence shows IC_{50} value of 6.42µM.
4. The study can be a basis for indicating that small, low molecular weight ligands as compared to those reported in the literature can also inhibit the BACE-1 enzyme. These compounds may also penetrate the blood brain barrier as indicated by *in silico* prediction. It can be proposed that many compounds reported in this thesis will have increased brain permeability due to low logP values, low molecular weight and low polar surface area.
5. Compound C24A represents a suitable starting point for extensive modifications for hit-to-lead conversion and eventually lead generation to effectively inhibit BACE-1 enzyme.

FUTURE PERSPECTIVES

The present work mainly focused on generation of structurally diverse library of small molecules to obtain leads of different structural scaffolds using computer aided drug design. Based on this work, following future studies may be planned:

1. The study has identified potential binding modes for the design of BACE-1 inhibitors. Using this information, several libraries can be designed of the molecules having improved binding interactions with BACE-1 active site and thus improved potency.

2. It can also be used in future design of new hits or in the development of hits to lead against various other targets such as aspartyl proteases.

3. The study has also shown that acridin-9-yl hydrazides, *N*-Phenyl-2-[(phenylsulfonyl)amino]acetamide, 2-amino- or 2-thio- pyrimidines and allylidene hydrazine carboximidamide derivatives have the potential to inhibit BACE-1 enzyme. Further to it,

a. specificity studies against other aspartyl proteases may be done

b. dose response curves for the best active compounds may be plotted to get the inhibition profile.

c. *in vivo* studies to prove efficacy/toxicity of these compounds in animal models may be performed.

d. modification in the active structures can be done to enhance potency and reduce failures.

CHAPTER 8

REFERENCES

1. Corrada MM, Brookmeyer R, Berlau D, *et al*. Prevalence of dementia after age 90. Results from 90+ study. *Neurol* 2008; 71(5): 337-343.
2. Ferrari CP, Prince M, Brayne C, et al. Global prevalence of dementia: A Delphi consensus study. *Lancet* 2005; 366(9503): 2112-2117.
3. Toni PM, Tanya EF, Sidney TB, *et al*. Dementia and race: Are there differences between African-American and Caucasians. *J Am Geriatr Soc* 2001; 49(4): 477-484.
4. Alzheimer's Association. http://sis.nlm.nih.gov/Tox/ToxMain.html (Accessed March 5, 2011).
5. Jack Diamond (2008). A report on Alzheimer's disease and current research, Alzheimer's society of Canada. http://www.alzheimer.ca/en/Research (Accessed May 25, 2009)
6. Christiane R, Richard M. Alzheimer disease: Epidemiology, diagnostic criteria, risk factors and biomarkers *Biochem Pharmacol* 2014; 88(4):640-651.
7. Michelle MM, Prashanthi V, Walter AR. Clinical epidemiology of Alzheimer's disease: assessing sex and gender differences. *Clin Epidemiol* 2014; 6:37–48.
8. Priti Jain and Hemant R. Jadhav. Therapeutic Advances in the Treatment of Alzheimer's disease: Present and Future, *Curr Drug Ther* 2011; 6:110-121.
9. http://www.mayoclinic.com/health/alzheimers-stages/AZ00041 (Accessed July 28,2011)
10. http://www.alzinfo.org/clinical-stages-of-alzheimers (Accessed May 25, 2009)
11. http://www.nia.nih.gov/alzheimers/topics/symptoms (Accessed May 25, 2009)
12. http://www.webmd.com/alzheimers/alzheimers-disease-stages (Accessed May 25, 2009)
13. Cumming JL. Alzheimer's disease: etiologies, pathophysiology, cognitive reserve and treatment opportunities. *Neurol* 1998; 51(1):512-517.
14. Tabet N. Acetylcholine inhibitors for Alzhiemer's disease: anti-inflammatories in acetylcholine chlothing. *Age and Ageing* 2006; 35(4):336-338.
15. Hogan DB. Progress update: Pharmacological treatment of Alzheimer's disease. *Neuropsychiatric Dis and Treat* 2007; 3(5):567-578.
16. Deachter I, Leuven FV. Secretases as a target for the treatment of Alzheimer's disease: the prospects. *Lancet Neurol* 2002; 1(7):409-416.
17. Suzuki N, Cheung TT, Cai XD *et al.* An increased percentage of long amyloid β protein secreted by familial amyloid β-protein precursor (βAPP717) mutants. *Science* 1994; 264(5163):1336-1340.

18. Asami OA, Ishibashi Y, Kikuchi T *et al.* Long amyloid β protein secreted from wild type human neuroblastoma IMR-32 cells. *Biochem* 1995; 34(32):10272-10278.
19. Walsh DM, Selkoe DJ. Deciphering the molecular basis of memory failure in Alzheimer's disease. *Neuron* 2004; 44(1):181-193.
20. Braak H, Braak E. Staging of Alzheimer's disease related neuroinflammatory changes. *Neurobiol Aging* 1995; 16:271-278.
21. Ballatore C, Lee VM, Trojanowski JQ. Tau-mediated neurodegeneration in Alzheimer's disease and related disorders. *Nat Rev Neurosci* 2007; 8(9):663-672.
22. Santacruz K, Lewis J, Spires T, *et al*. Tau suppression in neurodegenerative mouse model improves memory functions. *Science* 2006; 309(5733): 476-481.
23. Steinhilb ML, Dias-Santagata D, Mulkearns EE. S/P and T/P Phosphorylation Is Critical for Tau Neurotoxicity in Drosophila. *J Neurosci Res* 2007; 85(6):1271-1278.
24. Rogers J, Cooper NR, Webster S, *et al.* Complement activation by beta amyloid in Alzheimer's disease. *Proc Natl Acad Sci* 1992; 89(21):10016-10020.
25. Dickson DW, Lee SC, Mattiace LA, *et al*. Microglia and cytokines in neurological disease, with special reference to AIDS and Alzheimr's disease. *Glia* 1993; 7(1):75-83.
26. McGeer PL, Kawamata T, Walker DG, *et al.* Microglia in degenerative neurological diseases. *Glia* 1993; 7(1):84-92.
27. Eikelenboom P, Veerhuis R. Role of complement and activated microglia in the pathogenesis of Alzheimer's disease. *Neurobiol Aging* 1996; 17(5):673-680.
28. Akiyama H, Barger S, Barnum S, *et al.* Inflammation and Alzheimer's disease. *Neurobiol Aging* 2000; 21(3):383-421.
29. Ard MD, Cole GM, Wei J, *et al*. Scavenging of Alzheimer's amyloid beta-protein by microglia in culture. *J Neurosci Res* 1996; 43(2):190–202.
30. Koenigsknecht J, Landreth G. Microglial phagocytosis of fibrillar beta-amyloid through a beta1 integrin-dependent mechanism. *J Neurosci* 2004; 24(44):9838-9846.
31. Webster SD, Yang AJ, Margol L, *et al.* Complement component Cl q modulates phagocytosis of Ab by microglia. *Exp Neurol* 2000; 161:127-138.
32. Simard AR, Soulet D, Gowing G, *et al*. Bone marrow derived microglia play a critical role in restricitng senile plaques formation in Alzheimer's disease. *Neuron* 2006; 49(4):489-502.
33. El Khoury J, Toft M, Hickman SE. Ccr2 deficiency impairs microglial accumulation and accelerates progression of Alzheimer-like disease. *Nat Med* 2007; 13(4):432-438.

34. Yamamoto M, Horiba M, Buescher JL, *et al.* β-amyloid precursor protein transgenic mice show accelerated diffuse β-amyloid deposition. *Am J Pathol.* 2005; 166:1475–1485.

35. Bard F, Cannon C, Barbour R, *et al.* Peripherally administered antibodies against amyloid beta peptide enter the central nervous system and reduce pathology in a mouse model of alzheimer's disease. *Nat Med* 2000; 6(8):916-919.

36. Ellis JM. Cholinestrase inhibitors in the treatment of dementia. *J Am Osteo Assoc* 2005; 105(3): 145-153.

37. Hanna K. Zimmermann T, Hans PB, *et al* Cholinesterase inhibitors for patients with Alzheimer's disease: systematic review of randomised clinical trial. *BMJ* 2005; 331(7512): 321-327.

38. Tariot PN, Cumming JL, Katz IR, *et al*. A randomized, double-blind, placebo-controlled study of the efficacy and safety of donepezil in patients with Alzheimer's disease in the nursing home setting. *J Amer Geriat Soc*. 2001; 49(12): 1590-1599.

39. Winblad B, Engedal K, Soininen H, *et al.* A 1-year, randomized, placebo-controlled study of donepezil in patients with mild to moderate AD*. Neurol.* 2001; 57(3): 489-495.

40. Hogan DB. Progress update: Pharmacological treatment of Alzheimer's disease. *Neuropsychiatric Dis and Treat* 2007; 3(5): 567-578.

41. Rajesh R.T, Dyck CH. Memantine: Efficacy and safety in mild to severe Alzheimer's disease. *Neuropsychiatric Dis and Treat* 2007; 3(2): 245-258.

42. Tariot PN, Farlow MR, Grossberg GT, *et al.* Memantine treatment in patients with moderate to severe alzheimer disease already receiving donepezil: a randomized controlled trial. *J Am Med Assoc* 2004; 291(3):317-324.

43. Lim GP, Yang F, Chu T, *et al.* Ibuprofen suppresses plaque pathology and inflammation in a mouse model for alzheimer's disease. *J Neurosci.* 2000; 20(15):5709-5714.

44. Deachter I, Leuven FV. Secretases as a target for the treatment of Alzheimer's disease: the prospects. *Lancet Neurol* 2002; 1(7):409-416.

45. Suzuki N, Cheung TT, Tobun T, *et al.* An increased percentage of long amyloid β protein secreted by familial amyloid β-protein precursor (βAPP717) mutants. *Science* 1994; 264(5163):1336-1340.

46. Matti S, Janelle N, David H S. Regulation of APP cleavage by α-, β- and γ-secretases. *FEBS lett* 2000; 483(1):6–10.

47. Shimmyo Y, Kihara T, Akaike A, *et al.* Flavanols and flavones as BACE-1 inhibitors: structure-activity relationship in cell-free, cell-based and in-silico studies reveal novel pharmacophore features. *Biochem Biophys Acta* 2008; 1780(5):819-825.

48. Haass C. Take five- BACE and the γ-secretase quartet conduct Alzheimer's amyloid β-peptide generation. *The EMBO Journal* 2004; 23(3):485.

49. Dragana, S. and Wim, A. Building gamma-secretase- the bits and pieces. *J of Cell Sci* 2008; 121(4):413-420.

50. David HS, David WK, Lisa F. Presenilin and gamma secretase: Still a complex problem. *Molecular Brain* 2010; 3(7):1-6.

51. Moore CL, Leatherwood DD, Diehl TS, *et al.* Difluoro ketone peptidomimetics suggest a large S1 pocket for Alzheimer's γ-secretase: Implication for inhibitor design. *J. Med. Chem.* 2000; 43(18):3434-3442.

52. Lanz TA, Carol SA, Giovanni P, *et al.* The γ-secretase, DAPT reduces Aβ levels in vivo in plasma and CSF in young (plaque-free) and aged (plaque-bearing) Tg2576 mice. *JPET Fast Forward* 2003; 305(3):864-871.

53. Dovey HF, John V, Anderson JP, *et al.* Functional gamma-secretase inhibitors reduce beta-amyloid peptide levels in brain. *J Neurochem* 2001; 76(1):173-181.

54. Petit A, Pasini A, Alves DC, *et al.* JLK-isocoumarin inhibitors: Selective gamma secretase inhibitors that do not interfere with notch pathway in vitro or in vivo. *J. Neurosci. Res.* 2003; 74(3):370-377.

55. Andrea G, Steiner H, Willem M, *et al.* A γ-Secretase inhibitor blocks notch signaling in vivo and causes a severe neurogenic phenotype in zebrafish. *EMBO Reports* 2002; 3(7):688-694.

56. Wu WL, Lili Z. Gamma secretase inhibitors for the treatment of Alzheimer's disease. *Drug Dev. Res.* 2009; 70(2):94-100.

57. Mayer C, Kreft AF, Harrison B, *et al.* Discovery of begacestat, a notch-1-sparing γ-secretase inhibitor for the treatment of Alzheimer's disease. *J. Med. Chem* 2008; 51(23):7348-7351.

58. Henley DB, MayPC, Dean RA, *et al.* Development of Semagacestat (LY450139), a functional gamma secretase inhibitor, for the treatment of Alzheimer's disease. *Expert Opin Pharmacother.* 2009; 10(10):1657-1664.

59. Seimers ER, Quinn JF, Kaye J, *et al.* Effects of gamma secretase inhibitor in a randomized study of patients with Alzheimer's disease. *Neurol* 2006; 66(4):602-604.

60. Adam SF, Rema R. Phase II safety trial targeting amyloid beta production with a gamma-secretase inhibitor in Alzheimer's disease. *Arch Neurol.* 2008; 65(8):1031-1038.

61. Evin G. γ-secretase modulators: hopes and setbacks for the future of Alzheimer's treatment. *Neurother.* 2008; 8(11):1611-1613.

62. Lim GP, Yang F, Chu T, *et al.* Ibuprofen suppresses plaque pathology and inflammation in a mouse model for alzheimer's disease. *J. Neurosci.* 2000; 20(15):5709-5714.

63. Wilcock GK, Black SE, Hendrix SB, *et al.* Efficacy and safety of tarenflurbil in mild to moderate Alzheimer's disease: a randomized phase II trial. *Lancet* 2008; 7(6):483-493.

64. Robert CG. Effect of tarenflurbil on cognitive decline and activities of daily living in patients with mild alzheimer's disease: A randomised controlled trial*. J. Am. Med. Assoc.* 2009; 302(23):2557-2564.

65. Dale BS, Seubert P, Lieberberg I, *et al.* Beta peptide immunization: A possible treatment for alzheimer's disease. *Arch Neurol* 2000; 57(7):934-936.

66. Dara LD, Kaan EB, Maki U, *et al.* Aβ peptide immunization restores blood-brain barrier integrity in alzheimer's disease. *FASEB J.* 2006; 20(3):426-433.

67. Gilman S, Koller M, Black RS, *et al.* Clinical effects of Aβ immunization (AN1792) in patients with AD in an interrupted trial. *Neurol* 2005; 64(9):1553-1562.

68. Dale S, Hagen M, Seubert P. Current progress in beta-amyloid immunotherapy. *Curr. Opin. Immunol.* 2004; 16(5):599-606.

69. Dale S. Amyloid-β immunotherapy for Alzheimer's disease: the end of the beginning. *Neurosci* 2002; 3:282-284.

70. Anahit G, Irina P, Andrew L, *et al.* Aβ- immunotherapy for alzheimer's disease using mannan-amyloid-beta peptide immunoconjugates. *DNA Cell Biol.* 2006; 25(10):571-580.

71. Lemere CA. Developing novel immunogens for a safe and effective Alzheimer's disease vaccine. *Prog Brain Res* 2009; 175:83-93.

72. Edward T. New horizons in the treatment of alzheimer's disease-immunotherapeutics. *US Neurol* 2008; 4(1):34-36.

73. Bard F, Cannon C, Barbour R, *et al.* Peripherally administered antibodies against amyloid beta peptide enter the central nervous system and reduce pathology in a mouse model of Alzheimer's disease. *Nat Med* 2000; 6(8):916-919.

74. Lemere CA, Masliah E. Can alzheimer's disease be prevented by amyloid-β immunotherapy? *Nat Rev Neurol* 2010; 6(2):108-119.

75. Cheryl AH, Vivian N, JoAnne ML. Small molecule inhibitors of Aβ-aggregation and neurotoxicity. *Drug Dev. Res.* 2009; 70:111-124.

76. Frid P, Anisimov SV, Popovic N. Congo red and protein aggregation in neurogenerative diseases. *Brain Res Rev* 2007; 53(1):135-160.

77. Robert H, Ma Y, Molina HF, *et al.* Iron chelation as a potential therapy for neurodegenerative diseases. *Biochem. Soc. Trans.* 2008; 36(6):1304-1308.

78. Daniela G and Elio S. New Perspectives for the Treatment of Alzheimer's Disease. *Open Ger Med J,* 2008; 1:33-42.

79. Prasanthi JR, Schrag M, Dasari B. Deferiprone reduces amyloid-β and tau phosphorylation levels but not reactive oxygen species generation in hippocampus of rabbits fed a cholesterol-enriched diet. *J Alzheimers Dis*. 2012; 30(1):167-182.

80. Miao-Kun S. R*esearch progress in Alzheimers Disease and Dementia,* 1st Volume, Nova Science Publishers: New York, 2008.

81. Claude MW, Harrington CR, Storey JM. Tau-aggregation inhibitor therapy for Alzheimer's disease. *Biochem Pharmacol.* 2014; 4(15):529-539.

82. Congdon EE, Necula M, Blackstone RD, *et al.* Potency of a tau fibrillization inhibitor is influenced by its aggregation state. *Arch. Biochem. Biophys.* 2007; 465(1):127-135.

83. Pickhardt M, Gazova Z, Wang Y, *et al.* Anthraquinones inhibit tau aggregation and dissolve alzheimer's paired helical filaments in vitro and in cells. *J. Biol. Chem.* 2005; 280(5):3628-3635.

84. Bruno PI, V S, Francesco P. Are NSAIDs useful to treat Alzheimer's disease or mild cognitive impairment? *Front Aging Neurosci.* 2010; 2:1-14.

85. Brunden KR, John Q, Virginia MY. Advances in tau focused drug discovery for Alzheimer's disease and related tauopathies. *Nat Rev Drug Discov.* 2009; 8(10):783-793.

86. Cai H, Wang Y, McCarthy D, *et al*. BACE1 is the major [beta]-secretase for generation of A[beta] peptides by neurons. *Nat Neurosci* 2001; 4:233-234.

87. Bennett BD, Babu-Khan S, Loeloff R, *et al.* Expression Analysis of BACE2 in Brain and Peripheral Tissues. *J Biol Chem* 2000; 275(27):20647-20651.

88. Haass C, Lemere CA, Capell A, *et al*. The Swedish mutation causes early-onset Alzheimer's disease by [beta]-secretase cleavage within the secretory pathway. *Nat Med* 1995; 1:1291-1296.

89. Sinha S, Anderson JP, Barbour R. Purification and cloning of amyloid precursor protein [beta]-secretase from human brain. *Nature* 1999; 402(6761):537-540.

90. Yan R, Bienkowski MJ, Shuck ME. Membrane-anchored aspartyl protease with Alzheimer's disease [beta]-secretase activity. *Nature* 1999; 402(6761):533-537.

91. Hussain I, Powell D, Howlett DR. Identification of a Novel Aspartic Protease (Asp 2) as [beta]-Secretase. *Mol Cell Neurosci* 1999; 14(6):419-427.

92. Lin X, Koelsch G, Wu S. Human aspartic protease memapsin 2 cleaves the β-secretase site of β-amyloid precursor protein. *PNAS* 2000; 97(4):1456-1460.

93. Cai H, Wang Y, McCarthy D, *et al*. BACE1 is the major [beta]-secretase for generation of A[beta] peptides by neurons. *Nat Neurosci* 2001; 4:233-234.

94. Bennett BD, Babu-Khan S, Loeloff R, *et al.*Expression Analysis of BACE2 in Brain and Peripheral Tissues. *J Biol Chem* 2000; 275(27):20647-20651.

95. Fischer F, Molinari M, Bodendorf U, *et al*. The disulphide bonds in the catalytic domain of BACE are critical but not essential for amyloid precursor protein processing activity. *J Neurochem* 2002; 80(6):1079-1088.

96. Shimizu H, Tosaki A, Kaneko K, *et al.* Crystal structure of an active form of BACE-I, an enzyme responsible for amyloid protein production. *Mol. And Cell. Biol*. 2008; 28(11):3663-3671.

97. David H, David WK, Lisa F. Presenilin and gamma secretase: still a complex problem. *Molecular Brain* 2010; 3:1-7.

98. Xiaojie Z. and Weihong S. The role of APP and BACE1 trafficking in APP processing and amyloid- β, Generation, *Alzheimer's Res & Ther* 2013; 5:46.

99. Shi J, Zhang S, Tang M, *et al* The 1239G/C polymorphism in exon 5 of BACE1 gene may be associated with sporadic Alzheimer's disease in Chinese Hans. *Am J Med Genet B Neuropsychiatr Genet* 2004; 124B:54-57.

100. Patel S, Vuillard L, Cleasby A, *et al*. Apo and Inhibitor Complex Structures of BACE ([beta]-secretase). *J Mol Biol* 2004; 343(2):407-416.

101. Hong L, Tang J. Flap Position of Free Memapsin 2 (β-Secretase), a model for flap opening in aspartic protease catalysis. *Biochem* 2004; 43(16):4689-4695.

102. Hong L, Koelsch G, Lin X, *et al.* Structure of the protease domain of Memapsin 2 (beta-Secretase) complexed with inhibitor. *Science* 2000; 290(5489):150-153.

103. Ostermann N, Eder J, Eidhoff U. Crystal structure of Human BACE2 in complex with a Hydroxyethylamine transition-state inhibitor. *J Mol Biol* 2006; 355(2):249-261.

104. Arun KG and Heather LO. BACE1 (β-secretase) inhibitors for the treatment of Alzheimer's disease. *Chem. Soc. Rev.* 2014; 43(19): 6765-6813.

105. Vassar R, Cole SL. The alzheimer's disease β-secretase enzyme, BACE1. *Mol Neurogenerat* 2007; 2(22):1-25.

106. Miles Congreve, David Aharony, Jeffrey Albert. Application of fragment screening by X-ray crystallography to the discovery of aminopyridines as inhibitors of beta-secretase. *J Med Chem* 2007; 50(6):1124-1132.

107. Cai H, Wang Y, McCarthy D. BACE1 is the major beta - secretase for generation of Abeta peptides by neurons. *Nat Neurosci* 2001; 4(3):233–234.

108. Roberds SL, Anderson J, Basi G. BACE knockout mice are healthy despite lacking the primary beta - secretase activity in brain: implications for Alzheimer's disease therapeutics. *Hum Mol Genet* 2001; 10(12):1317–1324.

109. Godemann R, Madden JKramer J, *et al.* Fragment-based discovery of BACE inhibitors using functional assays. *Biochem* 2009; 48(45):10743-10751.

110. Hong L, Lin X, Wu S, *et al.* Structure of the protease domain of memapsin-2 (beta-secretase) complexed with inhibitor. *Science* 2000; 290(5489):150-153.

111. Haass C, Lemere CA, Capell A, *et al* Citron. The Swedish mutation causes early-onset Alzheimer's disease by [beta]-secretase cleavage within the secretory pathway. *Nat Med* 1995; 1:1291-1296.

112. McConlogue L, Buttini M, Anderson JP, *et al.* Partial reduction of BACE1 has dramatic effects on Alzheimer plaque and synaptic pathology in APP transgenic mice. *J Biol Chem* 2007; 282(36):26326–26334.

113. Arun KG, Margherita B and Jordan T. Developing β-secretase inhibitors for treatment of Alzheimer's disease. *J of Neurochem* 2012; 120(1):71–83.

114. Roberds SL, Anderson J, Basi G. BACE knockout mice are healthy despite lacking the primary beta - secretase activity in brain: implications for Alzheimer's disease therapeutics. *Hum Mol Genet* 2001; 10(12):1317–1324.

115. Luo Y, Bolon B, Brian DB, *et al*. Mice deficient in BACE1, the Alzheimer ' s beta - secretase, have normal phenotype and abolished beta-amyloid generation. *Nat Neurosci* 2001; 4(3):231–232.

116. McConlogue L, Buttini M, Anderson JP. Partial reduction of BACE1 has dramatic effects on Alzheimer plaque and synaptic pathology in APP transgenic mice. *J Biol Chem* 2007; 282(36):26326–26334.

117. Shuto D, Kasai S, Kimura T, *et al*. KMI-008, a novel beta-Secretase inhibitor containing a hydroxymethylcarbonyl isostere as a transition-State mimic: design and synthesis of substrate-based octapeptides. *Bioorg Med Chem Lett* 2003; 13(24):4273-4276.

118. Kimura T, Shuto D, Hamada Y, *et al.* Design and synthesis of highly active Alzheimer's [beta]-secretase (BACE1) inhibitors, KMI-420 and KMI-429, with enhanced chemical stability. *Bioorg Med Chem Lett* 2005; 15(1):211-215.

119. Asai M, Hattori C, Iwata N, *et al*. The novel β-secretase inhibitor KMI-429 reduces amyloid β peptide production in amyloid precursor protein transgenic and wild-type mice. *J Neurochem* 2006; 96(2):533-540.

120. Huang Wen-Hai, Sheng R, Yong-Zhou H. Progress in the development of nonpeptidomimetic BACE 1 Inhibitors for Alzheimers Disease. *Curr Med Chem* 2009; 16(14):1806-1820.

121. Ghosh AK, Kumaragurubaran N, Hong L. Design, synthesis, and X-ray structure of potent Memapsin 2 (β-secretase) inhibitors with isophthalamide derivatives as the P2-P3-ligands. *J Med Chem* 2007; 50(10):2399-2407.

122. Kimura T, Hamada Y, Stochaj M, *et al.* Design and synthesis of potent [beta]-secretase (BACE1) inhibitors with carboxylic acid bioisosteres. *Bioorg Med Chem Lett* 2006; 16(9):2380-2386.

123. Hussain I, Hawkins J, Harrison D, *et al.* Oral administration of a potent and selective non-peptidic BACE-1 inhibitor decreases β-cleavage of amyloid precursor protein and amyloid-β production in vivo. *J Neurochem* 2007; 100(3):802-809.

124. Huang D, Lüthi U, Kolb P, *et al.* Discovery of cell-permeable non-peptide inhibitors of β-secretase by high-throughput docking and continuum electrostatics calculations. *J Med Chem* 2005; 48(16):5108-5111.

125. Huang D, Luthi U, Kolb P. In silico discovery of beta-secretase inhibitors. *J Am Chem Soc* 2006; 128(16):5436 –5443.

126. Murray CW, Callaghan O, Chessari G, et al. Application of fragment screening by X – ray crystallography to beta - secretase. *J Med Chem,* 2007; 50(6):1116–1123.

127. Kuglstatter A, Stahl M, Peters J. U. Tyramine fragment binding to BACE-1. *Bioorg Med Chem Lett* 2008; 18(4):1304–1307.

128. Gianpaolo C, Angela DS, Mancini F, *et al.* A small library of 2-aminoimidazole derivatives as BACE-1 inhibitors: Structure based design, synthesis, and biological evaluation. *Eur J Med Chem* 2012; 48:206-213.

129. Malamas M. S, Robichaud A, Erdei J, *et al.* Design and synthesis of aminohydantoins as potent and selective human β-secretase (BACE-1) inhibitors with enhanced brain permeability. Bioorg Med Cem Lett, 2010; 20(22):6597-6605.

130. Malamas MS, Robichaud A, Erdei J, *et al.* New pyrazolyl and thienyl aminohydantoins as BACE-1 inhibitors: exploring the S2' region. *Bioorg Med Cem Lett* 2011; 21(28):5164-5170.

131. Gerritz S, Zhai W, Shi S. Acyl guanidine inhibitors of BACE-1: Optimization of a micromolar hit to a nanomolar lead via iterative solid- and solution –phase library synthesis. *J Med Chem* 2012; 55(21):9208-9223.

132. Peng L, Yan N, Chao W, *et al*. 4-Oxo-1,4-dihydroquinoline-3-carboxamides as BACE-1 inhibitors: Synthesis, biological evaluation and docking studies. *Eur J Med Chem* 2014; 79:413-421.

133. Leeson P. Drug discovery: Chemical beauty contest, *Nature* 2012; 481(7382): 455-456.

134. Azim MK, Waseem A, Ishtiaq AK. Identification of acridinyl hydrazides as potent aspartic protease inhibitors. *Bioorg Med Chem Lett* 2008; 18(9):3011-3015.

135. Molegro Virtual Docker (www.molegro.com) now available at CLC Genomics workbench 7.0.3 (www.clcbio.com)

136. Chemdraw Ultra 11 (www.cambridgesoft.com)

137. Halgren TA, Murphy RB, Friesner RA, *et al.* Glide: a new approach for rapid, accurate docking and scoring. 2. Enrichment factors in database screening. *J Med Chem* 2004; 47(7):1750-1759.

138. Marvin 5.2.6, 2009, ChemAxon (www.chemaxon.com).

139. Shelley JC, Cholleti A, Frye LL, *et al.* Epik: a software program for pK a prediction and protonation state generation for drug-like molecules. *J Comput Aid Mol Des* 2007; 21(12):681-691.

140. JChem for Excel (www.chemaxon.com/products/jchem-for-office/)

141. Fernandes J, Gattass CR. Topological polar surface area defines substrate transport by multidrug resistance associated protein 1 (MRP1/ABCC1). *J Med Chem.* 2009; 52(4):1214-1218.

142. Leeson, P. Drug discovery: Chemical beauty contest. *Nature* 2012; 481(7382):455-456.

143. Pajouhesh H and Lenz GR. Medicinal Chemical Properties of Successful Central Nervous System Drugs. *NeuroRx* 2005; 2: 541–553.

144. Sander T, Freyss J, von Korff M, *et al*. OSIRIS, an entirely in-house developed drug discovery informatics system. *J Chem Inf Model* 2009; 49(2):232-246.

145. Sander TL. Osiris Property Explorer (2001-2013). (www.organic-chemistry.org/prog/peo/)

146. Tetko IV, Tanchuk VY. Application of associative neural networks for prediction of lipophilicity in ALOGPS 2.1 program. *J Chem Inf Comput Sci* 2002; 42(5):1136-1145.

147. Pawel N, Derek C, Ann A. Discovery and initial optimization of 5, 5'–disubstituted aminohydantoins as BACE-1 inhibitors, *Bioorg Med Chem Lett* 2010; 20(2):632-635.

148. Taleb H, Mohammed HS, Raed A. Design, synthesis and quantitative structure-activity evaluations of novel beta secretase inhibitors as potential Alzheimer's drug leads. *J Med Chem* 2011;54(24):8373- 8385.

149. Azim MK, Waseem A, Ishtiaq AK. Identification of acridinyl hydrazides as potent aspartic protease inhibitors. *Bioorg Med Chem Lett* 2008; 18(9):3011-3015.

150. Pawel Z, Subra G, Verdie P, *et al*. Sulfonamides with the N-alkyl-N'-dialkylguanidine moiety as 5-HT7 receptor ligands. *Bioorg Med Chem Lett* 2009; 19(16):4827-4831.

151. Bogiel P, Gadella TW. FRET microscopy: from principle to routine technology in cell biology. *J Microsc* 2011; 241(2):111-118.

APPENDIX

List of publications

Journal Publications

1. Priti Jain, Hemant R Jadhav. Therapeutic Advances in the Treatment of Alzheimer's Disease: Present and Future. *Current Drug Therapy* 2011; 6(3):175-185
2. Lavika Jain, Priti Jain, Hemant R Jadhav. 1-(4-(Phenoxymethyl) benzyl) Piperidine Derivatives as H3 Histaminic Receptor Antagonists: A Quantitative Structure Activity Relationship study. *International Journal of Pharmaceutical Frontier Research* 2011; 1(2): 23-30.
3. Priti Jain, Hemant R Jadhav. Quantitative structure activity relationship analysis of aminoimidazoles as BACE-I inhibitors. *Medicinal Chemistry Research* 2013; 22:1740–1746.
4. Priti Jain, Multi target directed ligand: An approach to treat Alzheimer's disease. *J Alzheimers Dis Parkinsonism*, 2013, 3:4, http://dx.doi.org/10.4172/2161-0460.S1.004
5. Priti Jain, Naga Rajiv L, Hemant R Jadhav. Synthesis and antibacterial profile of cyclized diazonium compounds. *Journal of Drug Design and Discovery* 2014; 1(1):2014, 1-9.
6. Priti Jain, Pankaj K Wadhwa, Hemant R Jadhav. Reactive astrogliosis: Role in Alzheimer's Disease. *CNS & Neurological Disorders – Drug Targets*. 2015; 14:872-879.
7. Priti Jain, Pankaj K Wadhwa, Shilpa Rohilla, Hemant R Jadhav. Rational design, synthesis and in vitro evaluation of allylidene hydrazinecarboximidamide derivatives as BACE-1 inhibitors. *Bioorganic & Medicinal Chemistry Letters* 2015; 26(2016): 33-37.
8. Priti Jain, Pankaj K Wadhwa, Hemant R Jadhav. QSAR and Docking Studies of N-hydroxy Urea Derivatives as Flap Endonuclease-1 Inhibitors. *Current Computer Aided Drug Design* 2015; 12: DOI: 10.2174/1573409912666151124233628; E-pub ahead of print.
9. Priti Jain and Hemant R. Jadhav. Design, Synthesis and Evaluation of 2-thio-pyrimidine Derivatives as BACE-1 inhibitors. *International Journal of Pharmaceutical Sciences and Research: Scientific Proceeding APTICON 2015* 2015: 389-391.

Presentations

1. Bhanu Priy, Priti Jain, Hemant R Jadhav. Aminoimidazolesas Potent and Selective Human β-Secretase (BACE1) Inhibitors: A 2D-QSAR Study, presented at "62nd IPC", Manipal, Dec, 2010

2. Mohit Singh, Priti Jain, Hemant R Jadhav, 2-D QSAR study of novel pyrollones and imidazolones as $GABA_A$ receptor activity modulator presented at "62nd IPC", Manipal, Dec, 2010
3. Santosh C. V., Priti Jain, Hemant R Jadhav, 2D-QSAR analysis of cyanodihydrapyridines as potent mineralocorticoid receptor antagonists, presented at "62nd IPC", Manipal, Dec, 2010
4. Naga Rajiv L, Priti Jain, Hemant R Jadhav, 2D QSAR of pyrrole-indoline-2-ones as aurora kinase inhibitors, presented at "Contemporary Trends in Biological and Pharmaceutical Research", BITS, Pilani, 2011
5. Lavika Jain, Priti Jain, Hemant R. Jadhav, 2D-QSAR Studies of 1-(4-(Phenoxymethyl) benzyl) Piperidine Derivatives as H3 Histaminic Receptor Antagonists presented at "Contemporary Trends in Biological and Pharmaceutical Research", BITS, Pilani, 2011
6. Aneesh Karkhanis, Priti Jain, Hemant R. Jadhav, 2D QSAR of 4-alkylamino- [1, 7] naphthyridine-3- carbonitriles as selective TPL-2 kinase inhibitor presented at "Contemporary Trends in Biological and Pharmaceutical Research", BITS, Pilani, 2011
7. Christo Jose, Priti Jain, Hemant R Jadhav, Hydroxyethyl amine compounds as BACE-I inhibitors: A 2D-QSAR study presented at "Contemporary Trends in Biological and Pharmaceutical Research", BITS, Pilani, 2011
8. Ashar A. Faizee, Priti Jain, Hemant R. Jadhav, Aminohydantoin disubstituted derivatives as a potent and selective human β secretase (BACE1) inhibitors: A quantitative structure activity relationship, presented at "APTI, Moga, 7-9th October 2011.
9. Jigish J. Parmar, Priti Jain, Hemant R. Jadhav, 2D-QSAR study on the novel hydroxamates as TACE (TNF-α converting enzyme) inhibitors , presented at "APTI, Moga, 7-9th October 2011.
10. Neha Tickoo, Priti Jain, Hemant R. Jadhav, 2D-Quantitative structural activity relationship (2D-QSAR) studies of Inhibitors of Trypanosomal Cysteine Proteases, presented at "APTI, Moga, 7-9th October 2011.
11. Anupama Devarajan, Priti Jain, Hemant R. Jadhav. 2D-Quantitative structural activity relationship (2D-QSAR) studies of some new 4β-anilino-4'-O-demethyl-4-desoxypodophyllotoxin derivatives as potential antitumor agents, presented at "APTI, Moga, 7-9th October 2011.
12. Priti Jain, Naga Rajiv L Hemant R Jadhav. Synthesis and antibacterial profile of cyclized diazonium compounds, oral presentation at "International conference on global trends in pure and applied chemical sciences", Udaipur, 3rd-4th March 2012.

13. Pankaj Wadhwa, Priti Jain, Hemant R Jadhav. Docking study of indole derivatives as flap endonuclease inhibitor presented at “Recent advances in computational drug design”, IISc Bangalore, 16-17th September 2013.
14. Priti Jain, Shilpa Rohilla and Hemant R. Jadhav. Allylidene hydrazinecarboximidamide derivatives as BACE-1 inhibitors presented at “NDCS 2015: International Conference on Nascent Developments in Chemical Sciences: Opportunities for Academia- Industry Collaboration”, BITS Pilani, Pilani Campus, 16-18th October 2015.
15. Priti Jain and Hemant R. Jadhav. Design, Synthesis and Evaluation of 2-thio-pyrimidine Derivatives as BACE-1 inhibitors presented at “APTICON-2015: 20th Annual Convention of Association of Pharmaceutical Teachers of India”, Indore, 9-11th October 2015.

Brief Biography of Ms. Priti Jain

Ms. Priti Jain has completed her Bachelor`s degree in Pharmacy from Lachoo Memorial College of Science and Technology in the year 2005. She acquired her Master`s degree in Pharmacy in Pharmaceutical Chemistry from Manipal College of Pharmaceutical Sciences, Manipal in year 2007. She was gold medalist in her B. Pharm. and topper in M. Pharm. After that she worked in Glenmark Research Centre, Navi Mumbai as Research Associate from April 2007 to Jan. 2009. She joined BITS Pilani, Pilani campus as lecturer in Feb. 2009 and is continuing till date. She has successfully completed one UGC minor research project entitled, 'Design, synthesis and evaluation of novel beta secretase inhibitors for the treatment of Alzheimer's disease' (July 2012 to June 2014). She also has completed one industrial project. She has published research articles in peer reviewed journals and presented her work in various national and international conferences.

Brief Biography of Dr. Hemant R. Jadhav

Dr. Hemant R Jadhav is presently working in the capacity of Associate Professor, Department of Pharmacy and Associate Dean, Academic Research (Ph. D. Programme) Division, Birla Institute of Technology and Science Pilani, Pilani campus. He received his PhD degree in the year 2004 from National Institute of Pharmaceutical Education and Research (NIPER), Mohali, India. He has been involved in the research for last 15 years and in teaching for last 11 years. He has authored more than 20 research papers and 2 book chapters. He has presented his work in more than 40 national and international conferences. He is an expert reviewer of many national and international journals. He is a lifetime member of Association of Pharmacy Teachers of India. He has served as the post graduate and doctoral examiner for various universities.He has successfully completed two research projects, one under DST Fast Track Young Scientist Scheme and another sponsored by UGC, New Delhi. He also has completed one industrial project. He has guided three Ph. D students and is currently guiding five PhD students.